(NASA-CR-166448) CORRELATION AND EVALUATION OF INPLANE STABILITY CHARACTERISTICS FOR AN ADVANCED BEARINGLESS MAIN ROTOR Final Report (Textron Bell Helicopter) 85 p HC A05/MF A01 CSCL 01C G3/05

N83-25695

Unclas 11803

CORRELATION AND EVALUATION OF INPLANE STABILITY CHARACTERISTICS FOR AN ADVANCED BEARINGLESS MAIN ROTOR

By William H. Weller
May 1983

CR-166448

Prepared under Contract No. NAS2-11269 by

BELL HELICOPTER TEXTRON, INC.
Fort Worth, Texas

for

National Aeronautics and Space Administration

CORRELATION AND EVALUATION OF INPLANE STABILITY CHARACTERISTICS FOR AN ADVANCED BEARINGLESS MAIN ROTOR

By William H. Weller
May 1983

CR-166448

Prepared under Contract No. NAS2-11269 by

BELL HELICOPTER TEXTRON
Fort Worth, Texas

for

AMES RESEARCH CENTER
NATIONAL AERONAUTICS AND SPACE ADMINISTRATION

TABLE OF CONTENTS

SUMMARY

A program of experimental and analytical research has been performed to demonstrate the degree of correlation achieved between measured and computed rotor inplane stability characteristics. The experimental data were obtained from hover and wind tunnel tests of a scaled bearingless main rotor model. Both isolated rotor and free-hub conditions were tested. Test parameters included blade built-in cone and sweep angles; rotor inplane structural stiffness and damping; pitch link stiffness and location; and fuselage damping, inertia, and natural frequency. Analytical results for many test conditions were obtained, using current Bell Helicopter Textron Inc. analyses to compare with experimental data. In addition, the analytical and experimental results were examined to ascertain the effects of the test parameters on rotor ground and air resonance stability. The results from this program are presented herein in tabular and graphical form. The program documented herein was sponsored by contract (NAS2-11269) with the National Aeronautics and Space Administration, Ames Research Center.

INTRODUCTION

Many companies within the helicopter industry have worked toward the development of viable non-articulated rotor systems. Bell Helicopter Textron, Inc. (BHTI) has developed numerous multi-bladed hingeless rotor systems, where lead-lag and flap bearings are replaced with a structural flexure, to evaluate various design approaches. The development of viscoelastic materials, which can be efficiently used to provide high levels of inplane damping, caused BHTI to direct their efforts toward soft-inplane hingeless configurations with augmented inplane damping. This emphasis on soft-inplane configurations with viscoelastic dampers continued during the initiation of a program to design and test a bearingless rotor, where the pitch bearings were also eliminated. The bearingless hub has a soft-flapwise and soft-chordwise flexure that, at its outboard end, provides little restraint to blade feathering motions imposed through flexure twisting. Built-in inplane damping is provided primarily by using elastomeric material.

Concurrent with these hingeless and bearingless rotor development programs, BHTI has worked toward the establishment of analyses of sufficient accuracy to provide developmental support from preliminary design through flight test. The area of greatest difficulty has been predicting aeroelastic stability characteristics for hingeless and bearingless rotors. The fundamental problem lies in the fact that, unlike typical articulated rotors with a lag-flap-pitch hinge sequence, non-articulated rotors may have virtual flap and lag hinges that rotate with blade feathering (thereby possibly creating large kinematic coupling effects) and whose radial location varies with rotor speed. Other kinematic couplings may be intentionally induced through design. The structural design of a non-articulated rotor hub often includes redundant load paths. Finally, because of the higher effective hinge offsets typically associated with non-articulated rotors, blade elastic deflections are more pronounced. To be accurate, rotor stability analyses must reflect a sensitivity to structural detail and aeroelastic effects that have been substantiated by comparison to experimental results.

In an effort to substantiate current analyses, BHTI has constructed a small-scale model of a bearingless main rotor design. For this model the flap, lag, and torsional motions are accommodated in the hub flexure, with the inplane motions opposed by a damper-restrained, external cuff. Based on the use of this model, BHTI has embarked on a program to compare analytical predictions with measurements. In addition, both experimental and analytical results will be reviewed to obtain insight into the manner by which the physical characteristics of a bearingless

rotor influence isolated rotor and free-hub stability. The program began with the effort previously reported in reference 1, which investigated isolated rotor and free-hub stability characteristics in hover. To expand on those results and provide data more applicable to the full-scale system, the present study was done. Because the basic rotor and fuselage models were modified at the conclusion of the first phase, data from the two studies are not directly related. The details and results of the second study are discussed in this report. This study was performed in response to a contract (NAS2-11269) with the National Aeronautics and Space Administration, Ames Research Center. Mr. Randall L. Peterson served as the Technical Monitor.

SYMBOLS

Units used for the physical quantities defined in this paper are given in the International System of Units (SI).

C_d	airfoil aerodynamic drag coefficient
C_ℓ	airfoil aerodynamic lift coefficient
C_m	airfoil aerodynamic pitching moment coefficient referenced to the quarter chord
f_b	blade inplane frequency, Hz
I	natural mode generalized inertia, $kg \cdot m^2$
K	damper inplane stiffness, N/m
$\bar{K}_c$	control system stiffness normalized by the baseline value of 70.6 N·m/rad
$\bar{K}_{\zeta_i}$	damper inplane stiffness for ith blade normalized by the baseline value of 17513 N/m
R	rotor radius, m
r_{PL}	radial station of pitch link to pitch horn attachment, cm
T	rotor thrust normalized by 222.4 N, g
V	wind tunnel velocity, kn
x_{PL}	chordwise station of pitch link attachment (positive values ahead of blade quarter chord), cm

α	blade aerodynamic angle of attack, rad
α_s	rotor shaft angle of attack (positive nose up), deg
β_b	built-in coning angle of blade (positive tip up), deg
γ_b	built-in sweep of blade (positive tip aft), deg
δ	natural mode damper shear deflection, m
δ_3	pitch-flap coupling angle (positive for pitch down with flap up), deg
δ_4	pitch-lag coupling angle (positive for pitch up with lag aft), deg
ζ_b	blade inplane critical damping ratio (rotating system)
ζ_s	built-in inplane damping ratio (rotating system)
θ	blade collective pitch angle (positive nose up), deg
ϕ	blade damper material loss tangent angle, deg
ω	natural mode frequency, rad/s
$\bar{\Omega}$	rotor angular velocity normalized by 104.7 rad/s

EXPERIMENTAL APPARATUS AND PROCEDURES

The following paragraphs describe the bearingless rotor and fuselage models, test facilities, and the procedures used during the experiments associated with this study. The rotor model is designed to be functionally the same as a full-scale rotor system developed at BHTI and shown in figure 1. The major differences between the baseline model and full-scale rotors include a variation in blade design and the addition of certain hardware to effect the model parameter changes. The model hub, however, is an accurately scaled representation of the full-scale article. Model blade design variations from the full-scale design, including taper, airfoil and built-in twist, are believed to be of little consequence for this study.

Bearingless Rotor Model

The rotor model is a 2.42 m diameter, four-bladed, bearingless rotor. Rotor flap, lag, and pitch motions are accommodated by flexural arms extending outward from the centerline and preconed 2.75 degrees at their inboard end. The blades are untwisted and untapered with center of gravities and shear centers located at the quarter chord. Other rotor geometric and structural properties are shown in tables I and II.

One unique feature of this rotor is the hub design, shown pictorially in figures 2 and 3. The hub is formed by two flexural members, each continuing across the shaft attachment and connected to grips for opposite blade pairs. The two flexural members are stacked vertically and bolted to the mast at their centers. From the center of rotation, each flexural arm structurally transitions into a flat flapping flexure and then into a torsionally soft feathering element with cruciform cross-section. The cruciform shape is carried to station 21.9 cm, at which point the arm is built-up to contain the bushings for attachment of the blade grips. A torsionally stiff cuff encompasses each flexure. The cuff, used to control blade feathering, is bolted to the blade grip at its outboard end and is shear restrained to the flexure at its inboard end (6.1 cm from the rotor center). The shear restraint mechanism, shown schematically in figure 3, is pinned in the pitch direction; provides a beam shear load path to minimize beam-torsion coupling and flexure loads that would result from pitch link shears; and contains elastomeric shear pads for inplane damping augmentation. The pitch horn is attached to the inboard end of the cuff. Pitch link loads introduced to the horn will be reacted at the shear restraint in such a way as to generate a torsional couple, thereby rotating the cuff and twisting the attached flexure. The shear restraint rotates in pitch with the cuff and blade (fig. 3). With the blade and flexure at flat pitch, the shear restraint mechanism is rotated -11° (nose-down).

Two sets of blade grips can be used, providing either 0 or 3.0° coning angles. Blade sweep of 0 or 4° aft can be achieved through the use of eccentric bushings pressed into the inboard blade attachment blocks. Both blade coning and sweep are applied at 22 percent radius. The pitch horn is oversized to accommodate pitch link radial station changes by the use of various spacer arrangements. Inverting the cuff provides leading-edge pitch horn arrangements. Three sets of inplane dampers were tested. Two have stiffnesses of 17513 N/m with loss tangents of 0.467 and 0.600 (nominal). The third set has a stiffness of 35026 N/m and loss tangent of 0.246. The blade built-in damping level is proportional to the damper loss tangent value. The baseline

rotor pitch links contained a structural ring, shown in figure 2, to achieve the desired control system stiffness. Removal of this ring increased the control stiffness by 80 percent.

Two adjacent flexure arms are instrumented with four-arm strain gage bridges. Beamwise and chordwise bending moments are obtained at 3.1 and 5.9 percent radius and the flexure torsion is measured at 6.5 percent. The pitch link axial force and mast drive torque are also measured by strain gage bridges. Engineering load equivalents were recorded periodically with the data by using standard voltage level signals for each channel and noting the associated load level.

The model rotor is designed for Froude scale operation in air at atmospheric pressure based on a full-to-model scale factor of 5. Although compressibility and viscous effects on measured data are not representative, both static and dynamic deflections are properly simulated and the latter are more important for rotor stability testing. Scale factors relating the conceptual full-scale rotor to the model tested are listed in table III. Elastic simulation is based on matching the ratios of blade natural frequency to rotor speed. The calculated first inplane and out-of-plane frequency ratios for a nominal speed (78.54 rad/s) and moderate collective pitch (7°) are 0.69 and 1.04 per rev.

Fuselage Model

The fuselage model and drive system are shown in figures 4 to 6 which illustrate the more important features, as well as the hover and wind tunnel installations. The frame consists of an attachment shell, fuselage skin and ballast support structure, and rotor control system. The frame is mounted on a gimbal ring which, in turn, is connected to the drive stand. Connections between the frame, gimbal ring and stand are accomplished by soft rotary flexures that have very low rotational stiffness and damping. The flexures and gimbal provide fuselage freedom of motion in pitch and roll with respect to the drive stand. Steel leaf springs and adjustable viscous dampers are attached between the stand and fuselage or gimbal ring to tailor fuselage frequencies (pitch and roll stiffnesses) and damping levels. Ballast weights are mounted on the support structure to appropriately model the fixed-system inertia. The fuselage structure is covered by a fiberglass skin for wind tunnel testing.

The rotor shaft is direct driven by a variable-speed hydraulic motor. The motor is mounted within the lower portion of the drive stand, immediately above the thrust balance. A drive shaft is used to connect the motor with the rotor mast, extending

through the fuselage shell with two universal joints to accommodate fuselage motion. Rotor shaft angle of attack is controlled by an electric pitch actuator mounted to the drive stand above the balance.

The model has a complete rotor control system driven by remotely controlled electric motors. Two actuators, arranged 90° apart, are used to control cyclic blade feathering, and a single actuator is used for collective pitch. Linear potentiometers sense swashplate position and, therefore, rotor trim state. For the isolated rotor testing, one cyclic actuator was replaced by a spring-loaded stop. The spring holds the swashplate against the stop to maintain zero cyclic pitch during normal operation. When rotor excitation was desired, the swashplate was pulled down against the spring and released. The resulting cyclic feathering input led to a transient lead-lag motion of the blade. For free-hub testing, the fuselage was excited by pulling on one of two pluck cables attached to the fuselage at points removed from either pitch or roll axes. The ensuing fuselage motion caused transient blade lead-lag motions to occur.

The fuselage and drive stand are instrumented to read fuselage motions, rotor trim state, speed, thrust and torque. The gimbal rotary flexures are strain-gaged to measure fuselage pitch and roll motions. The linear potentiometers, connected to the swashplate, provide rotor trim state data and a potentiometer mounted to the pitch actuator indicates shaft angle of attack. Rotor thrust is measured by using a single component strain-gage balance mounted below the drive stand. Drive shaft torque is also sensed using a strain gage. Rotor shaft speed and azimuth position are determined using 1 and 60 per rev magnetic sensors. The rotating blade and shaft data are transferred to the fixed system through a 24-ring, slip-ring assembly using two brushes per ring. Rotor thrust, torque and trim positions are continuously displayed on analog meters mounted in a model operator's console. Rotor speed is read by using a frequency counter sensing the 60 per rev magnetic sensor signal.

The same fuselage and stand combination was used for both isolated rotor and free-hub tests. In the case of the isolated rotor testing, performed only in a hover condition, additions to the model were made to provide a large hub impedance and eliminate the free-hub effect. The model snubber was raised and locked to secure the fuselage and blocks were attached between the extremes of the fuselage attachment shell and the drive stand. These blocks were removed for free-hub testing in hover and in the wind tunnel and the snubber was used only to terminate unstable oscillations when incurred.

Test Facilities

Hover tests of the model were performed at the BHTI Model Test Cell. The test cell is 16.5 m in diameter with a ceiling height of 6.1 m. An adjacent control room houses all associated instrumentation and control apparatus. The model is mounted on a hydraulic hoist in the center of the test cell. Although the hoist is capable of raising the model 1.8 m, the hoist was kept in its down position to increase stand higher mode frequencies. As such, the rotor height above the floor, as tested, was approximately 2.4 m.

Wind tunnel tests were carried out at the Vought Corporation Low Speed Wind Tunnel (LSWT). The LSWT is a horizontal single-return, continuous-flow tunnel with a test section size 4.57 m by 6.10 m. The test section is 11.89 m long and velocities between 5 and 46 kn can be obtained.

Test Procedures and Data Reduction

Rotor inplane stability characteristics were measured in a hovering condition for numerous rotor and fuselage configurations. Operating conditions were varied over wide ranges of rotor thrust (44-400N) and rotational speed (63-100 rad/s). The nominal values of 1g rotor thrust and rotational speed were 222.4 N and 78.54 rad/s, respectively. Each hover run was initiated by bringing the rotor speed up to the desired value and setting collective pitch to yield the specified thrust. Sustained first harmonic rotor flapping was eliminated before recording data. Once the test conditions were established, the model was "plucked" and the transient response recorded on both oscillograph and magnetic tape recorders. For isolated rotor tests, the swashplate position was stepped using the spring-loaded stop mechanism which replaced one of the cyclic actuators. For free-hub tests, the fuselage was excited by pulling on one of the two pluck cables attached to the fuselage.

After transient data were recorded for a test point, the thrust and/or rotor speed was changed to the next value and the process repeated. The program consisted of data sets with varying thrusts at a constant rotor speed or varying speed at constant thrust. Eleven rotor configurations were tested and their parametric values are identified in table IV. In addition to the isolated rotor tests (designated as fuselage configuration F-1), four free-hub configurations were examined. Characteristics of the nominal fuselage case (F-2) are listed in table V. The remaining fuselage configurations are identified in table VI and involved variations in fixed-system damping, inertia, or natural frequency.

Appendix A lists the various combinations of rotor, fuselage and operating conditions that were examined. Note that the rotor speed, $\bar{\Omega}$, is normalized by a value of 104.72 rad/s. Rotor stability characteristics were recorded for each test point. Hub beam and chord bending moments at 0.031R, hub torsion at 0.065R and the pitch link axial force for adjacent blades and the hub chord moment at 0.059R for one blade were all recorded on magnetic tape. The fuselage pitch and roll motions and the 1 per rev rotor pulse signal were also recorded on magnetic tape. These same data channels were recorded by an oscillograph, as well. The oscillograph traces were analyzed to produce the hover stability data listed in Appendix A. Frequency was determined by counting the hub (0.031R) chord bending moment peaks and damping ratio was calculated by applying the logarithmic decrement technique to that trace.

The wind tunnel test was performed in a fashion analogous to the hover test. For the wind tunnel test the shaft angle of attack was varied systematically with the five tunnel speeds used. Isolated rotor tests were not performed in the tunnel, because inclusion of the excitation mechanism would have prevented full rotor control in forward flight. The resulting transient data were recorded on magnetic tape and reduced off-line. Data reduction was based on the chordwise bending measurement at 3.1 percent radius, using the in-house Prony Analysis (ref. 2). This process uses a least squares curve fit routine to represent the digitized transient record with an exponential series approximation. Each exponential term in the series corresponds to a mode evidenced in the response. The solution of these terms provides an approximation of the frequency and damping for the modes most characterizing the response. Generally, two seconds of data were used with a digitizing rate of 256 samples/second. The final solution was based on approximating the time history by up to 20 modes. The rotor and fuselage combinations tested and the associated operating conditions for the wind tunnel test are identified in Appendix B, along with the corresponding reduced inplane frequency and damping values. The characteristics of the various rotor and fuselage configurations are the same as those for the hover test listed in tables IV to VI.

ANALYTICAL MODELS

The analytical research was performed using BHTI computer programs DNAM06, DRAV21TI, and C81. Program DNAM06 is the current production version of the BHTI series of programs used to calculate blade modal characteristics. DRAV21TI is the production rotor stability analysis capable of determining both isolated rotor and ground resonance characteristics for hover. C81 is a helicopter flight simulation digital computer program that can

also be used to analyze models installed in the wind tunnel. Descriptions of these programs are presented in the following paragraphs.

Modal Analysis

The blade modal analysis is performed using the production version of BHTI computer program DNAM06, which is documented in reference 3. Program DNAM06 is used to compute the fully coupled rotating natural frequencies and mode shapes of the rotor blade in vacuo. Blade flexibility is modeled by piecewise uniform, untwisted, massless elastic elements with principal axis misalignment and shear center offsets from the reference axis. The inertial properties are represented by lumped elements that can be offset from the reference axis and oriented out of the hub plane to account for blade twist and collective pitch effects. Various combinations of blade pitch control system, pylon impedance, and hub structural detail can be modeled to represent the effects of most realistic hub configurations. The program calculates modal qualities assuming five degrees-of-freedom (radial vibrations are ignored). Program inputs include rotor geometry (radius, chord, twist, pitch link location, etc.), hub and blade structural parameters (mass, mass moment, and bending and torsional stiffness distributions), hub impedance parameters, and rotor operating conditions (rotor speed and blade pitch).

The DNAM06 program is capable of modeling the redundant structural details of a bearingless rotor with shear restrained cuff, such as that used in this program. The built-in damping ratio attributable to the cuff inplane restraint, normalized by damper material loss tangent, is computed for each mode using the following relationship.

$$\frac{\zeta_{s_v}}{\tan \phi} = \frac{K\delta^2}{2I\omega^2}$$

where δ represents the relative inplane deflection between cuff and flexure at the shear restraint radial station. This normalized damping ratio and the appropriate damper loss tangent value are combined only for the first inplane mode in performing subsequent stability analyses.

Hover Stability Analysis

Isolated rotor and free-hub stability characteristics in hover are predicted by the production version of BHTI computer program DRAV21TI which is an eigenvector analysis similar to the DRAV02

program documented in reference 4. DRAV21TI interfaces with program DNAM06 to model the elastic rotor by using up to ten fully coupled modes calculated by the latter program. In contrast, program DRAV02 uses a lumped mass and spring-restrained hinge representation for the blade. The fixed-system representation in DRAV21TI models both the pylon and fuselage as lumped masses, moments of inertia, and hinges having spring and damper restraint. The various elements are connected by massless, rigid rods. Pitch and roll of both the pylon and fuselage and combined system lateral and longitudinal translation are allowed. For this program, the analytical model considered only fuselage pitch and roll motion. The analysis treats various articulated, hingeless and bearingless rotor configurations and includes such parameters as hub precone and prelag; blade droop and sweep; and spanwise variations of center of gravity and aerodynamic center offsets, blade twist and chord. Other rotor structural properties, such as the redundant load path in the hub, are implicitly represented in the mode shapes calculated by program DNAM06.

Quasi-steady aerodynamic loads are derived from tabulations of C_ℓ, C_d, and C_m using a table look-up process dependent on local Mach number and aerodynamic angle of attack. A program option allows the use of nonlinear equations to formulate the aerodynamic coefficients. For this study, the optional equations were used to define the aerodynamic coefficients by

$$C_\ell = 5.73\alpha$$

$$C_d = 0.008 + 1.7\alpha^2$$

$$C_m = 0$$

where α is the aerodynamic angle of attack in units of radians. The aerodynamic loads are calculated using strip theory and include dynamic inflow. Fuselage aerodynamic loads are neglected.

For this study the stability analysis made use of the rotating first inplane mode and the first three flap modes. The built-in damping for the inplane mode was based on the normalized damping ratio from program DNAM06 and the loss tangent of the inplane damper material for the particular rotor configuration in question. For the flap modes the built-in damping ratio was assumed to be zero for the first and 0.02 for the other two modes.

A numerical iteration procedure is used to calculate the blade equilibrium position based on a linearized set of equations. These same equations, but with time dependent terms retained, are used in the perturbation analysis. The blade perturbation equations are transformed from the rotating coordinate system to the

fixed system, using a multiblade coordinate transformation, to eliminate the periodic coefficients from the equations of motion. The solution is based on the normal mode approach using generalized coordinates associated with each rotor mode and the fuselage pitch and roll motions.

The modal analysis, program DNAM06, includes only linear terms that arise from the structural character of a rotor blade. In the stability analysis, the resulting modes are first used in conjunction with static aerodynamic forcing functions to calculate the blade's equilibrium position for a hovering condition. For the subsequent stability analysis, certain nonlinear effects have been modeled to more completely describe the elastic bending and torsion motions of the blade. Differential equations 61(b), (c), and (d) of reference 5 contain higher order terms involving spatially differentiated elastic displacement variables. Because these terms were not included in the modal analysis, the stability equations have been formulated to reflect these nonlinear effects. These particular terms of reference 5 have been linearized about the blade equilibrium position to produce products of static and oscillatory bending curvatures. The static curvatures are defined from the calculated blade equilibrium position. The oscillatory curvatures are expressed in terms of the input mode shapes by differentiating the slopes computed in program DNAM06. These nonlinear terms introduce elastic torsional moments in the equations of motion that arise from moderate bending deflections and are combined with the aerodynamic loads as generalized forcing functions of the normal modes calculated by DNAM06.

Forward Flight Stability Analysis

The stability analysis for the model in the wind tunnel was accomplished using the Rotorcraft Flight Simulation Computer Program, C81 (ref. 6). This program is used for computing rotor loads and aeroelastic and air resonance stability characteristics. C81 models the major dynamic components of a helicopter in free flight, including main and tail rotors, elastic pylon, wing, elevators, and six rigid-body fuselage degrees of freedom. C81 can also be used to simulate model wind tunnel tests by omitting fuselage rigid body motions and altering the trim procedure to delete the requirement for an equilibrium balance of the fuselage. The math model is a nonlinear, open form, time history analysis. Computed results are also provided in integrated and frequency-domain formats.

The input data for C81 is grouped by rotorcraft component. C81 can model single, compound, tandem, or side-by-side helicopter rotor configurations in hover, cruise, maneuver, or wind tunnel

flight conditions. Each rotor can have 2 to 7 blades. The mathematical model incorporated in C81 permits analysis of inelastic or elastic rotors with full nonlinear steady or unsteady aerodynamics. The elastic rotor is represented by up to 11 normal modes furnished by the DNAM06 analysis. The C81 model also includes elastic pylon attachment to a rigid-body fuselage that can include wings, stabilizing surfaces, and stores. Up to 10 pylon modes can be described to provide a thorough dynamic representation of the fixed system.

The program is capable of analyzing a rotor-on-test-stand configuration, as in a wind tunnel, and steady-state or maneuvering flight of a complete aircraft. The maneuver section of the program numerically integrates the fully coupled, nonlinear equations of motion to determine the response of the simulated model to specific external excitations (such as oscillating cyclic/collective controls). The capability of harmonic control input in C81 can excite the swashplate (in the fixed system) or a blade (in the rotating system) in a sinusoidal manner (with up to three different frequencies and magnitudes) or in any random fashion. Other control inputs can be tailored to simulated pilot induced oscillations such as stick stirs used to excite the regressing inplane mode for air resonance studies.

For the forward flight study, rotor aerodynamic characteristics were described by equations using the same relationships as those for the hover analysis. Stability characteristics were computed using only the first inplane and flap modes. The built-in damping for the inplane mode was based on the normalized damping ratio from DNAM06 and the built-in damping for the flap mode was assumed to be zero. Studies, conducted during this program, have shown that use of only the first flap and lag modes is sufficient in calculating aeromechanical stability characteristics. Two elastic pylon modes were used to model fuselage pitch and roll degrees of freedom. The analytical procedure began by performing a trim analysis of the rotor at the prescribed tunnel operating conditions. Once the rotor trim state was established, a maneuver was simulated during which two cycles of counterclockwise cyclic stir were applied at the regressive inplane mode frequency. The stir was then stopped and a time history of the ensuing transient decay was computed based on a sample spacing of 0.004 seconds. One second of decay was analyzed by a Prony analysis, built into C81 and similar to that used for experimental data reduction. Calculated inplane frequency and damping values were obtained using up to 20 response modes.

PRESENTATION OF RESULTS

Measured rotor aerodynamic performance characteristics are shown in figures 7 and 8 for hover and forward flight conditions, respectively. These data were measured using rotor configuration R-1. Experimental stability characteristics are presented in Appendices A and B. Representative measured and, when applicable, corresponding analytical results are presented graphically in figures 9 to 33 and discussed in subsequent paragraphs. In the appendices the inplane damping and frequency are expressed as rotating coordinate system values. In the figures, the inplane frequency is shown in the fixed system, while the damping is presented exclusively in the rotating system. The calculated results are from the production analyses, DRAV21TI for hover and C81 for forward flight. The organization of the figures is as follows:

	Figures
Isolated Rotor Analytical Correlation.....	9 to 13
Free-hub Analytical Correlation in Hover.....	14 to 19
Free-hub Analytical Correlation in Forward Flight.....	20 to 26
Bearingless Rotor Aeromechanical Stability Trends.....	27 to 33

DISCUSSION OF RESULTS

Isolated Rotor Analytical Correlation

Comparisons of measured and calculated isolated rotor stability characteristics are illustrated for rotor configuration R-1 in figures 9 and 10. In the figures, 1g thrust refers to a value of 222.4 N. The calculated results are obtained from the production analyses, DNAM06 and DRAV21TI. In figures 9 and 10 the dashed curves represent the built-in inplane mode damping ratio which is approximately the same for rotor configurations R-1, R-2, R-4, R-7, R-8, R-9, and R-12. The damping ratios for R-5 and R-6 are approximately 52 and 78 percent, respectively, of the values in these figures. This built-in damping is derived from the modal analysis (DNAM06) and based on the loss tangent of the shear restraint damper material. Built-in damping is nearly invariant with thrust (collective pitch) and decreases slightly with increasing rotor speed. The latter trend is due mostly to the centrifugal stiffening of the flexure causing it to carry a greater portion of the inplane bending moments. The difference

between the solid and dashed curves of figures 9 and 10 represents the calculated contributions that arise from aeroelastic sources and from coupling with other modes. These contributions are much smaller, however, than that provided by the elastomeric damper.

As shown in figure 9, the agreement between measured and calculated inplane frequency is good both in regard to value and trend. The calculated damping is slightly unconservative, but the measured trend with rotor speed i. correctly reflected in the analytical results. The correlation is further illustrated by the data of figure 10. As rotor speed is decreased, the measured and predicted damping values show an increasing aeroelastic sensitivity to thrust level, the degree of which is properly reflected by the calculated data. Again, computed results are slightly unconservative. Based on the results presented in figures 9 and 10, the dependency of inplane damping on operating condition would seem to be properly represented by the analytical results.

Variations in analytical correlation between different rotor configurations are shown in figures 11 to 13. The analytical results correctly reflect the effects of blade coning as suggested by figure 11a. For an isolated rotor, both analytical and experimental data suggest that adding 3 degrees of blade coning yields an increment in inplane damping of approximately one percent across the range of rotor speeds considered. In order to achieve this degree of correlation, it was necessary to input a value of δ_4 (pitch-lag coupling) of 10.5 degrees for all analytical cases as the only change from the baseline rotor (R-1) input when executing DRAV21TI. This value of δ_4 was determined from another modal analysis, ARAM06 (described in ref. 1), which uses the operating equilibrium position of the blade in calculating modal characteristics. It was found that the first inplane mode shape for the coned blade, as determined by program ARAM06, had an elastic twist component which suggested the above δ_4 value. This effect was not evident in the DNAM06 results because that program assumes a straight blade axis, always perpendicular to the axis of rotation.

The analytical trend with blade sweep is shown in figure 11b. The analytical and experimental trends are similar, although the variation of damping with rotor speed is not completely predicted for the case of a swept blade. For this case, program ARAM06 indicated that blade sweep did not significantly effect the in vacuo mode shapes, although ref. 7 indicates that blade sweep acts in a manner analogous to pitch-flap coupling. The input to DRAV21TI used only the available sweep angle parameter in arriving at the results shown in figure 11b. From figures 12 and 13a,

the effects of pitch link location and blade built-in inplane damping are correctly predicted by the analyses. The observed stabilizing effect, which arises when the control system stiffness is increased, is not matched by the predictions in figure 13b.

Free-hub Analytical Correlation in Hover

The correlation between measured and calculated free-hub stability characteristics for rotor configuration R-1 and fuselage F-2 is depicted in figures 14 and 15 for a hovering condition. The frequency correlation shown in figure 14 is very good, although an approximate 0.03 $\bar{\Omega}$ overprediction of the resonance rotor speeds is evident from the damping minimum points. This shift appears across the range of rotor speed for which data are available. The minimum damping values at the resonance points are conservatively predicted, showing good agreement in figure 14 for the roll resonance ($\bar{\Omega} \sim 0.7$). The calculated damping at the pitch resonance ($\bar{\Omega} \sim 0.85$) is too low. The calculated results generally pertain to those eigenvectors which have the lowest associated damping and a significant inplane degree of freedom component. For rotor speeds below 0.65 or above 0.9, damping from a body-dominated mode is shown. Because the measured data were obtained by exciting the fuselage, at extreme rotor speeds experimental results may relate more to a mode other than the inplane dominated mode. This is also suggested by the measured frequencies at $\bar{\Omega}$ values of 0.6 and 0.95. Body-dominated modes are selected only if they contain significant inplane components.

Aeroelastic sensitivity of the damping with thrust and rotor speed is illustrated in figure 15. At the lowest rotor speed, occurring well within both measured and calculated damping "buckets," the correlation is excellent. At $\bar{\Omega}$ values of 0.75 or 0.85, the comparisons are not as close due mostly to the different rotor speeds for calculated and measured resonance points. For example, at $\bar{\Omega} = 0.75$ the measured data reflect a point well removed from either pitch or roll resonance, while the calculated data are within the roll bucket (fig. 14) where thrust is more destabilizing. At each rotor speed and for the lowest thrust condition, the agreement between measured and calculated damping is good.

Measured and predicted damping levels for various rotor and fuselage configurations and a hovering free-hub condition are presented in figures 16 to 19. In general, by comparing these figures to figure 14a the relative changes in calculated and measured damping attributable to the various rotor and fuselage parameters can be seen. From figures 14a and 16a, the effect of

blade cone angle is to increase the minimum damping level, but by only 0.001 to 0.002. Both analytical and experimental data reflect this trend. Experimental data suggest that blade sweep (fig. 16b) is stabilizing, particularly at the roll resonance operating point, in contrast to the destabilizing analytical projection. The stabilizing influence of blade sweep, as projected by the measured data, contradicts the results of ref. 1. From Appendix A of ref. 1, the minimum damping values either barely decrease or are unaffected by blade sweep. As will be shown subsequently, the effect of blade sweep varies with operating condition and with fuselage configuration.

Moving the trailing-edge pitch link from its nominal position for R-1 outboard to the R-7 location, slightly decreases both measured and predicted minimum damping values as shown by figures 14a and 17a. Based on analysis, the change of pitch link location causes the effective rotor δ_3 to vary from approximately 20° (R-1) to 0° (R-7). Thus, positive values of δ_3 achieved by pitch link location or by aft blade sweep are stabilizing for this configuration, further supporting the experimental projection for blade sweep shown in figure 16b. Moving the pitch link from the trailing to leading-edge (R-7 to R-8) stabilizes the rotor as seen from the measured data of figure 17. The calculated minimum for the pitch resonance supports this trend, but the analysis predicts that the roll resonance damping will be decreased by moving the pitch link to the leading-edge.

Both experimental and analytical results show a reduction in minimal damping level as blade built-in damping is decreased. From figures 14a and 18a, the minimum measured damping drops by 0.001 for rotor R-6 in comparison to R-1. Calculated damping levels change, however, by approximately 0.006 at the resonance point when the blade built-in damping is reduced by 22 percent. Also from figure 18b, stiffening the control system is stabilizing according to the measurements but ineffective from the analysis.

Reducing the fuselage built-in damping level also diminishes calculated damping as shown by figures 14a and 19a. The changes in minimum damping levels are approximately the same as predicted by experiment or analysis. The result of increasing fuselage inertia is also correctly predicted by the analysis, showing comparable damping ratio increases for both minimum values. Finally, the trend from reversing fuselage pitch and roll natural frequencies is well represented by the analysis and shows an extremely critical condition for a high frequency fuselage roll mode.

In summary, the results from programs DNAM06 and DRAV21TI project inplane stability characteristics for the basic rotor (R-1), whether isolated or mounted on a free-hub, that show good agreement with measured data. Measured trends with operating condition, blade cone angle, radial pitch link location, blade built-in damping and fuselage structural properties are reasonably reproduced by the calculations. The worst discrepancies arose when changes to blade sweep angle or chordwise location of the pitch link were made for a free-hub condition and for changes to the control system stiffness. These latter parameters are important in determining the amount of elastic torsion associated with the first inplane and, more importantly, flap modes which induce kinematic coupling (δ_4 or δ_3) effects on the rotor. It is possible that these kinematic effects are not completely represented in the analysis of a free-hub, where the degree of flapping associated with the eigenvector of interest is much larger than those for an isolated rotor condition.

Free-hub Analytical Correlation in Forward Flight

Measured and calculated free-hub stability characteristics, pertaining to rotor R-1 and fuselage F-2, are shown in figures 20 to 22. These data relate forward flight correlation and trends with the computed results obtained from program C81. The agreement between computed and measured inplane frequency is very good, especially in figure 20b where the variation with rotor speed is illustrated. The calculated frequencies of figure 21b are almost invariant with thrust (collective pitch), although the test data show a slight change. The calculated minimum damping levels of figure 20a are significantly higher for the roll resonance ($\bar{\Omega}$ = 0.7), but show good agreement for the pitch resonance ($\bar{\Omega} \simeq 0.85$). As with the hover data, the calculated rotor speeds for resonance (i.e., minimum damping) are slightly higher than measured values.

Although the measured trends with rotor speed variations are reasonably well predicted, the effect of thrust on damping is not. At low to moderate thrust levels the correlation is good, but for thrust values above 1g the analysis increasingly overpredicts damping level as shown by figure 21a. The measured data indicates a consistent destabilizing trend with thrust, similar to the hover trend shown in figure 15b. The analytical data better resembles isolated rotor characteristics. From figure 22 the variation of damping with flight speed is accurately projected by the analytical results at the rotor speeds for which data are shown. From figure 22, it is evident that both calculated and measured resonance minimum damping levels show an increase with flight speed from hover to 44.4 kn. At a nonresonant rotor speed ($\bar{\Omega}$ = 0.75), the measured and calculated damping

slightly decrease from hover to a moderate flight speed and increase for higher flight speeds. The discrepancy between the calculated and measured roll minimum damping ($\bar{\Omega}$ = 0.675) at the higher flight speeds is the largest difference, but the calculated pitch resonance and nonresonant damping levels correlate with measurement.

Comparing figure 20a with figures 23 to 26 provides an illustration of the analytical correlation achieved, using C81, with various rotor and fuselage parameter changes. The variation of inplane damping with rotor speed for rotor configurations having nonzero values of blade cone or sweep angle is presented in figure 23. Because C81 does not have provisions for inputs pertaining directly to blade cone and sweep angles including discrete δ_3 or δ_4 effects, the approach of applying lumped kinematic couplings to describe the effects of blade cone or sweep angle could not be used even though this method had worked for the hover correlation. Therefore, an alternate method was devised. Again, program ARAM06 (ref. 1) was used to determine blade equilibrium condition at the different operating conditions. The equilibrium condition was analyzed to calculate effective incremental aerodynamic center offsets for the blade stations relative to an assumed feathering axis. These offsets were input into C81 in conjunction with the modes pertaining to rotor configuration R-1 to simulate the effects of built-in blade cone or sweep angle. Only vertical offsets were required for a coned blade and horizontal offsets for a swept blade. As seen by comparing figure 20a for the baseline rotor (no offsets) with figure 23, this approach yielded good correlation as to the trends of blade damping with cone and sweep angles. The minimum damping values are unchanged for the roll resonance and increased for the pitch resonance by the addition of blade coning. The roll resonance damping ratio is decreased slightly and the pitch resonance damping increased by adding blade sweep. The incremental changes to the damping ratio due to blade cone and sweep angles are equally predicted by calculated and measured results.

Variation of inplane damping with pitch link location for forward flight is illustrated by figures 20a and 24. Moving the pitch link outboard along the trailing-edge (R-1 to R-7), reduces both calculated and measured damping ratios at roll resonance by 0.003 and 0.005, respectively. Both pitch resonance damping levels increase with the outboard pitch link, however, and the calculated increment is slightly larger. Relocating the pitch link from the trailing-edge to leading-edge position (R-7 to R-8), increases measured minimum damping ratios by 0.005 for both resonance points. The calculated minimum damping ratios also increase for R-8, but by approximately 0.008 to 0.019. Thus, measured trends with pitch link location are reflected by the analytical results, although the incremental changes differ in

magnitude. Good correlation is achieved in the relationship between system and blade structural damping as shown by comparing figures 20a and 25. The minimum damping ratio increments between R-1, R-5, and R-6 results are approximately the same as projected by measured and calculated data.

The correlation between calculated and measured damping for variations in fuselage structural characteristics is shown by comparing figures 20a and 26. The reduction in minimum damping ratios accompanying decreased fuselage built-in damping is well predicted by the analysis for both resonance points. The increased generalized inertia of fuselage configuration F-4 yields incremental levels to the minimum damping values which are slightly underpredicted for roll resonance and overpredicted for the pitch resonance point. The calculated roll resonance damping level, in fact, is insensitive to fuselage inertia. The trend from exchanging fuselage pitch and roll natural frequencies is partially predicted by the analysis. The agreement between computed and measured minimum damping at the roll resonance point ($\bar{\Omega}$ = 0.85) is comparable to that for F-2, when the roll resonance occurred at a normalized rotor speed of 0.7. The projected minimum damping pitch resonance at $\bar{\Omega}$ = 0.65 is not evident from the computed results.

The forward flight stability correlation achieved using program C81 is generally good for the baseline configuration (R-1/F-2). The minimum damping at roll resonance is overpredicted, as is the damping at thrust levels above 1g. Calculated frequencies and damping trends with flight speed are in good agreement with measured results. Calculated damping trends with blade cone and sweep angles, pitch link location, blade and fuselage built-in damping and fuselage inertia show acceptable agreement with measured data. The calculated damping for leading-edge pitch link locations is too high and this discrepancy should be remedied. The same is true for the roll resonance minimum damping associated with the baseline configuration.

Bearingless Rotor Aeromechanical Stability Trends

For over three decades the helicopter industry has concerned itself with the prevention of rotor dynamic instabilities which involve inplane motion of the blade, such as the aeromechanical type. Because earlier helicopters often employed articulated rotor systems, where large lead-lag motions were concentrated about the lag hinge, external viscous dampers could be used to provide large amounts of inplane damping and, thus, remedy these instabilities. Inplane instabilities could also be eliminated, as shown in ref. 8, by designing the hub to induce significant amounts of kinematic coupling between flap, lag and torsion

motions and, thus, provide damping from aerodynamic sources. As the industry evolved the hingeless rotor concept, where flap and lag motions were accommodated by long flexural arms, the problems of inplane dynamic instability resurfaced, particularly for soft-inplane rotor systems. Because inplane motion was no longer confined to a small area around the hinge, the use of external dampers became less viable. Further, the elimination of these dampers in improving hub aerodynamic characteristics became more desirable for these relatively clean systems. Reemphasis was placed on using hub and blade geometric and structural properties to elastically induce kinematic coupling effects and provide additional damping. Reference 7 demonstrates how effective these aeroelastic damping sources can be in enhancing inplane dynamic stability. Now, with the development of bearingless rotor systems, such as the BHTI M680, which also eliminate the feathering bearings of hingeless rotors, the aeromechanical stability traits of the former systems must be studied to determine the most efficient means of providing acceptable stability characteristics.

Prior to illustrating the inplane damping trends with various design parameters, it will be useful to consider certain operational trends of the baseline rotor system. As shown in figures 9 and 10, the greater portion of the isolated rotor inplane damping occurs due to the contribution of the hub elastomeric damper. Other aeroelastic contributions are present, although smaller, to yield the total observed damping ratio levels. One of these contributions arises from the relative flexure to shear restraint pitch inclination angle. As described previously, when the blade and hub flexure are at flat pitch the damper is inclined or indexed -11° (nose-down) as illustrated in figure 3. With this orientation aft bending of the blade causes a forward shearing of the damper and the inboard end of the cuff is lowered relative to the flexure by virtue of this index angle. Because the pitch horn is mounted to the trailing side of the cuff at its inboard end; the lowering of the cuff induces a nose-down pitch, creating a negative δ_4 (destabilizing) effect. As collective pitch is increased, the index angle and associated δ_4 effects are reduced. For pitch angles in excess of 11°, the coupling effect reverses to yield a stabilizing contribution. This variation of rotor kinematic δ_4, due to the shear restraint index angle, is one of the reasons the isolated rotor shows a stabilizing aeroelastic damping trend with higher thrust or lower rotor speeds at 1-g thrust.

Free-hub hover stability characteristics for the baseline rotor are shown in figures 14 and 15. The reduction in inplane damping at the points of frequency coalescence between the regressing blade inplane mode and fuselage roll ($\bar{\Omega}$ = 0.675) or pitch modes ($\bar{\Omega}$ = 0.825) is evident in figure 14. Damping levels are reduced

sufficiently to yield a mild instability at the inplane-roll resonance rotor speed and a damping ratio of only 0.004 at the pitch resonance. At a nonresonance operating rotor speed ($\bar{\Omega}$ = 0.75), the damping level has nearly recovered to its isolated rotor level, at least for 1-g thrust conditions. Comparisons of isolated and free-hub damping levels for variations in rotor thrust are shown by figures 10 and 15. The effect of a free-hub is generally destabilizing. At the rotor speeds shown in figure 10, the isolated rotor shows a consistent stabilizing trend with thrust, while the free-hub trends (fig. 15) are destabilizing for $\bar{\Omega} \leq 0.75$ and only slightly stabilizing at higher rotor speeds. Only at a nonresonance rotor speed and thrusts below 1-g are the damping levels for a free-hub comparable to those of the isolated rotor.

While the minimum resonance damping ratios in figure 14 depict a model which is unstable at one rotor speed range and only marginally stable at another, the full scale M680 helicopter has significantly higher stability margins with no observed instabilities as demonstrated by flight test. This lack of correlation between model and full scale is explained by the relative focal points for fuselage motions on the model and ship. The model gimbal is located at a waterline location which is very near the scaled aircraft's center of gravity. Thus the model fuselage was ballasted to yield mass moments of inertia which correspond to scaled ship inertias about its center of gravity. For the full scale helicopter the ground resonance fuselage mode is characterized by a motion focal point located below the landing gear due to translational motion accompanying airframe pitch and roll. The associated moments of inertia about this lower focal point are much higher than that for the center of gravity point. As was shown by figures 14a and 19b (F-4 case), this additional fixed-system inertia for the airframe is highly stabilizing. Because the purpose of this report is to illustrate bearingless rotor trends and correlation, the more critical center of gravity focal point inertias were used for the fuselage model. Better correlation with full scale results could be achieved, however, if the inertias for the fuselage model pertaining to figure 14 had been comparable to scaled inertias about a more representative focal point.

The variations of free-hub inplane damping with flight speed is illustrated, in part, by figure 22. At a nonresonant rotor speed damping variations with flight speed are small, being highest in hover and lowest at a moderate flight speed (fig. 22b). At the inplane-roll resonance rotor speed, the minimum damping ratio increases sharply in going from a hover to moderate flight speed (fig. 22a), but increases only slightly more as flight speed is further raised to 44.4 knots. Thus, the observed trend with flight speed at a nonresonance condition may not fully reflect trends at inplane-body resonance conditions. In contrast to the

roll resonance trend, minimum damping ratios at the inplane-pitch resonance rotor speed show a slight, but continuous, increase with flight speed from the lowest value in hover (fig. 22c). Besides these baseline rotor operational stability trends, the following paragraphs will illustrate trends observed by variation of design parameters.

As shown in ref. 7, the beamwise operating position of the blade relative to the feathering axis is extremely influencial in determining aeromechanical stability levels for a hingeless rotor, such as the BO-105. Overconing of the blade is beneficial, due to the nature of the elastically induced pitch-lag coupling, and its effect can be maximized by reducing feathering axis precone or increasing the built-in cone angle of the blade outboard of the feathering bearing. The degree to which feather axis precone and blade cone angles affect inplane stability is very dependent on the radial position of the feathering bearing or flexure. For a bearingless rotor such as the M680, where the torsional member is located well outboard of the flapping flexure, the effects of precone and cone angles on inplane stability should be diminished, because the blade and feathering axis elastically flap almost in unison. The results of applying 3° of blade coning were illustrated earlier in this report and figure 27 presents a summary of the free-hub measured data. Although a blade cone angle of 3° increases isolated rotor damping ratios by approximately 0.01 for 1g thrust (fig. 11a), the free-hub minimum damping levels are increased by only 0.001 to 0.003. Thus, the effectiveness of blade coning in increasing aeromechanical stability margins is significantly diminished for a free-hub condition. It is anticipated that the effect of flexure precone angle on a bearingless rotor would likewise be small in its effect on aeromechanical stability.

While refs. 7 and 9 suggest that aft blade sweep improves aeromechanical stability, partially by providing aerodynamic damping to the fuselage degrees of freedom, the results of ref. 10 indicate otherwise. From the isolated rotor test data, aft blade sweep reduces inplane damping as shown in figure 11b. Comparing figures 14a and 16b demonstrates that the hover free-hub minimum damping levels were increased for a swept-blade rotor on fuselage F-2. The greater increase occurred for the roll resonance ($\bar{\Omega}$ = 0.65). In forward flight a slight decrease in damping was observed in the roll resonance region by adding blade sweep (figs. 20a and 23b). Additional measured data are provided by figure 28 for the F-5 fuselage configuration, where the pitch and roll frequencies were reversed (see tables V and VI). The lower rotor speed resonance (pitch mode) is destabilized by blade sweep for both hover and forward flight with the latter condition showing a damping ratio loss of 0.005. The higher rotor speed resonance (roll mode) again shows an increase in damping from the swept blade. Quite possibly, the effect of blade sweep consistently

stabilizes the body modes, while for this rotor design it destabilizes the basic rotor stability characteristics. The net effect, then, will depend on the relative changes of blade sweep on rotor and body. What particular nature of fuselage configuration F-2 or of the operating characteristics of this rotor in the region $\bar{\Omega} \sim 0.65$ led to the stabilizing trend of figure 16b is unknown at this time. It is speculated that if the characteristics of the rotor could be changed such that the isolated rotor was stabilized or unaffected by blade sweep then blade sweep could be used to improve aeromechanical stability margins.

In a manner analogous to blade sweep, pitch link radial position influences the value of rotor pitch-flap coupling. Of the four pitch-link positions examined, the trailing-edge locations yielded δ_3 values of approximately 20° (R-1) and 0° (R-7) and the leading-edge locations had δ_3 values of 0° (R-8) and -20° (R-9). Unlike blade sweep, increasing rotor δ_3 by moving the pitch link did not degrade isolated rotor inplane damping for this configuration. As shown in figure 12a, isolated rotor damping levels were unaffected by moving the pitch link from R-1 and R-7. It is anticipated, therefore, that increased δ_3 conditions achieved by pitch link positioning might lead to improved aeromechanical stability margins. This assumption is supported by the data of figure 29, which shows minimum damping tends to increase for both leading- and trailing-edge configurations when the pitch link is moved to increase effective rotor δ_3. Figure 29 also shows that for comparable δ_3 values moving the pitch link from the trailing- to leading-edge (R-7 to R-8) further improves the minimum damping levels at 1g thrust, increasing the damping ratios by 0.008. This trend is due to the pitch inclination angle of the shear restraint and damper relative to the flexure axes as illustrated in figure 3. The action of this mechanism is described previously, where it was pointed out that blade inplane motions cause the inboard portion of the cuff to also move vertically and, depending on the location of the pitch link, to induce a torsional motion. This action generates an effective δ_4, or pitch-lag coupling, which is stabilizing at 1g thrust for leading-edge configurations and destabilizing for trailing-edge pitch links. The stabilizing tendencies of leading-edge pitch links were also observed throughout the forward flight operating envelope as shown in figure 30.

The effects of blade built-in damping on aeromechanical stability were demonstrated earlier and are again illustrated in figure 31a. The variation in loss tangent values for figure 31a represents an approximate change in damping ratio of 0.011 for the damper alone. The reduced built-in damping leads to a reduction

of 0.005 in the measured minimum damping ratios. A similar effect was observed by varying fuselage damping. Based on these results it appears that system built-in damping is one of the strongest parameters in affecting the aeromechanical stability of bearingless rotors. The effect of stiffening the rotor control system by 80 percent is shown in figure 31b. From ref. 7, it was pointed out that control system stiffness was influential in determining hingeless rotor aeromechanical stability margins. For this bearingless rotor configuration, control system stiffness changes were ineffective in varying forward flight minimum damping ratios based on the results depicted in figure 31b. For hover, the stiffened control system led to a slight increase in minimum damping ratios (figs. 14a and 18b).

In an effort to find other means of improving aeromechanical stability margins, consideration has been given to using an anisotropic hub design. In this instance the rotor anisotropy was created by varying the inplane damper stiffnesses among the four rotor blades. For this study two dampers were employed. those used for rotor configurations R-5 and R-6 which have stiffnesses differing by a factor of two. The relative measured isolated rotor characteristics for R-5 and R-6 and in hover are shown in figure 32. The isolated rotor damping levels are nearly equal for the rotors, because the stiffer rotor used an elastomeric material with lower loss tangent value. The inplane frequencies differ by only 0.032 per rev at a moderate rotor speed. Note that the rotor with the stiff dampers has a higher inplane frequency in the rotating system, which leads to a lower frequency in the fixed coordinate system used for figure 32b. The free-hub damping characteristics for R-5 and R-6 are shown in figure 33. Note that the curves were derived by fairing measured data, where either the soft of stiff dampers are installed in all four blades. The minimum damping ratios are about the same at the roll resonance points and R-5 shows a minimum damping 0.005 below that for R-6 at the pitch resonance points. Further, the resonance points for R-5 occur at a higher rotor speed due to the relative inplane frequencies of the two rotors.

Free-hub anisotropic rotor damping characteristics for hover are also presented in figure 33, where the dampers were arranged in two patterns. Due to the anisotropic nature of rotor configurations R-10 and R-11, it was necessary to reduce the transient response on both blade numbers 1 and 2. At each operating condition the smallest of the two damping ratio values was used in figure 33 and Appendix A. Minimum damping ratios for rotor configuration R-10, where adjacent blade pairs have the same damper characteristics, are higher than those for R-5 and R-6 by 0.003 to 0.008 (fig. 33a). For configuration R-11, with opposite blade pairs having the same damper characteristics, the increase in minimum damping ratios is only 0.001 to 0.004 (fig. 33b). Thus, the improvement in stability margins for R-11 is only

one-half that for R-10. In fact, the minimum damping ratios for configuration R-11 on a free-hub average the minimum ratios observed for configurations R-5 and R-6. For R-11 opposite blades both achieve a fuselage resonance condition at the same rotor speed. Because aeromechanical stability is influenced by the joint action of opposite blades in offsetting the rotor center of gravity from the axis of rotation, greater stability margins are achieved when opposite blades are dynamically distinct. The stability characteristics of rotor configuration R-10 might be further improved upon if all four blades had different damper characteristics and if the frequency separation was greater than the 0.032 per rev value used for this study.

As part of this study, model fuselage pitch and roll damping, moments of inertia and natural frequencies were independently varied to investigate their effects on rotor inplane damping. Parametric changes to the fuselage are identified in tables V and VI and measured results for hover are shown in figures 14a and 19, while results for forward flight are presented in figures 20a and 26. Figures 19a and 26a illustrate the effect of reducing fixed-system damping ratios from 0.06 to 0.03. The results of increasing fuselage pitch and roll inertias by 29 and 82 percent, respectively, are shown in figures 19b and 26b. Reversing fuselage natural frequencies, such that the pitch and roll normalized resonance rotor speeds are approximately 0.65 and 0.8, affects inplane damping in the manner shown in figures 19c and 26c.

By halving fuselage structural damping, hover minimum damping ratios at the pitch and roll resonance points are reduced by only 0.003 as shown from figures 14a and 19a. This amount is comparable to the reductions observed as rotor structural damping was reduced by approximately 1 percent. Fuselage built-in damping does influence stability margins, as does rotor damping. Increasing fuselage pitch and roll inertias led to improvements in minimum damping ratios by increments of 0.004 and 0.008 (figs. 14a and 19b) with the larger change relating to the roll resonance. Thus, minimum damping ratios at both resonances showed comparable sensitivities to fuselage inertia. Increasing fuselage natural frequency increases the associated resonance rotor speed and decreases minimum damping ratios (figs. 14a and 19c). For example increasing roll natural frequency from 2.8 to 4.9 Hz caused an increase in roll resonance rotor speed from 0.675 to 0.800 and a decrease in minimum damping of 0.012. The resonance damping ratio, associated with the fuselage degree of freedom having the least inertia, shows the greater sensitivity to natural frequency. Similar trends were observed from the forward flight test results as shown by comparing figures 20a and 26.

CONCLUSIONS

A program of experimental and analytical research has been performed to demonstrate the correlation achieved between measured and computed inplane stability characteristics for a model bearingless helicopter rotor. Data were obtained for an isolated rotor in hover and free-hub configurations in hover and forward flight. In addition to correlation objectives, the results were used to ascertain the effects of rotor and fuselage design parameters on aeromechanical stability. From the results of this program the follcwing conclusions are drawn:

I. Hover Stability Correlation

1. Results from program DRAV21TI show excellent correlation with measurement for the baseline rotor (R-1), whether isolated or mounted on a free-hub.

2. Measured trends with operating condition, blade cone angle, radial pitch link location, blade built-in damping and fuselage structural properties are reasonably predicted by the analysis.

3. Significant discrepancies arose when changes to blade sweep angle or chordwise location of the pitch link were considered for a free-hub condition and for changes to the control system stiffness.

II. Forward Flight Stability Correlation

1. The forward flight stability characteristics, as predicted by program C81, show generally good agreement for the baseline rotor and fuselage configuration (R-1/F-2), although the roll resonance minimum damping ratio is overpredicted as are the damping ratios at thrust levels above 1g.

2. Calculated damping trends with flight speed, blade cone and sweep angles, radial pitch link location, blade and fuselage built-in damping, and fuselage inertia show acceptable agreement with measured data.

3. Calculated damping ratios for rotors with leading-edge pitch link locations were too high and the agreement for measurements from a fuselage with low pitch natural frequency was not acceptable.

III. Bearingless Rotor Aeromechanical Stability Trends

1. The effects on stability margins of most of the rotor geometric and structural design parameters considered in this bearingless rotor study are small.

2. Built-in blade cone angle; leading-edge pitch link locations and those that provide the largest rotor δ_3; and increased rotor built-in damping lead to improved aeromechanical stability margins.

3. Variation in damper inplane stiffnesses among the blades to create an anisotropic rotor also improves aeromechanical stability margins.

4. Aft sweep of the rotor blades generally degrades stability margins, while increasing control system stiffness slightly improves hover stability but is ineffective in forward flight.

5. Increased fuselage damping, mass moments of inertia, and decreased fuselage natural frequencies all yield improvements in aeromechanical stability margins.

6. Acceptable aeromechanical stability traits for a bearingless rotor of the type used in this study can best be achieved by incorporating sufficient levels of built-in damping into the rotor.

APPENDIX A

EXPERIMENTAL INPLANE STABILITY CHARACTERISTICS FOR HOVER

Rotor Conf	Fuse Conf	$\bar{\Omega}$	T g	f_b Hz	ζ_b	Rotor Conf	Fuse Conf	$\bar{\Omega}$	T g	f_b Hz	ζ_b
R-1	F-1	0.650	0.2	8.6	3.8	R-1	F-2	0.825	1.0	9.1	0.4
"	"	"	0.6	8.4	3.5	"	"	0.875	"	9.4	1.5
"	"	"	1.0	8.2	4.8	"	"	0.900	"	9.9	2.1
"	"	"	1.4	8.2	6.3	"	"	0.950	"	10.6	3.5
"	"	0.750	0.2	9.2	3.2	R-1	F-3	0.750	0.2	9.0	5.8
"	"	"	0.6	8.8	3.0	"	"	"	0.6	8.9	5.5
"	"	"	1.0	8.7	3.8	"	"	"	1.0	8.8	4.3
"	"	"	1.4	8.6	4.5	"	"	"	1.4	8.8	2.3
"	"	"	1.6	8.5	5.4	"	"	"	1.6	8.8	0.9
"	"	"	1.8	8.4	6.3	"	"	0.600	1.0	7.2	1.3
"	"	0.850	0.2	9.3	2.5	"	"	0.625	"	7.5	0.5
"	"	"	0.6	9.3	2.5	"	"	0.650	"	7.8	-0.4
"	"	"	1.0	9.1	3.0	"	"	0.675	"	8.1	0.0
"	"	"	1.4	8.9	3.3	"	"	0.700	"	8.4	0.6
"	"	"	1.6	8.8	3.7	"	"	0.725	"	8.7	1.9
"	"	"	1.8	8.7	4.0	"	"	0.775	"	8.5	1.2
R-1	F-2	0.650	0.2	8.2	2.4	"	"	0.800	"	8.8	0.7
"	"	"	0.6	8.0	1.4	"	"	0.825	"	9.0	0.3
"	"	"	1.0	7.9	0.2	"	"	0.850	"	9.3	1.1
"	"	"	1.3	7.8	-1.2	"	"	0.875	"	9.6	2.1
"	"	0.750	0.2	9.0	3.7	"	"	0.900	"	9.7	3.5
"	"	"	0.6	8.8	3.4	"	"	0.925	"	10.0	5.1
"	"	"	1.0	8.6	3.1	"	"	0.950	"	10.2	5.9
"	"	"	1.4	8.7	2.8	R-1	F-4	0.750	0.2	9.1	6.3
"	"	"	1.6	8.6	2.7	"	"	"	0.6	8.8	6.4
"	"	"	1.8	8.6	2.0	"	"	"	1.0	8.8	6.4
"	"	0.850	0.2	9.3	0.9	"	"	"	1.4	8.7	6.3
"	"	"	0.6	9.3	0.8	"	"	"	1.6	8.9	6.1
"	"	"	1.0	9.2	0.8	"	"	"	1.8	8.7	5.4
"	"	"	1.4	9.0	0.9	"	"	0.600	1.0	7.3	1.5
"	"	"	1.6	9.3	1.1	"	"	0.625	"	7.7	1.2
"	"	"	1.8	9.3	1.2	"	"	0.650	"	7.8	0.8
"	"	0.600	1.0	7.3	1.9	"	"	0.675	"	8.1	0.7
"	"	0.625	"	7.6	0.6	"	"	0.700	"	8.4	0.8
"	"	0.675	"	8.0	-0.1	"	"	0.725	"	8.7	1.8
"	"	0.700	"	8.5	0.9	"	"	0.775	"	8.4	1.8
"	"	0.775	"	9.1	2.3	"	"	0.800	"	8.7	1.3
"	"	0.800	"	8.9	0.7	"	"	0.825	"	8.9	1.0

APPENDIX A (Continued)

Rotor Conf	Fuse Conf	$\bar{\Omega}$	T g	f_b Hz	ζ_b	Rotor Conf	Fuse Conf	$\bar{\Omega}$	T g	f_b Hz	ζ_b
R-1	F-4	0.850	1.0	9.2	0.9	R-2	F-2	0.750	0.6	9.3	3.0
"	"	0.875	"	9.4	1.2	"	"	"	1.0	8.6	2.6
"	"	0.900	"	9.7	1.5	"	"	"	1.4	8.7	2.5
"	"	0.925	"	10.0	3.9	"	"	"	1.6	8.5	2.4
"	"	0.950	"	10.0	6.3	"	"	"	1.8	8.5	1.9
R-1	F-5	0.750	0.2	8.5	1.4	"	"	0.600	1.0	7.2	1.7
"	"	"	0.6	8.4	0	"	"	0.625	"	7.6	0.6
"	"	"	1.0	8.3	-0.8	"	"	0.650	"	7.7	0.1
"	"	"	1.4	8.2	-1.1	"	"	0.675	"	8.1	0
"	"	"	1.6	8.2	-1.5	"	"	0.700	"	8.4	1.0
"	"	0.600	1.0	7.3	2.0	"	"	0.725	"	8.6	2.3
"	"	0.625	"	7.8	1.0	"	"	0.775	"	8.7	1.5
"	"	0.650	"	8.0	1.1	"	"	0.800	"	8.9	0.7
"	"	0.675	"	8.2	2.1	"	"	0.825	"	9.2	0.6
"	"	0.700	"	8.3	6.1	"	"	0.850	"	9.3	1.1
"	"	0.725	"	8.2	3.2	"	"	0.875	"	9.6	1.6
"	"	0.775	"	8.4	-1.2	"	"	0.900	"	10.0	2.8
"	"	0.800	"	8.8	-1.3	"	"	0.950	"	10.5	3.9
"	"	0.825	"	9.0	-0.7	R-2	F-5	0.750	0.2	9.0	2.9
"	"	0.850	"	9.1	0.1	"	"	"	0.6	8.7	1.8
"	"	0.875	"	9.2	0.9	"	"	"	1.0	8.4	0.3
"	"	0.900	"	9.4	1.3	"	"	"	1.4	8.3	-0.5
"	"	0.925	"	9.5	2.3	"	"	"	1.6	8.2	-0.9
"	"	0.950	"	9.7	3.3	"	"	"	1.8	8.2	-1.3
R-2	F-1	0.750	0.2	9.0	4.1	"	"	0.600	1.0	7.3	2.8
"	"	"	0.6	8.9	3.7	"	"	0.625	"	7.6	1.6
"	"	"	1.0	8.7	4.5	"	"	0.650	"	7.9	1.2
"	"	"	1.4	8.5	5.3	"	"	0.675	"	8.3	1.9
"	"	"	1.6	8.6	6.6	"	"	0.700	"	8.4	3.9
"	"	"	1.8	8.6	7.5	"	"	0.725	"	8.4	3.1
"	"	0.600	1.0	8.2	6.8	"	"	0.775	"	8.5	-1.1
"	"	0.650	"	8.5	6.0	"	"	0.800	"	8.8	-1.0
"	"	0.700	"	8.6	5.2	"	"	0.825	"	9.1	-0.7
"	"	0.800	"	8.8	4.1	"	"	0.850	"	9.1	0.4
"	"	0.850	"	9.1	3.9	"	"	0.875	"	9.4	0.8
"	"	0.900	"	9.2	3.5	"	"	0.900	"	9.6	1.7
"	"	0.950	"	9.5	2.9	"	"	0.925	"	9.8	2.2
R-2	F-2	0.750	0.2	9.4	3.0	"	"	0.950	"	9.9	3.4

APPENDIX A (Continued)

Rotor Conf	Fuse Conf	$\bar{\Omega}$	T g	f_b Hz	ζ_b	Rotor Conf	Fuse Conf	$\bar{\Omega}$	T g	f_b Hz	ζ_b
R-4	F-1	0.750	0.2	9.2	3.0	R-4	F-5	0.700	1.0	8.7	2.7
"	"	"	0.6	9.1	2.7	"	"	0.725	"	8.8	6.2
"	"	"	1.0	8.9	3.1	"	"	0.775	"	8.6	-0.4
"	"	"	1.4	8.8	3.6	"	"	0.800	"	8.7	-1.1
"	"	"	1.6	8.6	4.1	"	"	0.825	"	9.0	-1.2
"	"	"	1.8	8.6	4.9	"	"	0.850	"	9.3	-0.7
"	"	0.600	1.0	8.5	4.6	"	"	0.875	"	9.4	0.0
"	"	0.650	"	8.7	4.0	"	"	0.900	"	9.5	0.5
"	"	0.700	"	8.9	3.6	"	"	0.925	"	9.7	1.4
"	"	0.800	"	9.2	2.6	"	"	0.950	"	10.0	2.1
"	"	0.850	"	9.4	2.3	R-5	F-1	0.750	0.2	9.0	3.4
"	"	0.900	"	9.6	2.1	"	"	"	0.6	8.9	3.2
"	"	0.950	"	9.8	2.0	"	"	"	1.0	8.8	3.3
R-4	F-2	0.750	0.2	9.4	2.0	"	"	"	1.4	8.7	3.9
"	"	"	0.6	9.1	1.8	"	"	"	1.6	8.6	4.9
"	"	"	1.0	9.0	1.4	"	"	"	1.8	8.5	5.6
"	"	"	1.4	8.8	1.3	"	"	0.600	1.0	8.2	4.6
"	"	"	1.6	8.8	1.1	"	"	0.650	"	8.4	4.1
"	"	"	1.8	8.8	0.8	"	"	0.700	"	8.6	3.7
"	"	0.600	1.0	7.4	3.8	"	"	0.800	"	9.0	2.9
"	"	0.625	"	7.7	2.5	"	"	0.850	"	9.2	2.6
"	"	0.650	"	7.9	0.8	"	"	0.900	"	9.3	2.3
"	"	0.675	"	8.2	0.7	"	"	0.950	"	9.5	1.9
"	"	0.700	"	8.4	0.7	R-5	F-2	0.750	0.2	9.1	2.3
"	"	0.725	"	8.7	1.1	"	"	"	0.6	9.1	1.6
"	"	0.775	"	8.9	3.4	"	"	"	1.0	8.9	1.0
"	"	0.800	"	8.9	1.0	"	"	"	1.4	8.9	0
"	"	0.825	"	9.2	0.7	"	"	"	1.6	8.7	-0.3
"	"	0.850	"	9.4	0.5	"	"	"	1.8	8.8	-0.6
"	"	0.875	"	9.7	1.0	"	"	0.600	1.0	7.5	4.3
"	"	0.900	"	10.0	2.2	"	"	0.625	"	8.0	2.6
"	"	0.925	"	10.1	2.3	"	"	0.650	"	8.1	0.6
"	"	0.950	"	10.3	2.4	"	"	0.675	"	8.4	0.2
R-4	F-5	0.750	0.2	8.8	3.0	"	"	0.700	"	8.5	-0.3
"	"	"	0.6	8.7	2.4	"	"	0.725	"	8.7	0.0
"	"	"	1.0	8.5	1.0	"	"	0.775	"	9.0	1.8
"	"	"	1.4	8.3	0.2	"	"	0.800	"	9.1	1.2
"	"	"	1.6	8.3	-0.6	"	"	0.825	"	9.1	-0.2
"	"	"	1.8	8.1	-0.9	"	"	0.850	"	9.3	0.2
"	"	0.600	1.0	7.2	2.6	"	"	0.875	"	9.4	0.8
"	"	0.625	"	7.6	1.7	"	"	0.900	"	9.6	1.3
"	"	0.650	"	8.0	0.9	"	"	0.925	"	9.8	2.1
"	"	0.675	"	8.2	1.5	"	"	0.950	"	10.4	3.2

APPENDIX A (Continued)

Rotor Conf	Fuse Conf	$\tilde{\Omega}$	T g	f_b Hz	ζ_b	Rotor Conf	Fuse Conf	$\tilde{\Omega}$	T g	f_b Hz	ζ_b
R-6	F-1	0.750	0.2	8.9	3.2	R-7	F-1	0.850	1.0	8.9	3.0
"	"	"	0.6	8.6	3.1	"	"	0.900	"	9.1	2.9
"	"	"	1.0	8.6	3.2	"	"	0.950	"	9.2	2.5
"	"	"	1.4	8.5	3.4	R-7	F-2	0.750	0.2	8.9	4.5
"	"	"	1.6	8.3	3.9	"	"	"	0.6	8.7	4.0
"	"	"	1.8	8.3	4.7	"	"	"	1.0	8.7	2.9
"	"	0.600	1.0	7.7	4.3	"	"	"	1.4	8.7	2.0
"	"	0.650	"	8.1	3.9	"	"	"	1.6	8.7	1.6
"	"	0.700	"	8.3	3.6	"	"	"	1.8	8.6	1.1
"	"	0.800	"	8.6	2.9	"	"	0.600	1.0	7.4	2.4
"	"	0.850	"	8.8	2.7	"	"	0.625	"	7.7	0.7
"	"	0.900	"	8.9	2.5	"	"	0.650	"	7.9	-0.1
"	"	0.950	"	9.1	2.0	"	"	0.675	"	8.0	0.0
R-6	F-2	0.750	0.2	8.7	2.9	"	"	0.700	"	8.5	1.0
"	"	"	0.6	8.6	2.8	"	"	0.725	"	8.6	1.3
"	"	"	1.0	8.6	2.4	"	"	0.775	"	8.5	1.4
"	"	"	1.4	8.6	2.2	"	"	0.800	"	8.9	0.6
"	"	"	1.6	8.6	1.9	"	"	0.825	"	9.0	-0.1
"	"	"	1.8	8.5	1.6	"	"	0.850	"	9.2	0.3
"	"	0.600	1.0	7.4	1.8	"	"	0.875	"	9.5	1.6
"	"	0.625	"	7.7	0.8	"	"	0.900	"	9.7	2.4
"	"	0.650	"	7.8	-0.2	"	"	0.925	"	9.9	3.0
"	"	0.675	"	8.1	0.0	"	"	0.950	"	10.1	4.1
"	"	0.700	"	8.3	0.7	R-7	F-5	0.750	0.2	8.9	2.3
"	"	0.725	"	8.6	1.6	"	"	"	0.6	8.4	0.5
"	"	0.775	"	8.5	1.0	"	"	"	1.0	8.3	-0.3
"	"	0.800	"	8.8	0.4	"	"	"	1.4	8.3	-0.9
"	"	0.825	"	9.0	0.3	"	"	"	1.6	8.2	-1.7
"	"	0.850	"	9.1	1.1	"	"	"	1.8	8.2	-1.9
"	"	0.875	"	9.3	1.4	"	"	0.600	1.0	7.3	3.4
"	"	0.900	"	9.4	2.1	"	"	0.625	"	7.7	2.5
"	"	0.925	"	10.0	2.7	"	"	0.650	"	7.9	1.3
"	"	0.950	"	10.2	3.7	"	"	0.675	"	8.2	2.0
R-7	F-1	0.750	0.2	9.0	3.5	"	"	0.700	"	8.8	3.6
"	"	"	0.6	9.0	3.3	"	"	0.725	"	8.9	5.8
"	"	"	1.0	8.7	3.9	"	"	0.775	"	8.6	-0.8
"	"	"	1.4	8.7	4.7	"	"	0.800	"	8.8	-1.3
"	"	"	1.6	8.6	5.5	"	"	0.825	"	9.1	-0.9
"	"	"	1.8	8.3	6.7	"	"	0.850	"	9.2	-0.2
"	"	0.600	1.0	8.1	5.3	"	"	0.875	"	9.3	0.4
"	"	0.650	"	8.0	4.9	"	"	0.900	"	9.4	1.1
"	"	0.700	"	8.4	4.3	"	"	0.925	"	9.5	1.7
"	"	0.800	"	8.8	3.4	"	"	0.950	"	9.7	2.0

APPENDIX A (Continued)

Rotor Conf	Fuse Conf	$\bar{\Omega}$	T g	f_b Hz	ζ_b	Rotor Conf	Fuse Conf	$\bar{\Omega}$	T g	f_b Hz	ζ_b
R-8	F-1	0.750	0.2	8.9	6.2	R-9	F-1	0.850	1.0	8.9	5.7
"	"	"	0.6	8.7	7.2	"	"	0.900	"	9.7	5.0
"	"	"	1.0	8.7	7.2	"	"	0.950	"	9.7	4.3
"	"	"	1.4	8.7	6.8	R-9	F-2	0.750	0.2	9.2	3.7
"	"	"	1.6	8.7	6.5	"	"	"	0.6	9.2	3.4
"	"	"	1.8	8.6	6.1	"	"	"	1.0	9.0	2.9
"	"	0.600	1.0	7.9	7.0	"	"	"	1.4	8.8	2.3
"	"	0.650	"	8.2	7.2	"	"	"	1.6	8.9	1.5
"	"	0.700	"	8.2	7.3	"	"	"	1.8	8.7	1.2
"	"	0.800	"	8.8	6.7	"	"	0.600	1.0	7.4	2.1
"	"	0.850	"	9.2	5.9	"	"	0.625	"	7.7	0.6
"	"	0.900	"	9.4	5.0	"	"	0.650	"	7.9	0.0
"	"	0.950	"	9.8	4.5	"	"	0.675	"	8.1	0.2
F-8	F-2	0.750	0.2	9.2	3.9	"	"	0.700	"	8.4	0.7
"	"	"	0.6	8.9	3.6	"	"	0.725	"	8.8	1.7
"	"	"	1.0	8.8	3.0	"	"	0.775	"	8.6	1.8
"	"	"	1.4	8.7	2.5	"	"	0.800	"	8.8	1.0
"	"	"	1.6	8.7	1.6	"	"	0.825	"	9.0	0.9
"	"	"	1.8	8.6	1.2	"	"	0.850	"	9.4	1.4
"	"	0.600	1.0	7.4	3.2	"	"	0.875	"	9.5	1.8
"	"	0.625	"	7.6	1.5	"	"	0.900	"	9.7	2.7
"	"	0.650	"	7.8	0.6	"	"	0.925	"	9.9	3.8
"	"	0.675	"	8.2	0.8	"	"	0.950	"	10.4	4.4
"	"	0.700	"	8.4	1.2	R-10	F-2	0.750	0.2		4.0
"	"	0.725	"	8.8	2.0	"	"	"	0.6		3.7
"	"	0.775	"	8.5	1.2	"	"	"	1.0		2.7
"	"	0.800	"	8.9	1.0	"	"	"	1.4		1.9
"	"	0.825	"	9.0	0.9	"	"	"	1.6		1.3
"	"	0.850	"	9.3	1.6	"	"	"	1.8		0.6
"	"	0.875	"	9.6	2.2	"	"	0.600	1.0		1.8
"	"	0.900	"	9.7	2.8	"	"	0.625	"		0.6
"	"	0.925	"	10.0	4.2	"	"	0.650	"		0.0
"	"	0.950	"	10.3	5.7	"	"	0.675	"		0.2
R-9	F-1	0.750	0.2	9.4	5.9	"	"	0.700	"		0.4
"	"	"	0.6	8.9	6.7	"	"	0.725	"		1.5
"	"	"	1.0	8.7	6.9	"	"	0.775	"		1.4
"	"	"	1.4	8.7	6.9	"	"	0.800	"		0.6
"	"	"	1.6	8.7	6.5	"	"	0.825	"		1.0
"	"	"	1.8	8.6	6.2	"	"	0.850	"		0.8
"	"	0.600	1.0	7.9	6.7	"	"	0.875	"		0.9
"	"	0.650	"	8.0	7.1	"	"	0.900	"		1.2
"	"	0.700	"	8.2	7.2	"	"	0.925	"		1.6
"	"	0.800	"	8.8	6.5	"	"	0.950	"		2.1

APPENDIX A (Concluded)

Rotor Conf	Fuse Conf	$\bar{\Omega}$	T g	f_b Hz	ζ_b	Rotor Conf	Fuse Conf	$\bar{\Omega}$	T g	f_b Hz	ζ_b
R-11	F-2	0.750	0.2		3.4	R-12	F-1	0.650	1.0	8.3	5.4
"	"	"	0.6		3.2	"	"	0.700	"	8.6	4.9
"	"	"	1.0		2.7	"	"	0.800	"	8.8	3.7
"	"	"	1.4		2.6	"	"	0.850	"	9.0	3.4
"	"	"	1.6		2.3	"	"	0.900	"	9.2	3.2
"	"	"	1.8		1.8	"	"	0.950	"	9.5	3.0
"	"	0.600	1.0		1.2	R-12	F-2	0.750	0.2	9.0	5.1
"	"	0.625	"		-0.2	"	"	"	0.6	8.8	4.4
"	"	0.650	"		-0.1	"	"	"	1.0	8.7	3.7
"	"	0.675	"		0.2	"	"	"	1.4	8.7	2.9
"	"	0.700	"		0.4	"	"	"	1.6	8.7	2.5
"	"	0.725	"		1.9	"	"	"	1.8	8.7	1.6
"	"	0.775	"		0.8	"	"	0.600	1.0	7.3	4.0
"	"	0.800	"		0.2	"	"	0.625	"	7.6	1.4
"	"	0.825	"		1.2	"	"	0.650	"	8.0	1.1
"	"	0.850	"		1.2	"	"	0.675	"	8.2	0.8
"	"	0.875	"		1.0	"	"	0.700	"	8.4	0.9
"	"	0.900	"		1.2	"	"	0.725	"	8.7	1.4
"	"	0.925	"		2.8	"	"	0.775	"	8.7	2.2
"	"	0.950	"		3.8	"	"	0.800	"	8.7	0.7
R-12	F-1	0.750	0.2	8.9	4.0	"	"	0.825	"	8.8	0.6
"	"	"	0.6	8.6	4.0	"	"	0.850	"	9.3	1.8
"	"	"	1.0	8.6	4.3	"	"	0.875	"	9.5	2.4
"	"	"	1.4	8.6	5.2	"	"	0.900	"	9.7	3.8
"	"	"	1.6	8.5	5.9	"	"	0.925	"	9.9	4.2
"	"	"	1.8	8.5	6.5	"	"	0.950	"	10.2	4.9
"	"	0.600	1.0	8.2	5.9						

APPENDIX B

EXPERIMENTAL INPLANE STABILITY CHARACTERISTICS FOR FORWARD FLIGHT

Rotor Conf	Fuse Conf	V kn	α_s deg	$\bar{\Omega}$	T g	f_b Hz	ζ_b
R-1	F-2	27.7	-3	0.750	0.2	9.2	2.8
"	"	"	"	"	0.6	9.1	2.6
"	"	"	"	"	1.0	8.8	2.2
"	"	"	"	"	1.4	8.7	1.8
"	"	"	"	"	1.6	8.6	1.5
"	"	9.2	-1	"	1.0	8.8	2.7
"	"	18.5	-2	"	"	8.8	2.4
"	"	37.0	-4	"	"	8.7	2.0
"	"	44.4	-5	"	"	8.6	2.4
"	"	27.7	+1	"	"	8.9	2.0
"	"	"	-1	"	"	8.8	2.1
"	"	"	-5	"	"	8.8	2.3
"	"	"	-7	"	"	8.8	2.3
"	"	"	-3	0.600	"	7.5	3.3
"	"	"	"	0.625	"	7.5	2.5
"	"	"	"	0.650	"	7.8	1.7
"	"	"	"	0.675	"	8.1	1.5
"	"	"	"	0.700	"	8.2	1.5
"	"	"	"	0.775	"	8.9	3.2
"	"	"	"	0.800	"	8.9	2.6
"	"	"	"	0.825	"	9.1	0.8
"	"	"	"	0.850	"	9.1	0.6
"	"	"	"	0.875	"	9.2	1.4
"	"	"	"	0.900	"	9.6	1.7
"	"	"	"	0.925	"	9.7	1.9
"	"	"	"	0.950	"	9.8	2.1
"	"	44.4	-5	0.625	"	7.6	3.0
"	"	"	"	0.650	"	7.9	2.1
"	"	"	"	0.675	"	8.2	1.8
"	"	"	"	0.700	"	8.4	1.6
"	"	"	"	0.725	"	8.7	1.7
"	"	"	"	0.775	"	8.7	2.8
"	"	"	"	0.800	"	8.8	1.6
"	"	"	"	0.825	"	9.1	0.9
"	"	"	"	0.850	"	9.2	1.2
"	"	"	"	0.875	"	9.4	2.1
"	"	"	"	0.900	"	9.5	2.5
"	"	"	"	0.925	"	9.7	2.6

APPENDIX B (Continued)

Rotor Conf	Fuse Conf	V kn	α_s deg	$\bar{\Omega}$	T g	f_b Hz	ζ_b
R-1	F-3	27.7	-3	0.750	0.2	9.1	2.9
"	"	"	"	"	0.6	9.0	2.9
"	"	"	"	"	1.0	8.9	2.5
"	"	"	"	"	1.4	8.6	1.9
"	"	"	"	"	1.6	8.7	1.7
"	"	9.2	-1	"	1.0	8.9	3.1
"	"	18.5	-2	"	"	8.9	2.6
"	"	37.0	-4	"	"	8.9	2.4
"	"	44.4	-5	"	"	8.9	3.2
"	"	27.7	-3	0.600	"	7.2	3.6
"	"	"	"	0.625	"	7.7	2.1
"	"	"	"	0.650	"	7.9	1.4
"	"	"	"	0.675	"	8.2	1.2
"	"	"	"	0.700	"	8.4	1.5
"	"	"	"	0.725	"	8.7	1.8
"	"	"	"	0.775	"	8.5	1.3
"	"	"	"	0.800	"	8.8	0.3
"	"	"	"	0.825	"	9.0	0.3
"	"	"	"	0.850	"	9.2	0.6
"	"	"	"	0.875	"	9.6	1.8
"	"	"	"	0.900	"	10.2	2.7
"	"	"	"	0.925	"	9.9	3.4
"	"	"	"	0.950	"	9.8	3.3
R-1	F-4	"	"	0.750	0.2	9.2	3.7
"	"	"	"	"	0.6	9.1	3.5
"	"	"	"	"	1.0	8.8	3.3
"	"	"	"	"	1.4	8.7	3.2
"	"	"	"	"	1.6	8.7	3.1
"	"	9.2	-1	"	1.0	8.9	4.2
"	"	18.5	-2	"	"	8.9	3.8
"	"	37.0	-4	"	"	8.9	3.1
"	"	44.4	-5	"	"	8.7	3.4
"	"	27.7	-3	0.600	"	7.4	3.9
"	"	"	"	0.625	"	7.7	3.3
"	"	"	"	0.650	"	8.0	1.9
"	"	"	"	0.675	"	8.2	1.9
"	"	"	"	0.700	"	8.5	2.1
"	"	"	"	0.725	"	8.7	2.5
"	"	"	"	0.775	"	8.6	4.7
"	"	"	"	0.800	"	8.8	1.8
"	"	"	"	0.825	"	9.0	1.1
"	"	"	"	0.850	"	9.3	0.9
"	"	"	"	0.875	"	9.6	1.2

APPENDIX B (Continued)

Rotor Conf	Fuse Conf	V kn	α_s deg	$\bar{\Omega}$	T g	f_b Hz	ζ_b
R-1	F-4	27.7	-3	0.900	1.0	9.9	2.6
"	"	"	"	0.925	"	10.0	3.5
"	"	"	"	0.950	"	9.9	3.8
R-1	F-5	"	"	0.750	0.2	9.3	4.2
"	"	"	"	"	0.6	8.9	3.3
"	"	"	"	"	1.0	8.4	1.8
"	"	"	"	"	1.4	8.2	0.4
"	"	"	"	"	1.6	8.2	-1.3
"	"	9.2	-1	"	1.0	8.3	-0.3
"	"	18.5	-2	"	"	8.4	0.7
"	"	37.0	-4	"	"	8.6	2.1
"	"	44.4	-5	"	"	8.5	0.3
"	"	27.7	-3	0.600	"	7.3	3.3
"	"	"	"	0.625	"	7.6	2.0
"	"	"	"	0.650	"	8.0	1.5
"	"	"	"	0.675	"	8.4	2.1
"	"	"	"	0.700	"	8.8	4.3
"	"	"	"	0.725	"	9.0	6.2
"	"	"	"	0.775	"	8.6	0.3
"	"	"	"	0.800	"	8.8	-0.5
"	"	"	"	0.825	"	9.0	-0.8
"	"	"	"	0.875	"	9.4	0.1
"	"	"	"	0.900	"	9.5	0.6
"	"	"	"	0.925	"	9.7	1.2
"	"	"	"	0.950	"	9.8	2.1
R-2	F-2	"	"	0.750	0.2	9.3	3.1
"	"	"	"	"	0.6	9.0	2.6
"	"	"	"	"	1.0	8.9	2.1
"	"	"	"	"	1.4	8.6	1.6
"	"	"	"	"	1.6	8.5	1.2
"	"	9.2	-1	"	1.0	8.9	3.2
"	"	18.5	-2	"	"	8.9	2.5
"	"	37.0	-4	"	"	8.5	2.1
"	"	44.4	-5	"	"	8.7	2.4
"	"	27.7	-3	0.600	"	7.3	3.4
"	"	"	"	0.625	"	7.7	2.5
"	"	"	"	0.650	"	7.9	1.6
"	"	"	"	0.675	"	8.2	1.5
"	"	"	"	0.725	"	8.6	1.8
"	"	"	"	0.775	"	8.9	2.6
"	"	"	"	0.800	"	9.0	1.9
"	"	"	"	0.825	"	9.1	1.2
"	"	"	"	0.850	"	9.3	0.9

APPENDIX B (Continued)

Rotor Conf	Fuse Conf	V kn	α_s deg	$\bar{\Omega}$	T g	f_b Hz	ζ_b
R-2	F-2	27.7	-3	0.875	1.0	9.4	1.4
"	"	"	"	0.900	"	9.6	1.8
"	"	"	"	0.925	"	9.8	1.9
"	"	"	"	0.950	"	10.0	2.1
R-2	F-5	"	"	0.750	0.2	9.2	4.8
"	"	"	"	"	0.6	8.7	2.8
"	"	"	"	"	1.0	8.4	0.8
"	"	"	"	"	1.4	8.3	-0.5
"	"	"	"	"	1.6	8.1	-1.7
"	"	9.2	-1	"	1.0	8.4	0.3
"	"	18.5	-2	"	"	8.4	0.9
"	"	37.0	-4	"	"	8.4	0.5
"	"	44.4	-5	"	"	8.4	0.2
"	"	27.7	-3	0.625	"	7.6	2.4
"	"	"	"	0.650	"	7.8	1.6
"	"	"	"	0.675	"	8.4	1.9
"	"	"	"	0.700	"	8.7	5.4
"	"	"	"	0.725	"	8.5	4.0
"	"	"	"	0.775	"	8.6	-0.3
"	"	"	"	0.800	"	8.8	-0.5
"	"	"	"	0.825	"	9.1	-0.5
"	"	"	"	0.850	"	9.1	0.2
"	"	"	"	0.875	"	9.4	1.0
"	"	"	"	0.900	"	9.7	1.4
"	"	"	"	0.925	"	9.8	1.4
"	"	"	"	0.950	"	9.9	1.7
R-4	F-2	"	"	0.750	0.2	9.2	2.9
"	"	"	"	"	0.6	9.2	2.5
"	"	"	"	"	1.0	9.0	1.9
"	"	"	"	"	1.4	8.7	0.9
"	"	"	"	"	1.6	8.6	0.4
"	"	9.2	-1	"	1.0	8.9	2.2
"	"	18.5	-2	"	"	8.9	1.9
"	"	37.0	-4	"	"	8.8	1.7
"	"	44.4	-5	"	"	8.8	1.9
"	"	27.7	-3	0.600	"	7.4	2.8
"	"	"	"	0.625	"	7.6	2.0
"	"	"	"	0.650	"	8.0	1.4
"	"	"	"	0.675	"	8.2	1.4
"	"	"	"	0.700	"	8.4	1.2
"	"	"	"	0.725	"	8.6	1.4
"	"	"	"	0.775	"	9.1	2.0
"	"	"	"	0.800	"	9.3	1.7

APPENDIX B (Continued)

Roter Conf	Fuse Conf	V kn	α_s deg	$\bar{\Omega}$	T g	f_b Hz	ζ_b
R-4	F-2	27.7	-3	0.825	1.0	9.2	1.0
"	"	"	"	0.850	"	9.4	0.8
"	"	"	"	0.875	"	9.4	0.8
"	"	"	"	0.900	"	9.7	1.1
"	"	"	"	0.925	"	9.9	1.2
"	"	"	"	0.950	"	10.1	1.2
R-4	F-5	"	"	0.750	0.2	9.4	3.5
"	"	"	"	"	0.6	9.2	2.9
"	"	"	"	"	1.0	8.7	2.3
"	"	"	"	"	1.4	8.5	0.5
"	"	"	"	"	1.6	8.3	-1.2
"	"	9.2	-1	"	1.0	8.5	1.9
"	"	18.5	-2	"	"	8.7	2.2
"	"	37.0	-4	"	"	8.6	2.4
"	"	44.4	-5	"	"	8.5	1.8
"	"	27.7	-3	0.600	"	7.3	3.9
"	"	"	"	0.625	"	7.7	1.7
"	"	"	"	0.650	"	7.9	1.0
"	"	"	"	0.675	"	8.4	1.7
"	"	"	"	0.700	"	8.8	3.6
"	"	"	"	0.725	"	8.7	4.8
"	"	"	"	0.775	"	8.7	0.4
"	"	"	"	0.800	"	8.9	-0.5
"	"	"	"	0.825	"	9.1	-0.5
"	"	"	"	0.850	"	9.3	-0.2
"	"	"	"	0.875	"	9.5	0.1
"	"	"	"	0.900	"	9.8	0.5
"	"	"	"	0.925	"	9.9	1.1
"	"	"	"	0.950	"	10.1	1.2
R-5	F-2	"	"	0.750	0.2	9.2	1.5
"	"	"	"	"	0.6	9.1	1.0
"	"	"	"	"	1.0	9.0	0.6
"	"	"	"	"	1.4	8.9	-0.1
"	"	"	"	"	1.6	8.8	-0.6
"	"	9.2	-1	"	1.0	9.0	0.5
"	"	18.5	-2	"	"	9.0	0.6
"	"	37.0	-4	"	"	8.9	0.6
"	"	44.4	-5	"	"	9.0	0.7
"	"	27.7	-3	0.600	"	7.9	6.6
"	"	"	"	0.625	"	8.0	4.3
"	"	"	"	0.650	"	8.2	2.6
"	"	"	"	0.675	"	8.4	1.1
"	"	"	"	0.700	"	8.6	0.6

APPENDIX B (Continued)

Rotor Conf	Fuse Conf	V kn	α_s deg	$\bar{\Omega}$	T g	f_b Hz	ζ_b
R-5	F-2	27.7	-3	0.725	1.0	8.8	0.5
"	"	"	"	0.775	"	9.1	0.7
"	"	"	"	0.800	"	9.2	1.0
"	"	"	"	0.825	"	9.1	-0.3
"	"	"	"	0.850	"	9.3	-0.1
"	"	"	"	0.875	"	9.4	0.2
"	"	"	"	0.900	"	9.7	0.6
"	"	"	"	0.925	"	9.9	1.1
"	"	"	"	0.950	"	10.0	1.1
R-6	F-2	"	"	0.750	0.2	9.1	2.3
"	"	"	"	"	0.6	8.9	2.2
"	"	"	"	"	1.0	8.8	1.6
"	"	"	"	"	1.4	8.6	1.0
"	"	"	"	"	1.6	8.6	0.6
"	"	9.2	-1	"	1.0	8.8	1.7
"	"	18.5	-2	"	"	8.8	1.6
"	"	37.0	-4	"	"	8.7	1.7
"	"	44.4	-5	"	"	8.7	1.7
"	"	27.7	-3	0.600	"	7.6	4.6
"	"	"	"	0.625	"	7.8	2.6
"	"	"	"	0.650	"	8.0	1.9
"	"	"	"	0.675	"	8.1	1.1
"	"	"	"	0.700	"	8.4	1.1
"	"	"	"	0.725	"	8.6	1.3
"	"	"	"	0.775	"	8.8	2.1
"	"	"	"	0.800	"	8.8	1.0
"	"	"	"	0.825	"	9.0	0.1
"	"	"	"	0.850	"	9.2	0.4
"	"	"	"	0.875	"	9.3	0.9
"	"	"	"	0.900	"	9.5	1.2
"	"	"	"	0.925	"	9.6	1.3
"	"	"	"	0.950	"	9.7	1.0
R-7	F-2	"	"	0.750	0.2	9.2	3.1
"	"	"	"	"	0.6	8.9	2.4
"	"	"	"	"	1.0	8.9	1.7
"	"	"	"	"	1.4	8.7	1.0
"	"	"	"	"	1.6	8.6	0.7
"	"	9.2	-1	"	1.0	8.7	2.1
"	"	18.5	-2	"	"	8.8	2.0
"	"	37.0	-4	"	"	8.7	1.5
"	"	44.4	-5	"	"	8.7	1.9
"	"	27.7	-3	0.600	"	7.4	4.9
"	"	"	"	0.625	"	7.7	2.6

APPENDIX B (Continued)

Rotor Conf	Fuse Conf	V kn	α_s deg	$\bar{\Omega}$	T g	f_b Hz	ζ_b
R-7	F-2	27.7	-3	0.650	1.0	8.0	1.3
"	"	"	"	0.675	"	8.2	0.9
"	"	"	"	0.700	"	8.4	1.0
"	"	"	"	0.725	"	8.6	1.1
"	"	"	"	0.775	"	8.9	1.8
"	"	"	"	0.800	"	9.0	1.7
"	"	"	"	0.825	"	9.0	0.9
"	"	"	"	0.850	"	9.0	0.7
"	"	"	"	0.875	"	9.3	0.9
"	"	"	"	0.900	"	9.5	1.2
"	"	"	"	0.925	"	9.6	1.2
"	"	"	"	0.950	"	9.8	1.3
R-7	F-5	"	"	0.750	0.2	8.7	3.5
"	"	"	"	"	0.6	8.6	2.5
"	"	"	"	"	1.0	8.4	1.4
"	"	"	"	"	1.4	8.2	-0.8
"	"	"	"	"	1.6	8.2	-1.4
"	"	9.2	-1	"	1.0	8.2	-0.9
"	"	18.5	-2	"	"	8.4	0.3
"	"	37.0	-4	"	"	8.5	1.6
"	"	44.4	-5	"	"	8.4	0.8
"	"	27.7	-3	0.600	"	7.4	4.3
"	"	"	"	0.625	"	7.6	2.4
"	"	"	"	0.650	"	8.0	0.8
"	"	"	"	0.675	"	8.3	2.5
"	"	"	"	0.700	"	8.8	4.7
"	"	"	"	0.725	"	8.6	5.8
"	"	"	"	0.775	"	8.5	-0.7
"	"	"	"	0.800	"	8.7	-0.7
"	"	"	"	0.825	"	8.9	-0.4
"	"	"	"	0.850	"	9.1	0.0
"	"	"	"	0.875	"	9.2	0.3
"	"	"	"	0.900	"	9.4	0.5
"	"	"	"	0.925	"	9.6	0.8
"	"	"	"	0.950	"	9.8	0.8
R-8	F-2	"	"	0.750	0.2	9.4	3.7
"	"	"	"	"	0.6	9.1	2.6
"	"	"	"	"	1.0	9.0	2.0
"	"	"	"	"	1.4	8.7	1.4
"	"	"	"	"	1.6	8.6	1.1
"	"	9.2	-1	"	1.0	8.9	2.6
"	"	18.5	-2	"	"	8.8	2.2
"	"	37.0	-4	"	"	8.8	2.2
"	"	44.4	-5	"	"	8.7	2.2

APPENDIX B (Continued)

Rotor Conf	Fuse Conf	V kn	α_s deg	$\bar{\Omega}$	T g	f_b Hz	ζ_b
R-8	F-2	27.7	-3	0.600	1.0	7.5	2.9
"	"	"	"	0.625	"	7.7	2.0
"	"	"	"	0.650	"	7.9	1.7
"	"	"	"	0.675	"	8.2	1.5
"	"	"	"	0.700	"	8.5	1.5
"	"	"	"	0.725	"	8.7	1.7
"	"	"	"	0.775	"	9.1	2.6
"	"	"	"	0.800	"	9.4	1.9
"	"	"	"	0.825	"	9.0	1.3
"	"	"	"	0.850	"	9.3	1.2
"	"	"	"	0.875	"	9.5	1.2
"	"	"	"	0.900	"	9.7	2.3
"	"	"	"	0.925	"	9.8	2.6
"	"	"	"	0.950	"	9.8	3.0
R-8	F-5	"	"	0.750	0.2	9.1	4.1
"	"	"	"	"	0.6	8.7	2.8
"	"	"	"	"	1.0	8.6	2.1
"	"	"	"	"	1.4	8.3	0.1
"	"	"	"	"	1.6	8.2	-0.5
"	"	9.2	-1	"	1.0	8.4	1.1
"	"	18.5	-2	"	"	8.5	1.8
"	"	37.0	-4	"	"	8.5	1.7
"	"	44.4	-5	"	"	8.6	1.4
"	"	27.7	-3	0.600	"	7.3	2.7
"	"	"	"	0.625	"	7.6	2.2
"	"	"	"	0.650	"	8.0	1.9
"	"	"	"	0.675	"	8.3	2.3
"	"	"	"	0.700	"	8.7	4.5
"	"	"	"	0.725	"	8.5	4.9
"	"	"	"	0.775	"	8.6	0.1
"	"	"	"	0.800	"	8.8	-0.3
"	"	"	"	0.825	"	9.0	0.4
"	"	"	"	0.850	"	9.2	0.7
"	"	"	"	0.875	"	9.5	1.0
"	"	"	"	0.900	"	9.7	1.4
"	"	"	"	0.925	"	9.8	1.7
"	"	"	"	0.950	"	10.0	2.3
R-9	F-2	"	"	0.750	0.2	9.1	3.7
"	"	"	"	"	0.6	9.1	3.0
"	"	"	"	"	1.0	8.9	2.4
"	"	"	"	"	1.4	8.7	2.0
"	"	"	"	"	1.6	8.6	1.8
"	"	9.2	-1	"	1.0	8.9	3.5

APPENDIX B (Concluded)

Rotor Conf	Fuse Conf	V kn	α_s deg	$\bar{\Omega}$	T g	f_b Hz	ζ_b
R-9	F-2	18.5	-2	0.750	1.0	8.9	2.7
"	"	37.0	-4	"	"	8.8	2.9
"	"	44.4	-5	"	"	8.8	3.5
"	"	27.7	-3	0.600	"	7.4	1.9
"	"	"	"	0.625	"	7.6	1.2
"	"	"	"	0.650	"	8.0	1.0
"	"	"	"	0.675	"	8.2	1.1
"	"	"	"	0.700	"	8.5	1.2
"	"	"	"	0.725	"	8.7	1.8
"	"	"	"	0.775	"	9.0	2.9
"	"	"	"	0.800	"	8.9	2.1
"	"	"	"	0.825	"	9.1	1.4
"	"	"	"	0.850	"	9.2	1.2
"	"	"	"	0.875	"	9.5	1.5
"	"	"	"	0.900	"	9.8	1.9
"	"	"	"	0.925	"	9.9	3.3
"	"	"	"	0.950	"	10.1	3.5
R-12	F-2	"	"	0.750	0.2	9.4	2.3
"	"	"	"	"	0.6	9.2	2.2
"	"	"	"	"	1.0	8.9	1.8
"	"	"	"	"	1.4	8.7	1.3
"	"	"	"	"	1.6	8.6	1.1
"	"	9.2	-1	"	1.0	8.9	2.2
"	"	18.5	-2	"	"	8.9	1.9
"	"	37.0	-4	"	"	8.7	1.8
"	"	44.4	-5	"	"	8.7	2.1
"	"	27.7	-3	0.600	"	7.4	3.4
"	"	"	"	0.625	"	7.7	2.7
"	"	"	"	0.650	"	8.0	1.9
"	"	"	"	0.675	"	8.2	1.5
"	"	"	"	0.700	"	8.5	1.5
"	"	"	"	0.725	"	8.7	1.4
"	"	"	"	0.775	"	9.0	2.5
"	"	"	"	0.800	"	9.0	1.7
"	"	"	"	0.825	"	9.0	0.9
"	"	"	"	0.850	"	9.3	0.7
"	"	"	"	0.875	"	9.5	0.7
"	"	"	"	0.900	"	9.6	1.5
"	"	"	"	0.925	"	9.8	1.9
"	"	"	"	0.950	"	9.9	1.9

REFERENCES

1. Weller, William H.: Correlating Measured and Predicted Inplane Stability Characteristics for an Advanced Bearingless Rotor. NASA CR-166280, January 1982.

2. Kelly, Louis G.: Handbook of Numerical Methods and Applications. Addison-Wesley Publishing Co., Inc., c. 1967.

3. Sadler, S. G.; and Ellis, D. B.: Documentation of Myklestad Analysis (DNAM06). Bell Helicopter Textron Report Number 299-099-608, August 1979.

4. Viswanathan, Sathy P.: Ground and Air Resonance Analyses of Multibladed Rotors. Bell Helicopter Textron Report Number 599-270-900, October 1975.

5. Hodges, D. H.; and Dowell, E. H.: Nonlinear Equations of Motion for the Elastic Bending and Torsion of Twisted Nonuniform Rotor Blades. NASA TN D-7818, December 1974.

6. Van Gaasbeek, James R.: Rotorcraft Flight Simulation Computer Program C81 with Datamap Interface. Volume I - User's Manual. USAAVARDCOM-TR-80-D-38A, U.S. Army, December 1979.

7. Huber, H. B.: Effect of Torsion-Flap-Lag Coupling on Hingeless Rotor Stability. Preprint No. 731, American Helicopter Society, May 1973.

8. Chou, Pei Chi: Pitch-Lag Instability of Helicopter Rotors. Journal of the American Helicopter Society, Vol. 3, No. 3, July 1958, pages 30-39.

9. Burkam, John E.; and Miao, Wen-Liu: Exploration of Aeroelastic Stability Boundaries with a Soft-in-Plane Hingeless-Rotor Model. Preprint No. 610, American Helicopter Society, May 1972.

10. Hodges, Dewey H.: An Aeromechanical Stability Analysis for Bearingless Rotor Helicopters. Journal of the American Helicopter Society, January 1979.

TABLE I. ROTOR MODEL DISTRIBUTED STRUCTURAL PROPERTIES

Outboard Station of Segment, m	Mass, kg/m	Structural Stiffness, N-m^2			Chordwise Radius of Gyration, m
		Beamwise	Chordwise	Torsion	
0.030	0.536	286.98	717.4	860.94	0.0102
0.046	0.129	1.49	189.4	0.72	0.0083
0.061	0.129	1.49	189.4	0.72	0.0083
0.076	0.129	1.49	189.4	0.72	0.0037
0.090	0.113	1.43	130.9	0.57	0.0033
0.104	0.093	3.44	62.3	0.29	0.0029
0.140	0.077	4.88	35.3	0.14	0.0024
0.180	0.068	4.59	28.4	0.11	0.0021
0.218	0.068	4.59	28.4	0.11	0.0021
0.269	2.143	860.94	2295.9	860.94	0.0058
0.292	1.250	86.09	2295.9	250.00	0.0189
0.333	0.607	12.34	1607.1	143.49	0.0271
0.427	0.518	11.19	430.5	14.35	0.0131
0.526	0.339	7.17	215.2	5.74	0.0145
0.602	0.339	7.17	215.2	5.74	0.0145
0.678	0.339	7.17	215.2	5.74	0.0145
0.754	0.339	7.17	215.2	5.74	0.0145
0.831	0.339	7.17	215.2	5.74	0.0145
0.907	0.339	7.17	215.2	5.74	0.0145
0.983	0.339	7.17	215.2	5.74	0.0145
1.059	0.339	7.17	215.2	5.74	0.0145
1.135	0.339	7.17	215.2	5.74	0.0145
1.212	0.446	10.04	215.2	5.74	0.0147

TABLE II. ROTOR BLADE DISCRETE PROPERTIES

Number of blades	4
Radius	1.212 m
Lock number	4.7
Solidity	.0734
Airfoil	NACA 0012
Blade chord	.0699 m
Blade twist	0 deg
Nominal rotor speed	78.54 rad/s
Nominal control system stiffness	70.6 N-m/rad
Precone angle	2.75 deg
Radius of built-in precone	.0305 m
Radius of applied blade coning and sweep	.2692 m
Cuff weight	.135 kg
Cuff beamwise bending stiffness	373 $N-m^2$
Cuff inplane bending stiffness	1062 $N-m^2$
Cuff torsional stiffness	201 $N-m^2$
Shear restraint radial station	.0610 m
Nominal shear restraint inplane stiffness	17513 N/m
Flat pitch inplane damper nose-down inclination	11 deg

TABLE III. MODEL SCALE FACTORS

Item	Units	Scale Factor (a)
Length	m	5.0
Weight	N	125.0
Structural stiffness	$N\text{-}m^2$	3125.0
Angular velocity	rad/s	0.447
Linear velocity	m/s	2.236
Force	N	125.0
Moment	N-m	625.0
Power	N-m/s	279.5
Froude number		1.0
Rotor Lock number		1.0
Structural frequency ratio		1.0

[a]Ratio of full scale to model.

TABLE IV. ROTOR CONFIGURATION PARAMETRIC VALUES

Conf	β_b deg	γ_b deg	tan ϕ	$\bar{K}_{\zeta_i}$ i=1	2	3	4	x_{PL} cm	r_{PL} cm	$\bar{K}_c$
R-1	0	0	0.600	1	1	1	1	-3.56	3.56	1.0
R-2	3	0	0.600	1	1	1	1	-3.56	3.56	1.0
R-3	(not used)									
R-4	0	4	0.600	1	1	1	1	-3.56	3.56	1.0
R-5	0	0	0.246	2	2	2	2	-3.56	3.56	1.0
R-6	0	0	0.467	1	1	1	1	-3.56	3.56	1.0
R-7	0	0	0.600	1	1	1	1	-3.56	4.95	1.0
R-8	0	0	0.600	1	1	1	1	3.56	4.95	1.0
R-9	0	0	0.600	1	1	1	1	3.56	3.56	1.0
R-10	0	0	-	1	2	2	1	-3.56	3.56	1.0
R-11	0	0	-	1	2	1	2	-3.56	3.56	1.0
R-12	0	0	0.600	1	1	1	1	-3.56	3.56	1.8

TABLE V. ROTOR-OFF FUSELAGE PARAMETRIC VALUES FOR CONFIGURATION F-2

Item	Value
Mass moment of inertia in pitch about the c.g.	3.390 $kg \cdot m^2$
Mass moment of inertia in roll about the c.g.	.542 $kg \cdot m^2$
Undamped natural frequency in pitch	4.9 Hz
Undamped natural frequency in roll	2.8 Hz
Height of rotor above gimbal	.339 m
Height of c.g. above gimbal	.018 m
Fuselage weight	386 N
Damping ratio in pitch	.06
Damping ratio in roll	.06

TABLE VI. PARAMETRIC CHANGES FROM F-2 VALUES FOR EACH FUSELAGE CONFIGURATION

Fuse Conf	Item	Value
F-3	Damping ratio in pitch	.03
	Damping ratio in roll	.03
F-4	Inertia in pitch about the c.g.	4.381 $kg \cdot m^2$
	Inertia in roll about the c.g.	.989 $kg \cdot m^2$
	Fuselage weight	600 N
	Height of c.g. above gimbal	.009 m
F-5	Natural frequency in pitch	2.8 Hz
	Natural frequency in roll	4.9 Hz

Figure 1. M680 Bearingless Main Rotor on the M222 Helicopter.

Figure 2. Bearingless Rotor Model Hardware.

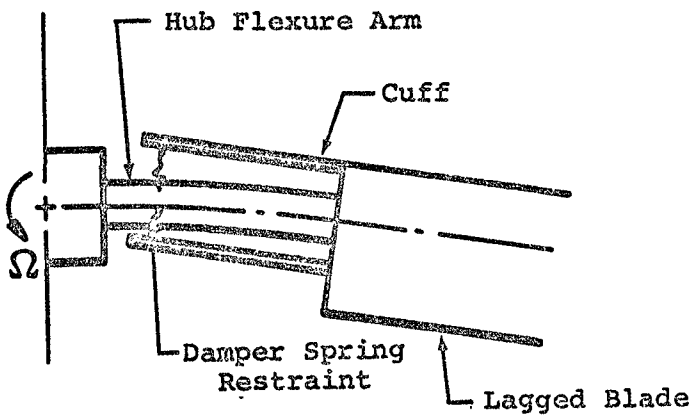

Cuff Inplane Restraint Schematic

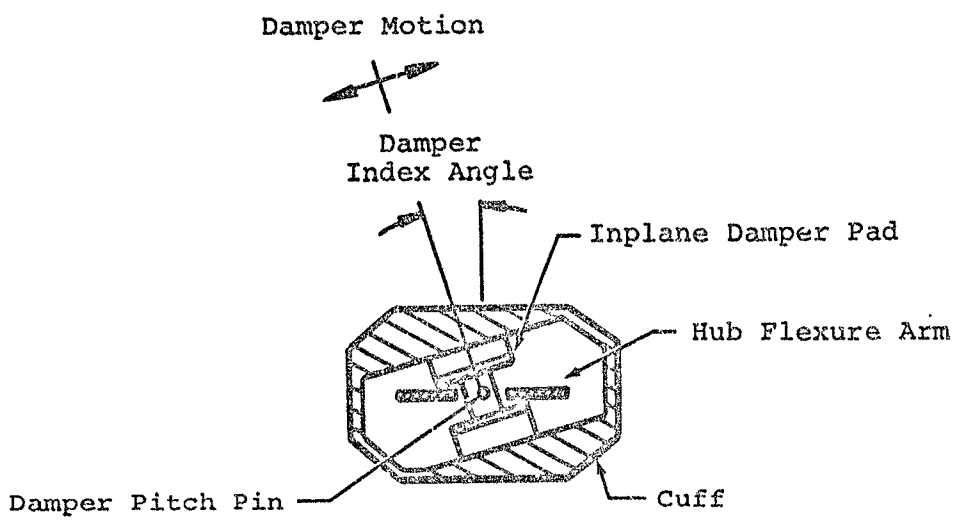

Cross Section of Damper Mechanism

Figure 3. Illustration of Model Shear Restraint Mechanism.

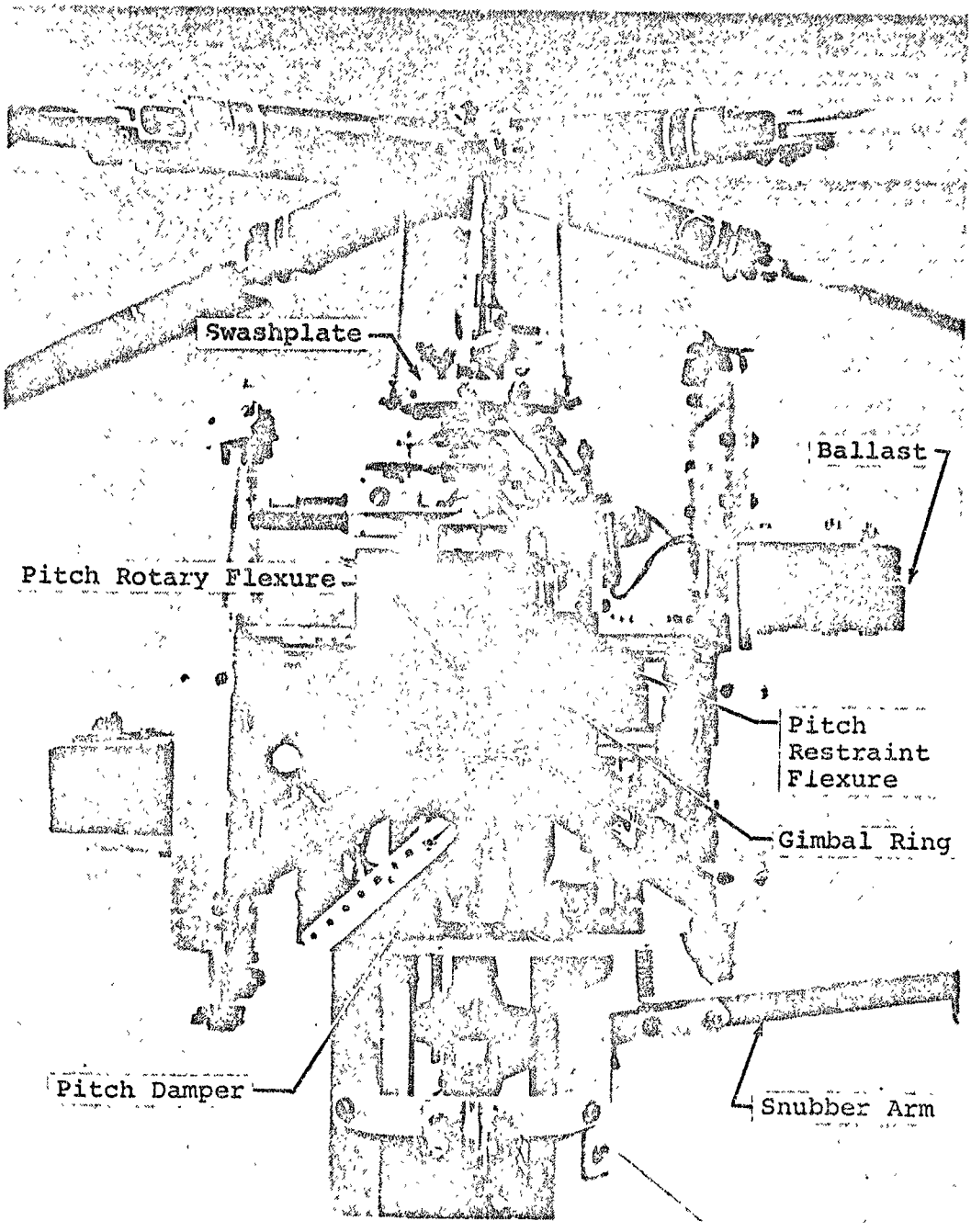

Figure 4. Fuselage Model Detailed Features.

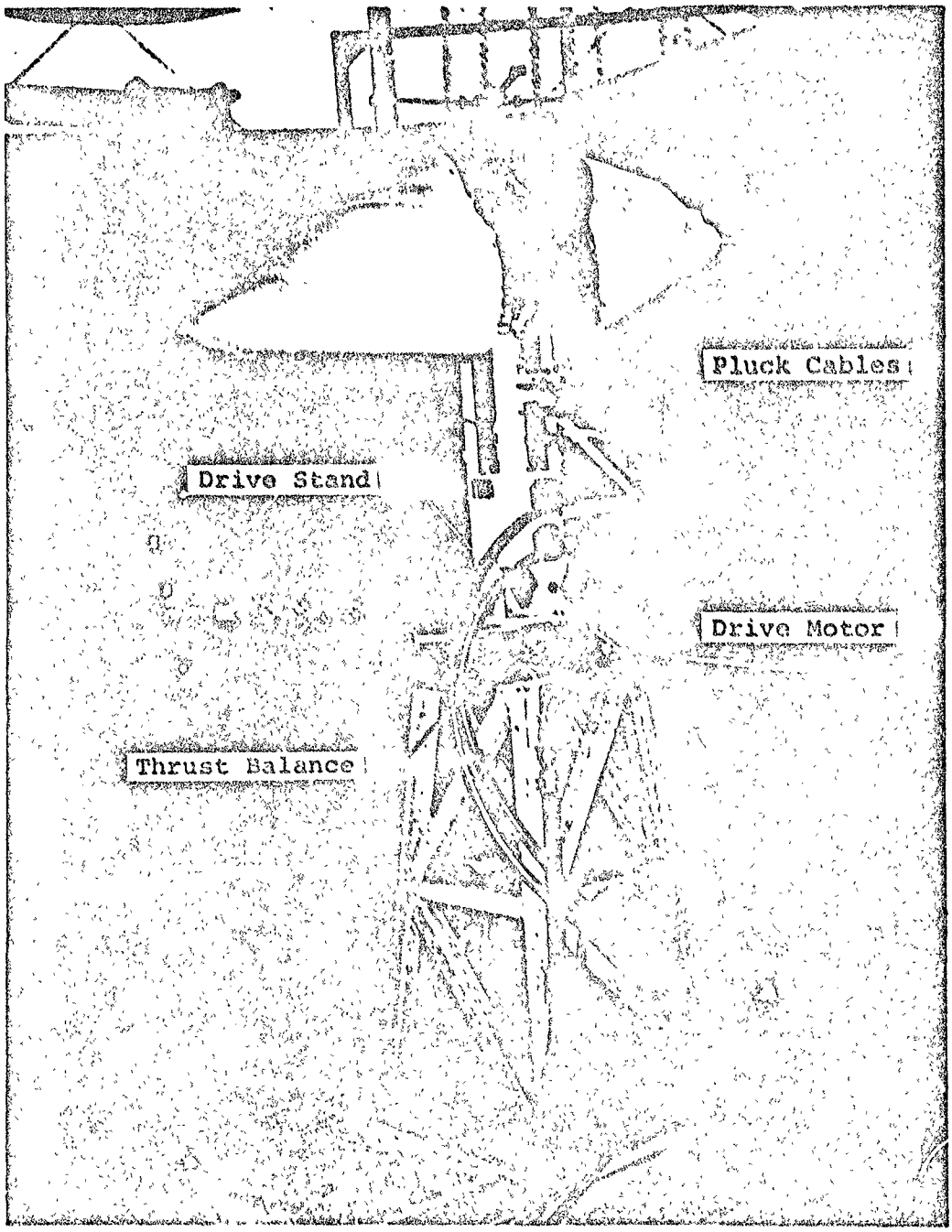

Figure 5. Model Hover Test Installation.

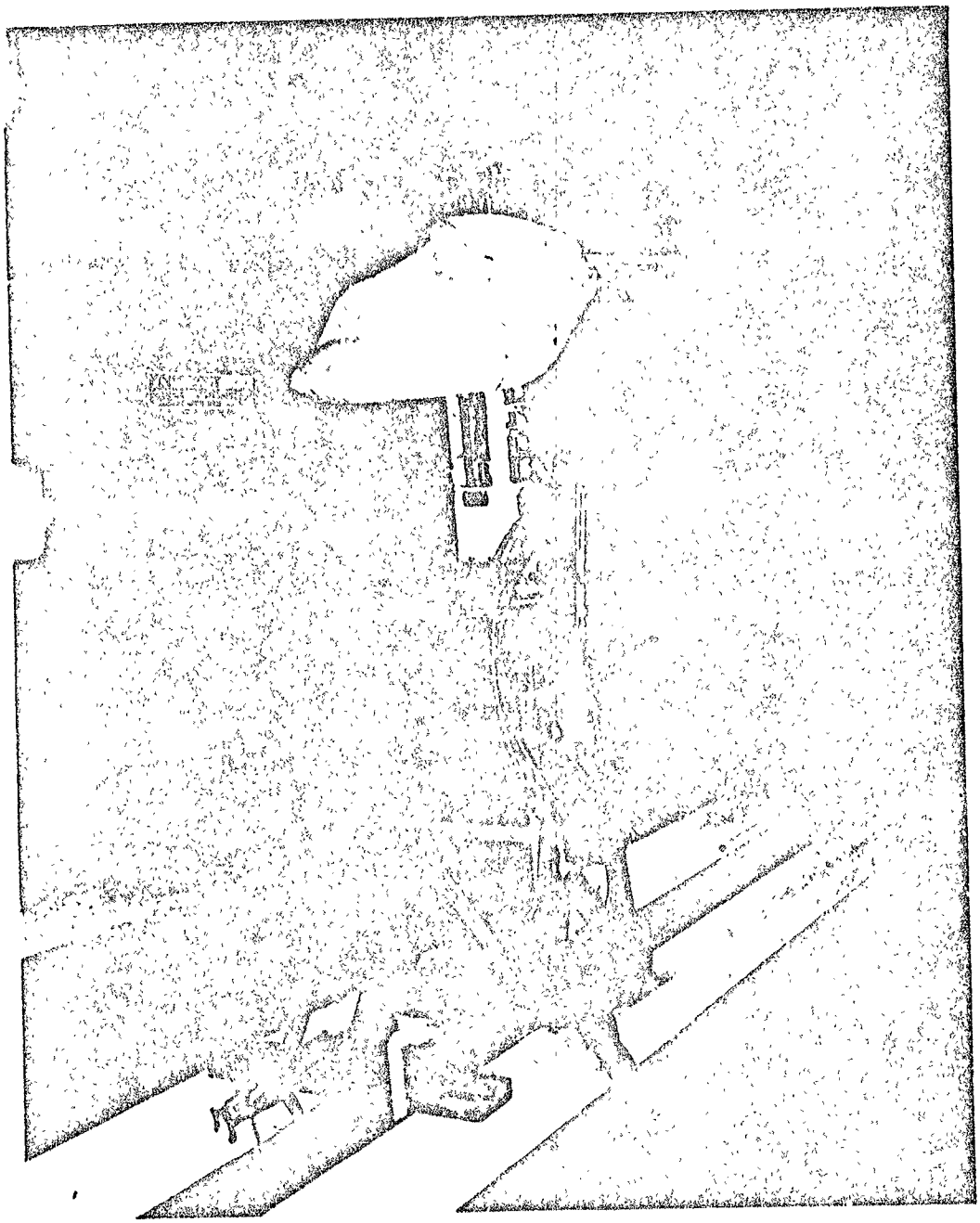

Figure 6. Model Wind Tunnel Installation.

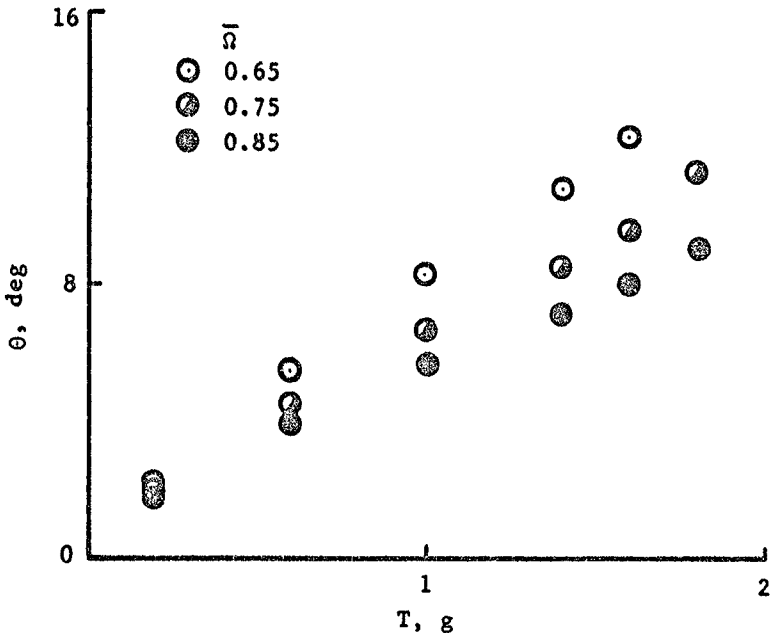

(a) Thrust Variation

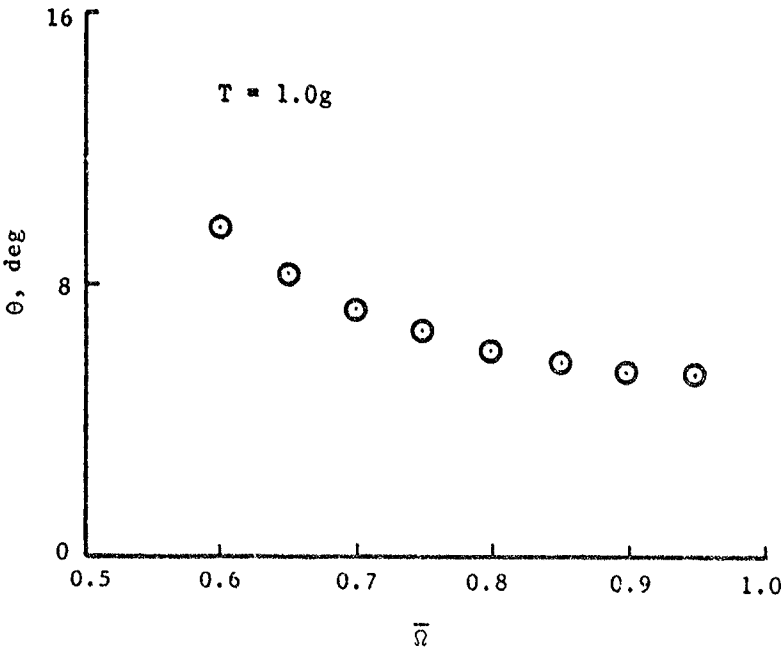

(b) Rotor Speed Variation

Figure 7. Hover Aerodynamic Performance for R-1.

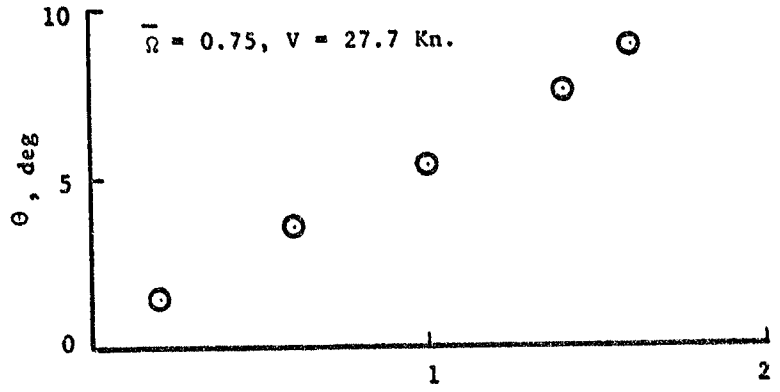

(a) Thrust Variation

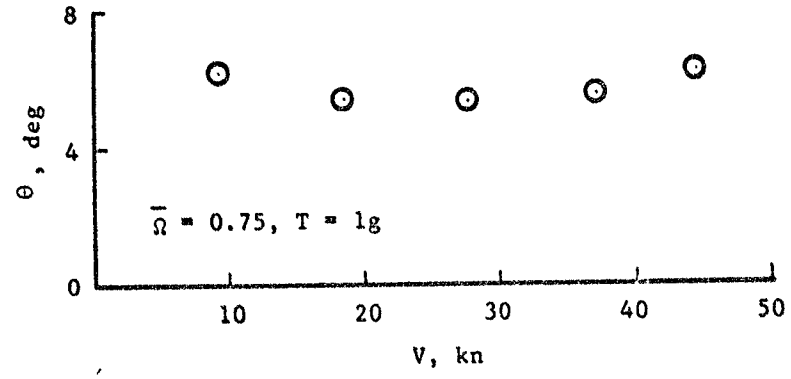

(b) Flight Speed Variation

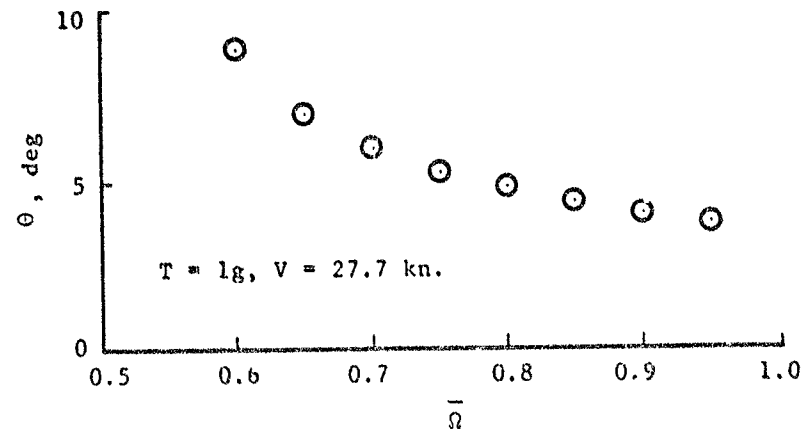

(c) Rotor Speed Variation

Figure 8. Forward Flight Aerodynamic Performance for R-1.

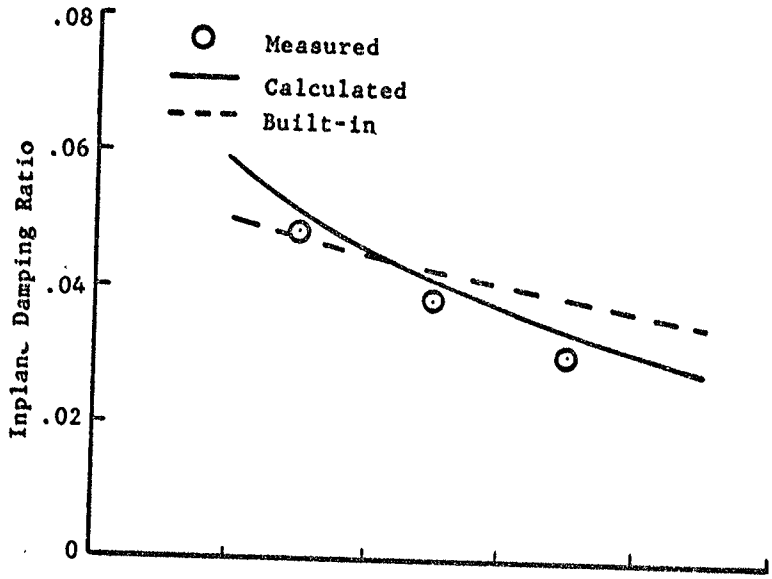

(a) Damping Correlation

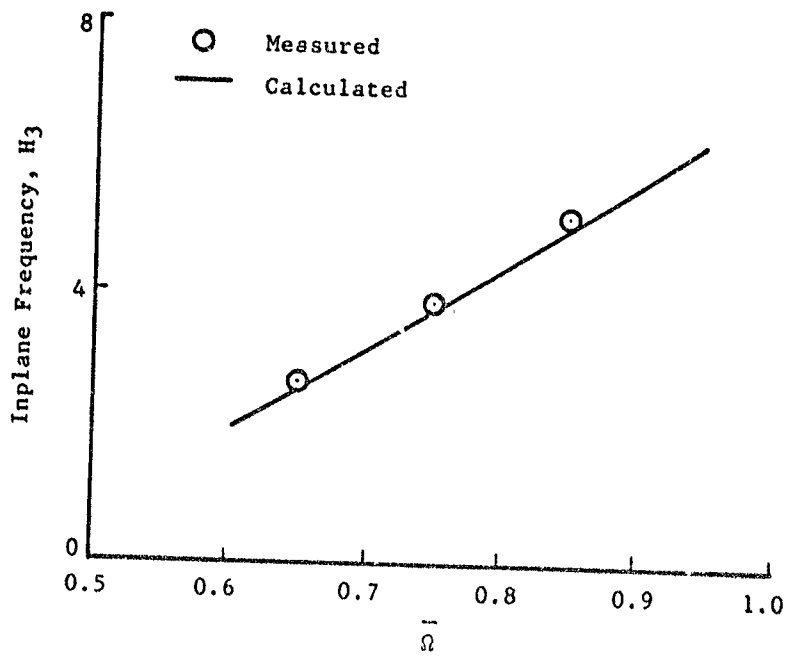

(b) Frequency Correlation

Figure 9. Inplane Damping and Frequency Correlation for Isolated Rotor (R-1) in Hover ($T \approx 1g$).

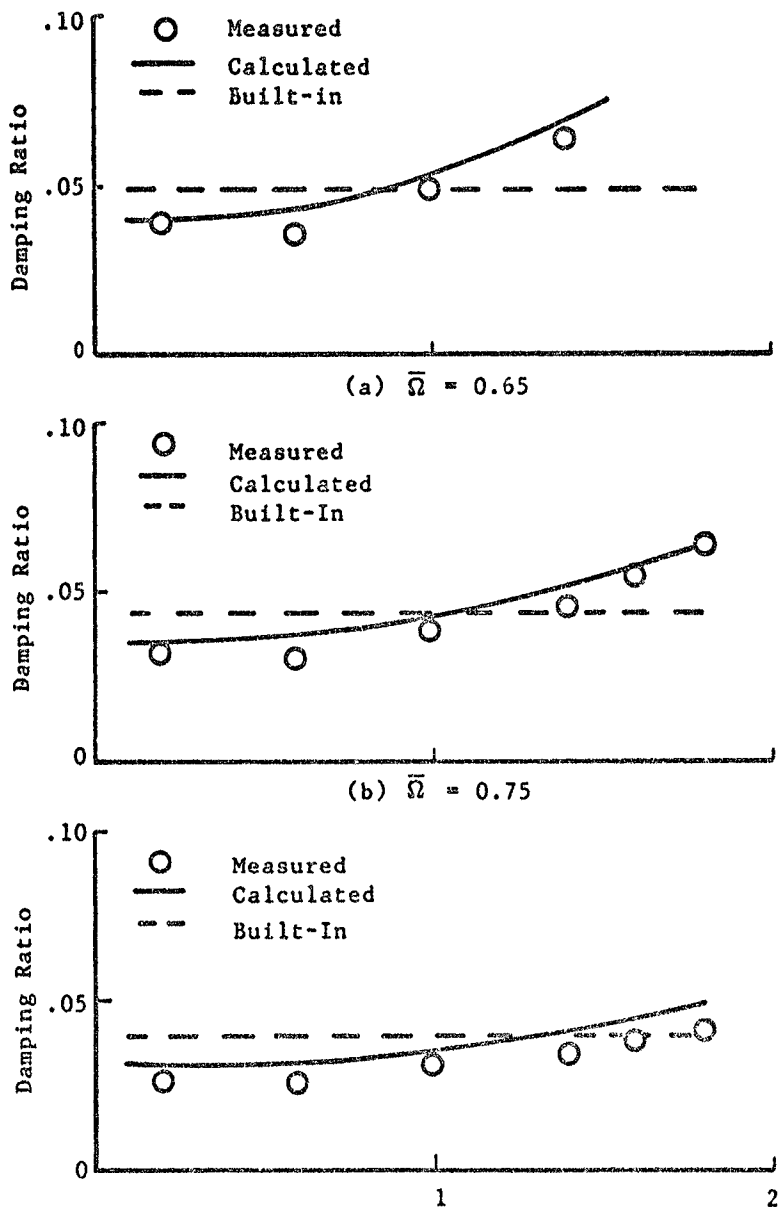

Figure 10. Inplane Damping Variation With Thrust for Isolated Rotor (R-1) in Hover.

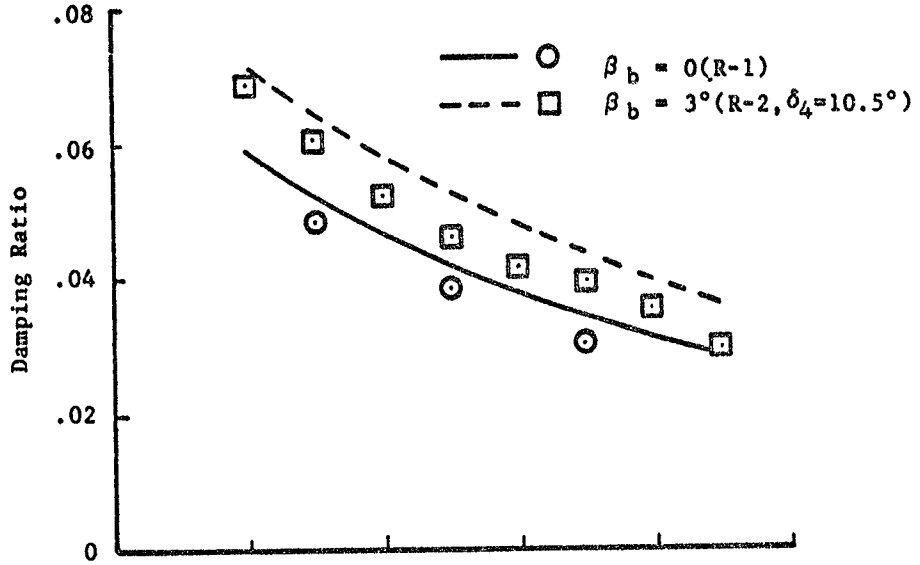

(a) Blade Cone Angle Effect

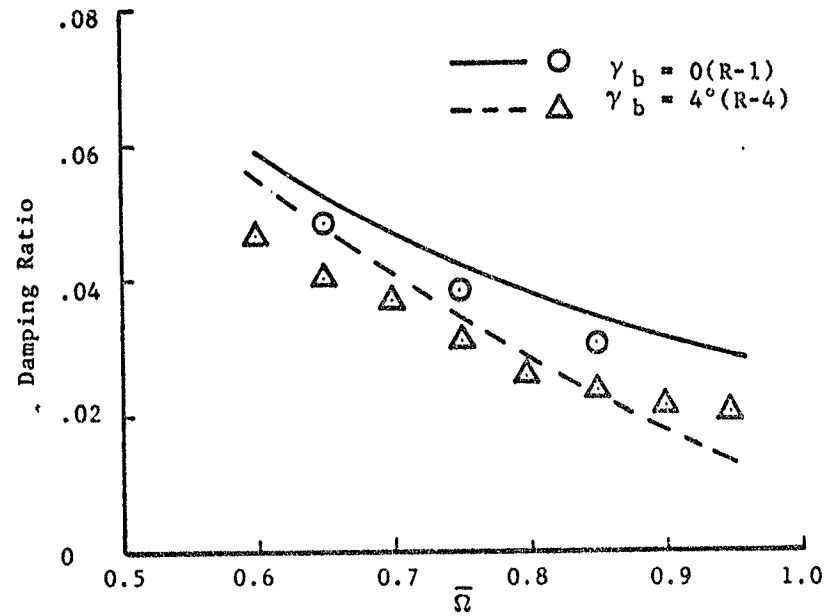

(b) Blade Sweep Angle Effect

Figure 11. Inplane Damping Variation With Blade Cone and Sweep Angles for Isolated Rotor in Hover (T = 1g).

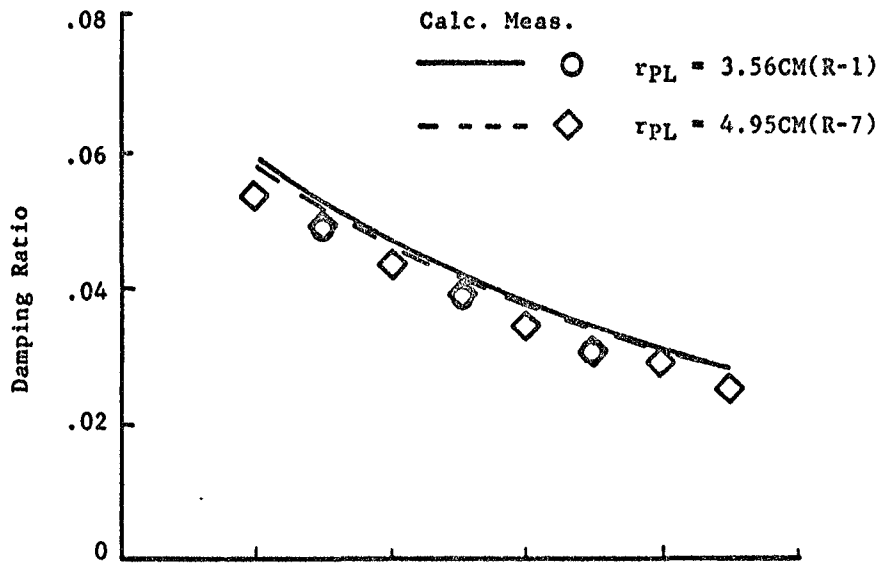

(a) Radial Location Effect

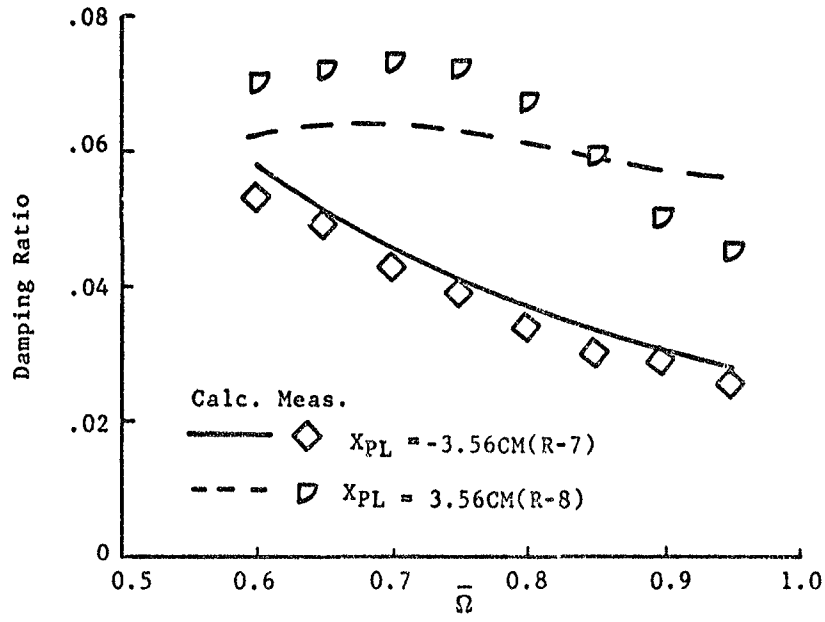

(b) Chordwise Location Effect

Figure 12. Inplane Damping Variation With Pitch Link Location For Isolated Rotor in Hover (T = 1g).

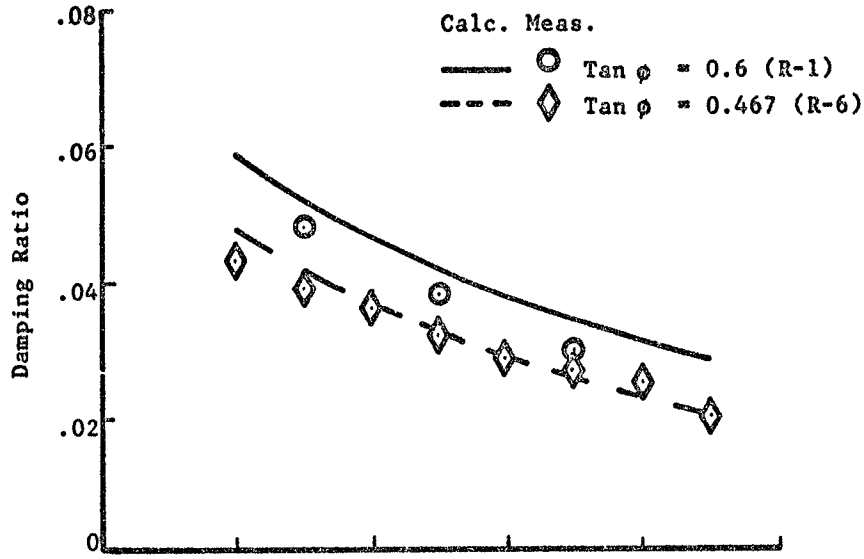

(a) Built-in Damping Effect

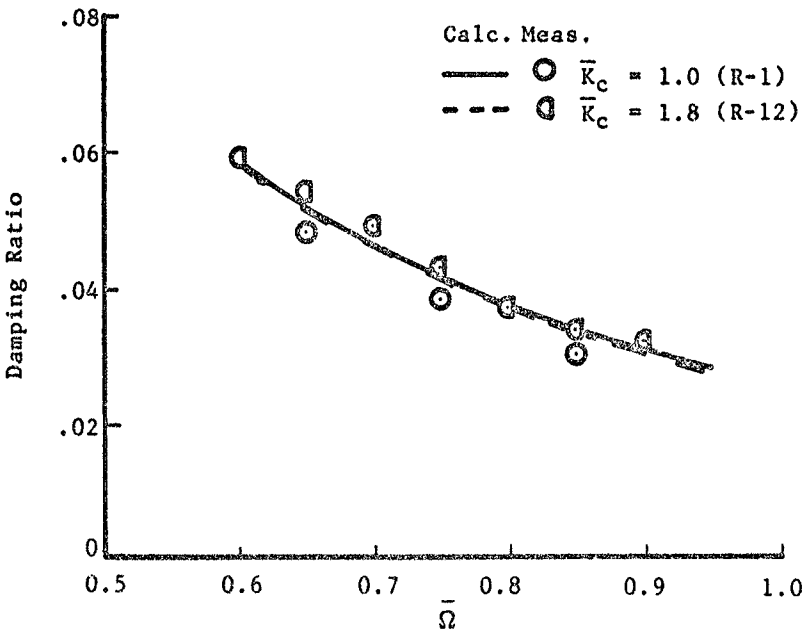

(b) Control System Stiffness Effect

Figure 13. Inplane Damping Variation With Blade Built-in Damping and Control System Stiffness for Isolated Rotor in Hover (T-1g).

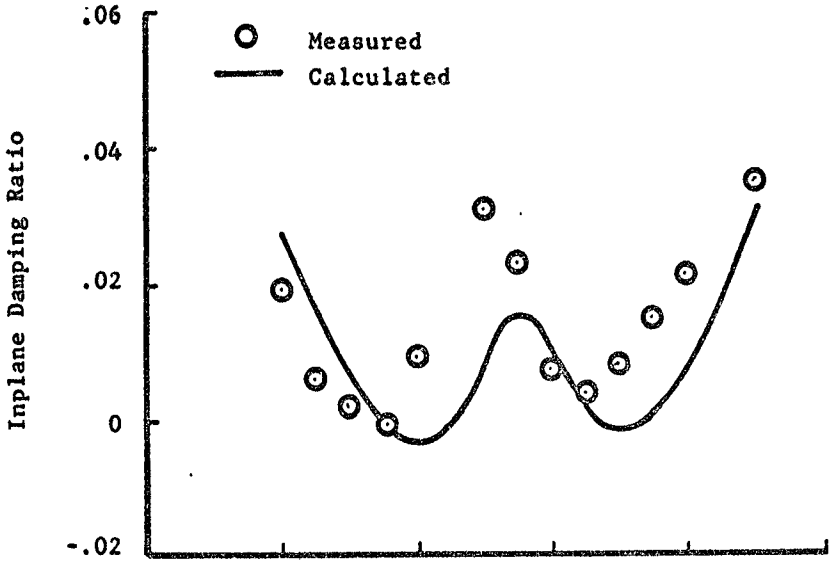

(a) Damping Correlation

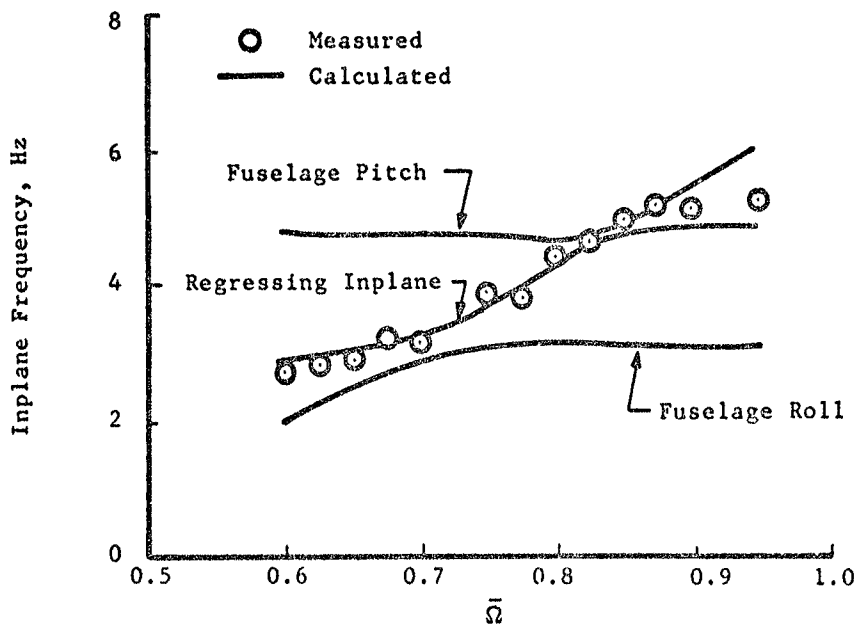

(b) Frequency Correlation

Figure 14. Inplane Damping and Frequency Correlation for Free-Hub (R-1/F-2) in Hover (T=1g).

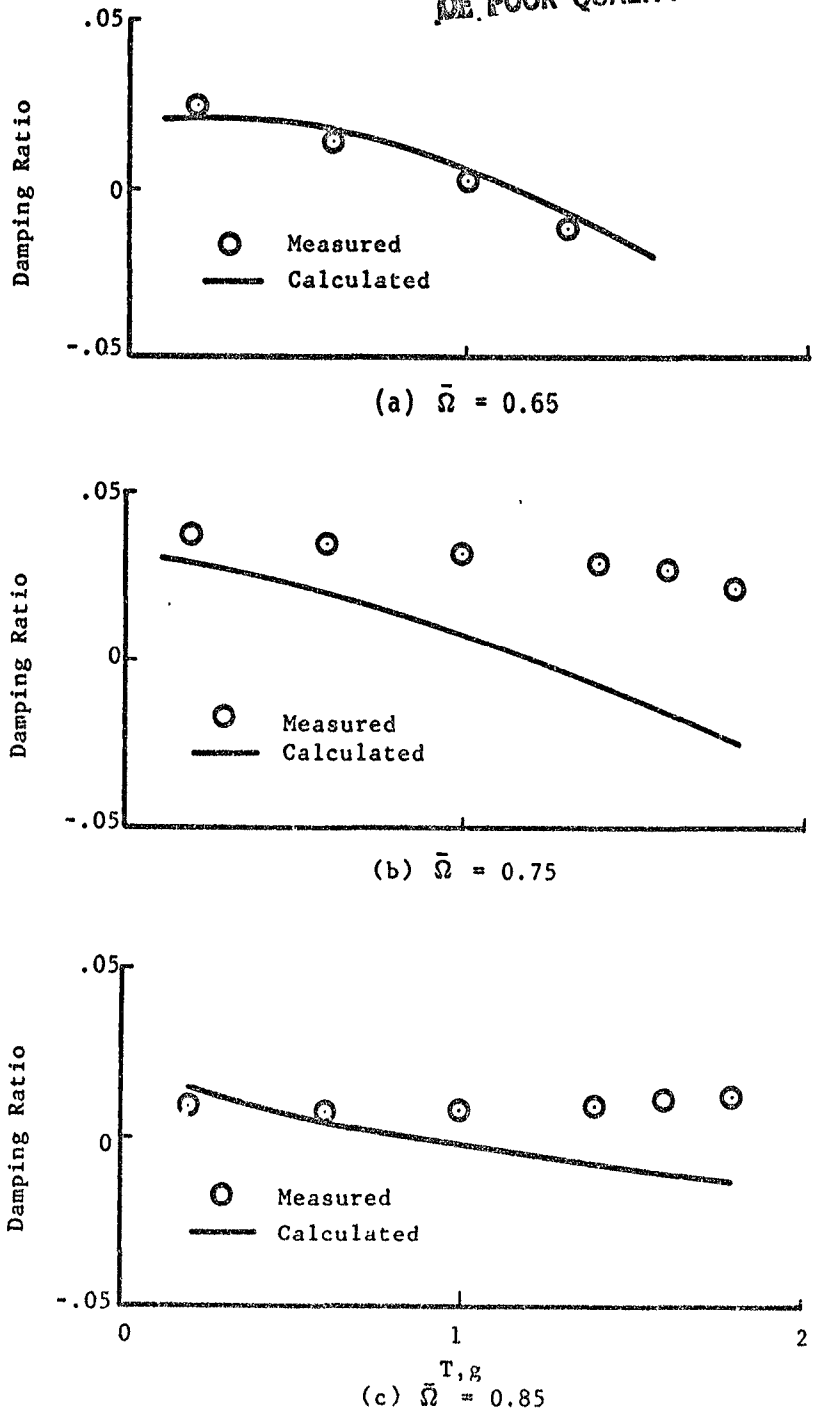

Figure 15. Inplane Damping Variation With Thrust for Free-Hub (R-1/F-2) in Hover.

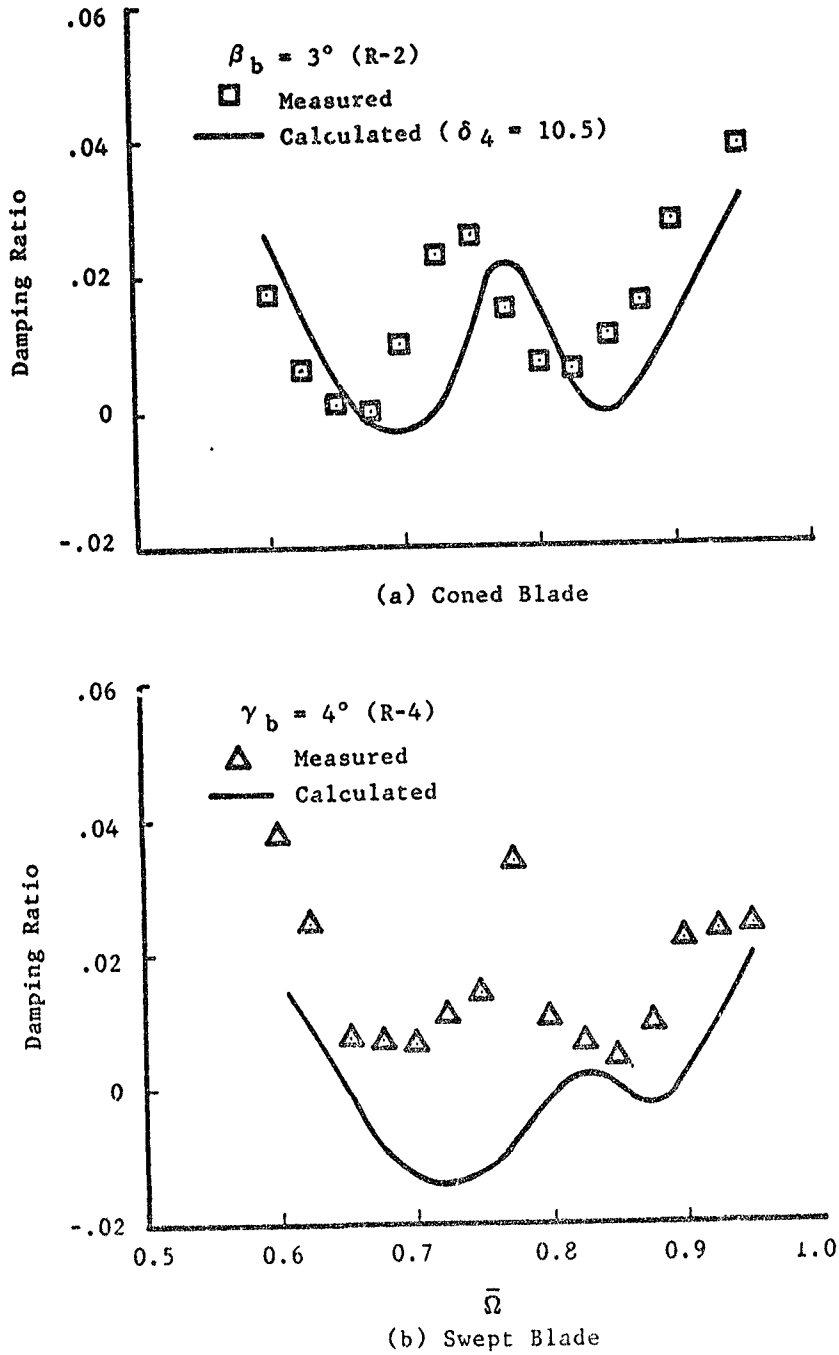

Figure 16. Inplane Damping Variation With Blade Cone and Sweep Angles for Free-Hub (F-2) in Hover (T-1g).

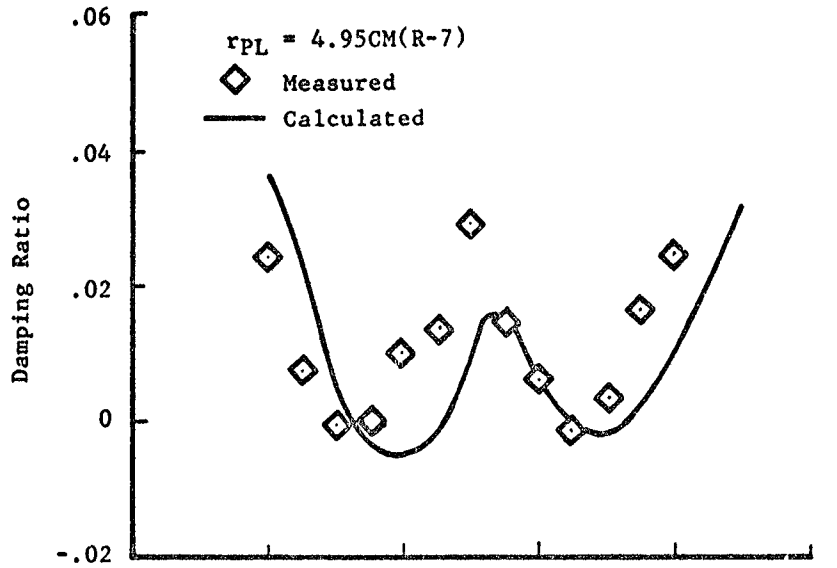

(a) Outboard Pitch Link

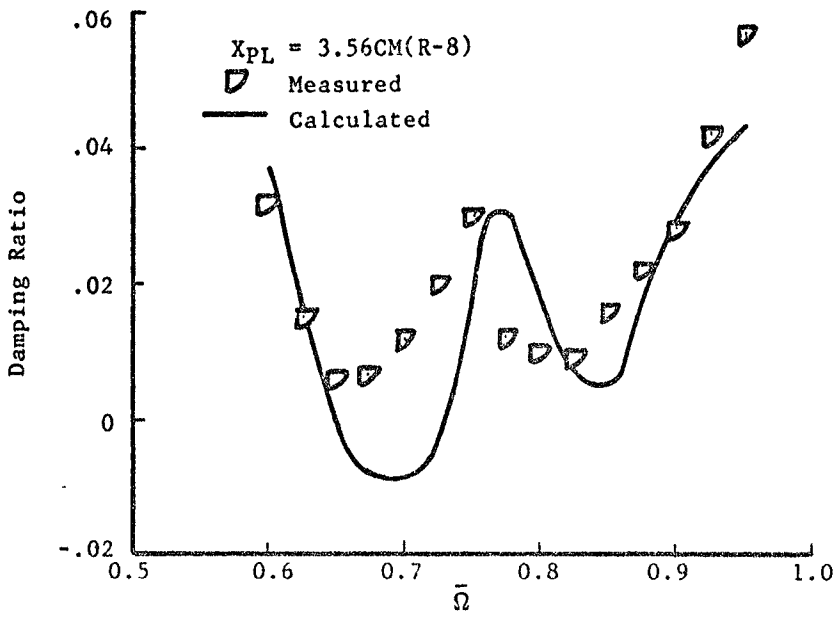

(b) Leading-edge Pitch Link

Figure 17. Inplane Damping Variation With Pitch Link Location for Free-hub (F-2) in Hover (T=1g).

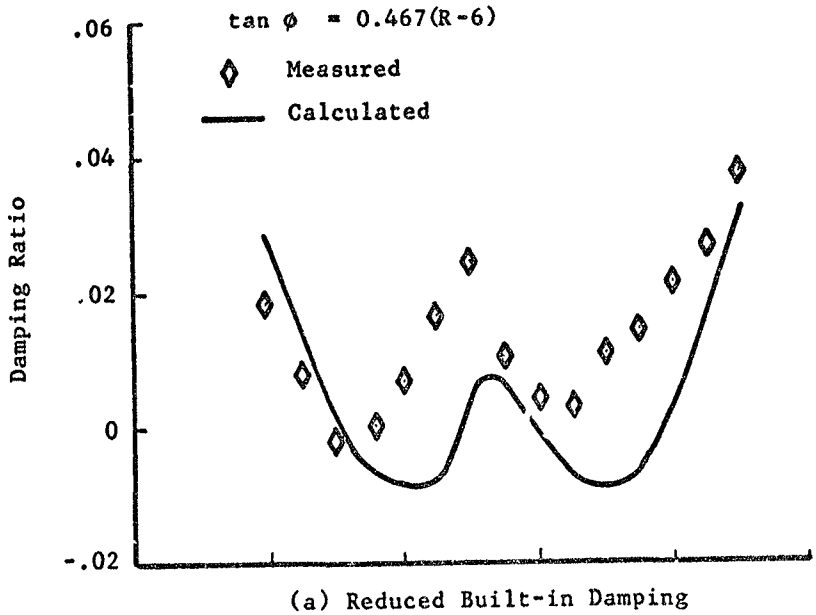

(a) Reduced Built-in Damping

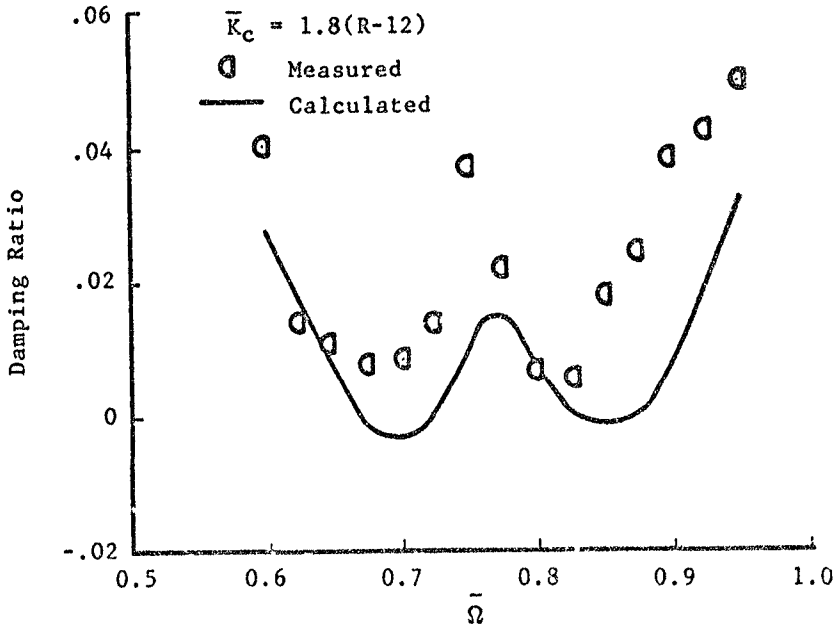

(b) Stiffened Control System

Figure 18. Inplane Damping Variation With Built-in Damping and Control System Stiffness for Free-hub (F-2) in Hover (T-1g).

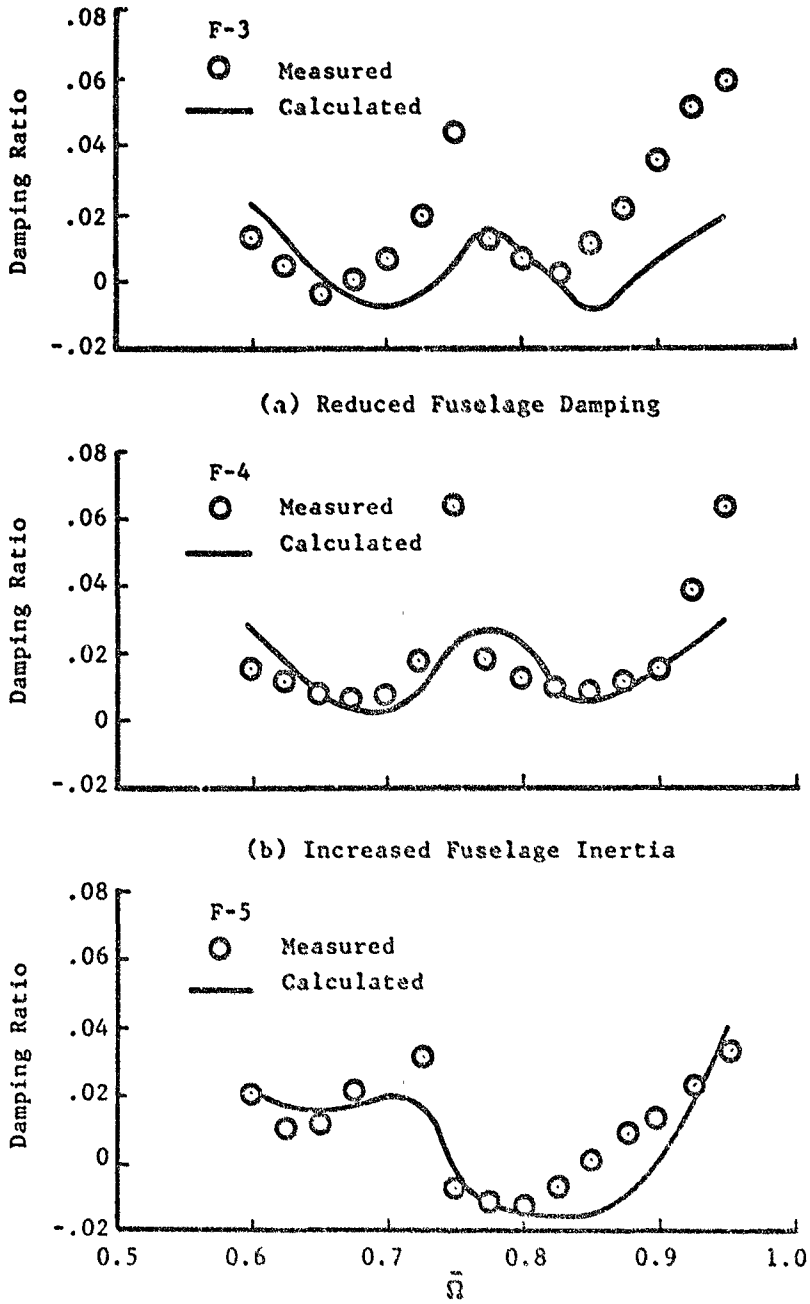

Figure 19. Inplane Damping Variation With Fuselage Structural Properties for Free-hub With R=1 in Hover (T=1g).

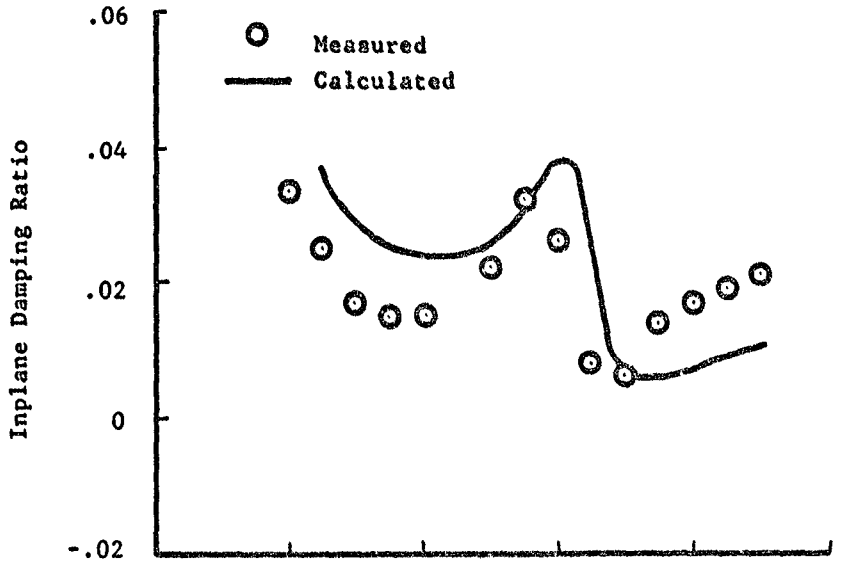

(a) Damping Correlation

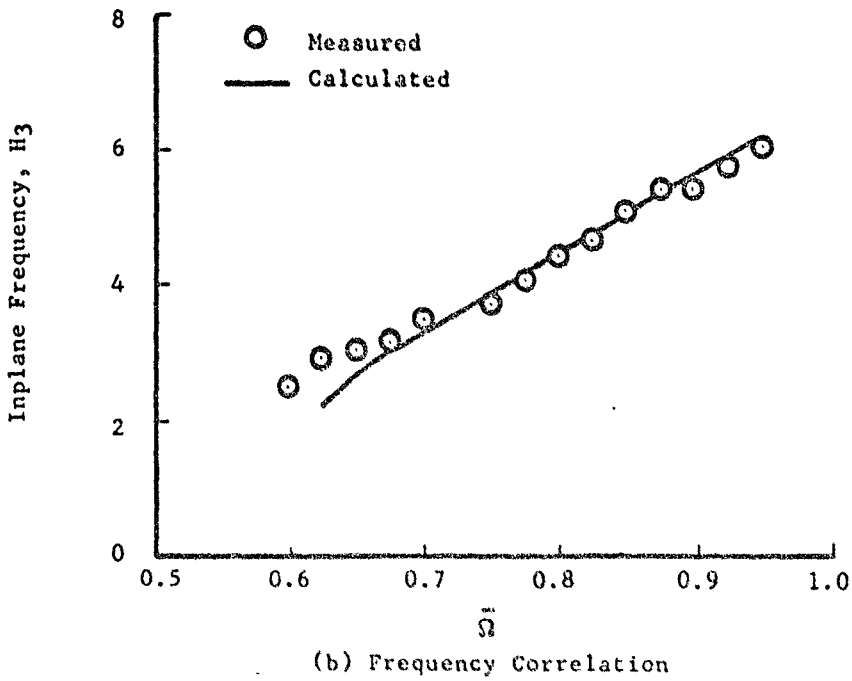

(b) Frequency Correlation

Figure 20. Inplane Damping and Frequency Correlation for Free-Hub (R-1/F-2) in Forward Flight (T=1g, V=27.7kn).

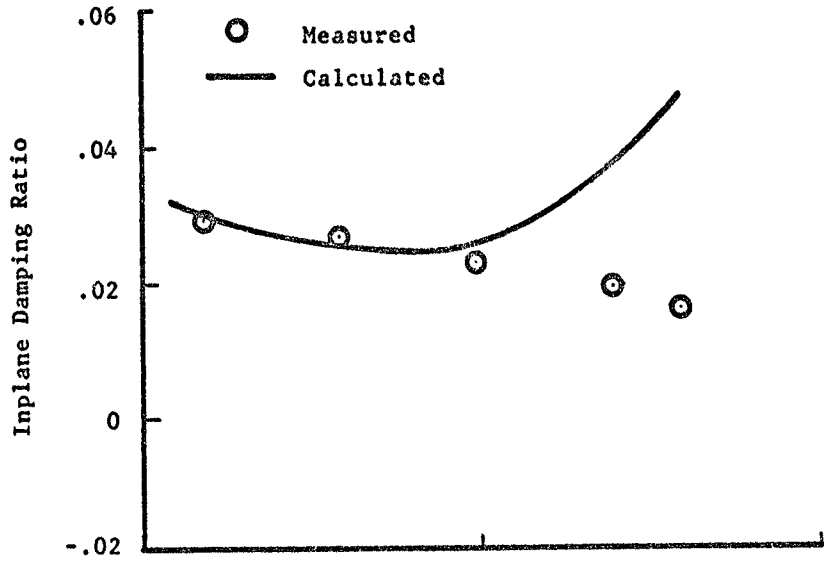

(a) Damping Variation

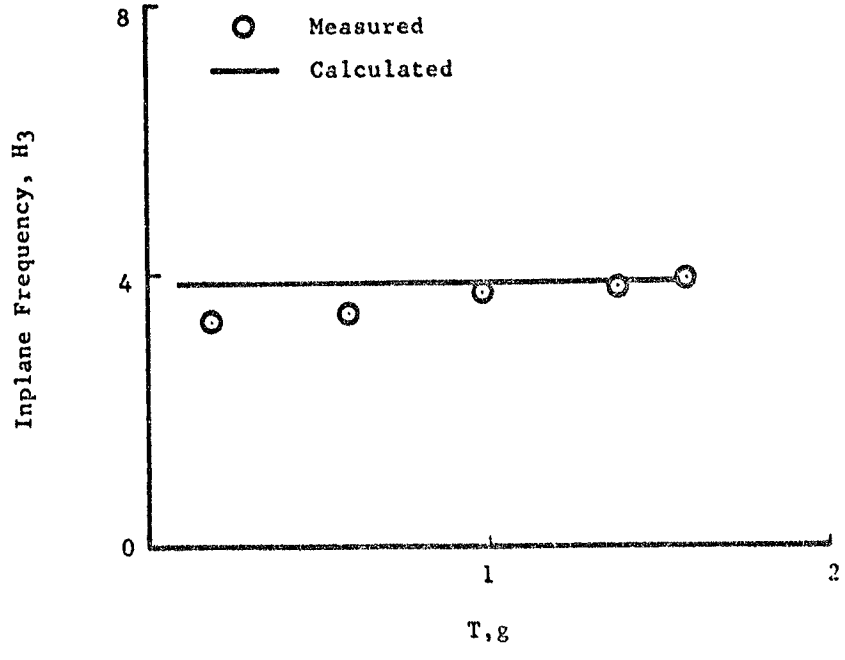

(b) Frequency Variation

Figure 21. Inplane Damping and Frequency Variations with Thrust for Free-Hub (R-1/F-2) in Forward Flight ($\bar{\Omega}$ = 0.75, V = 27.7 kn).

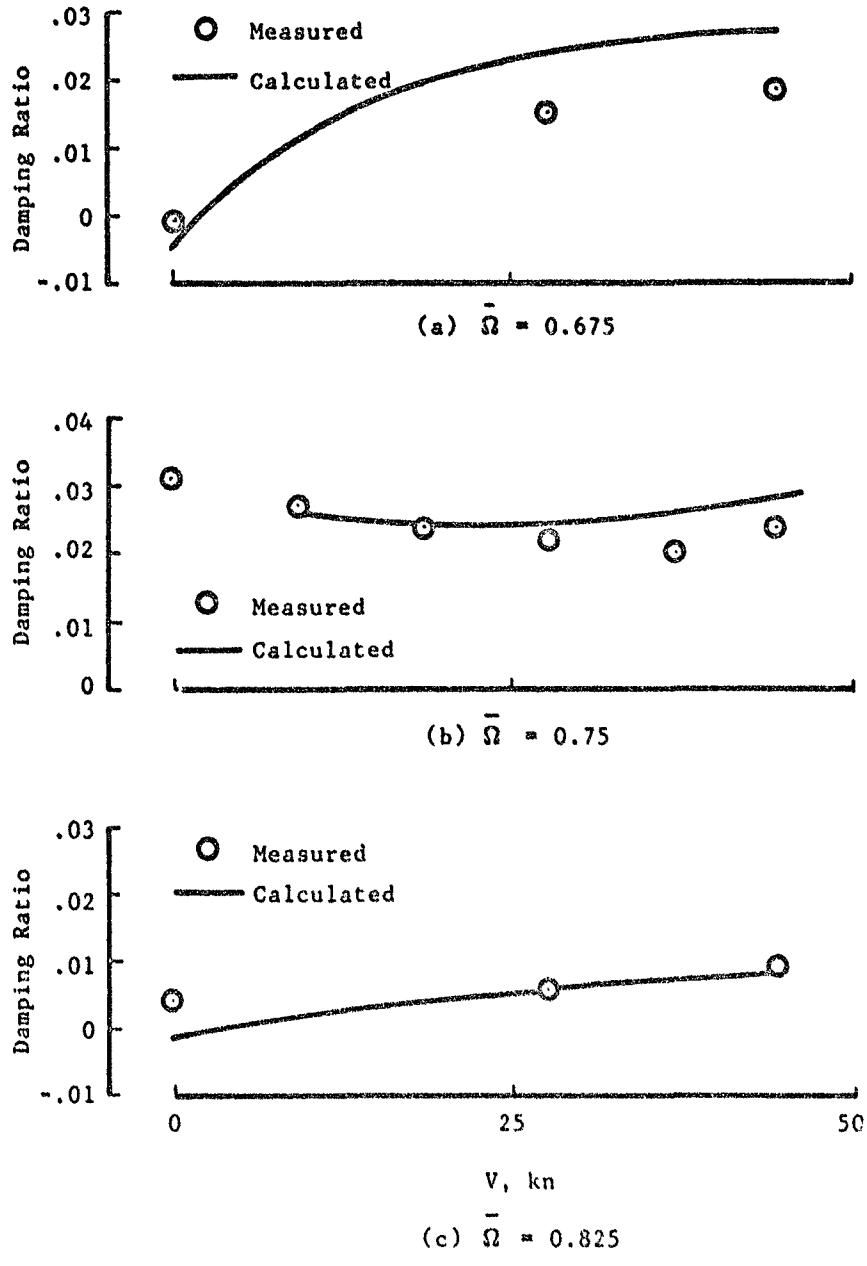

Figure 22. Inplane Damping Variation With Flight Speed for Free-Hub (R-1/F-2) and T=1g.

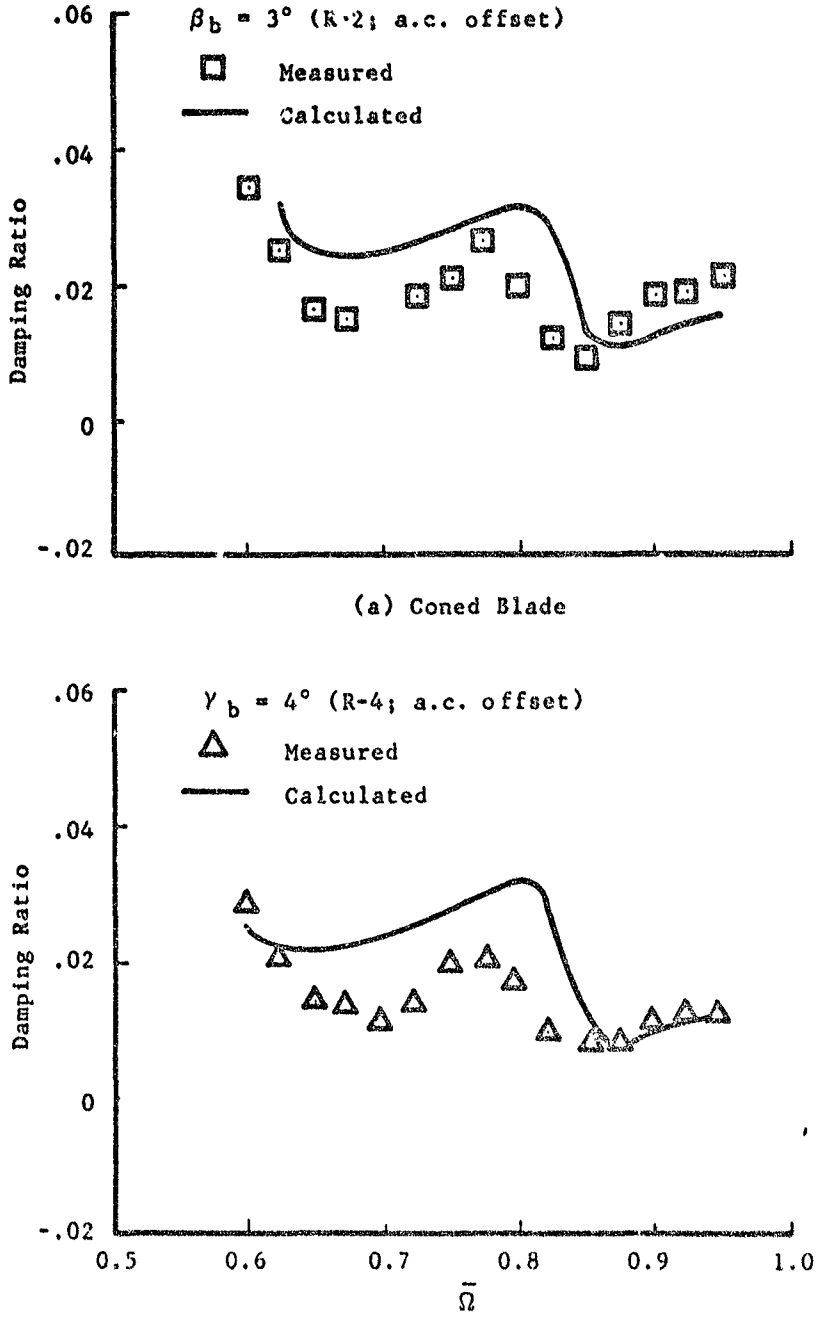

Figure 23. Inplane Damping Variation With Blade Cone and Sweep Angles for Free-Hub (F-2) in Forward Flight (T-1g, V=27.7 kn).

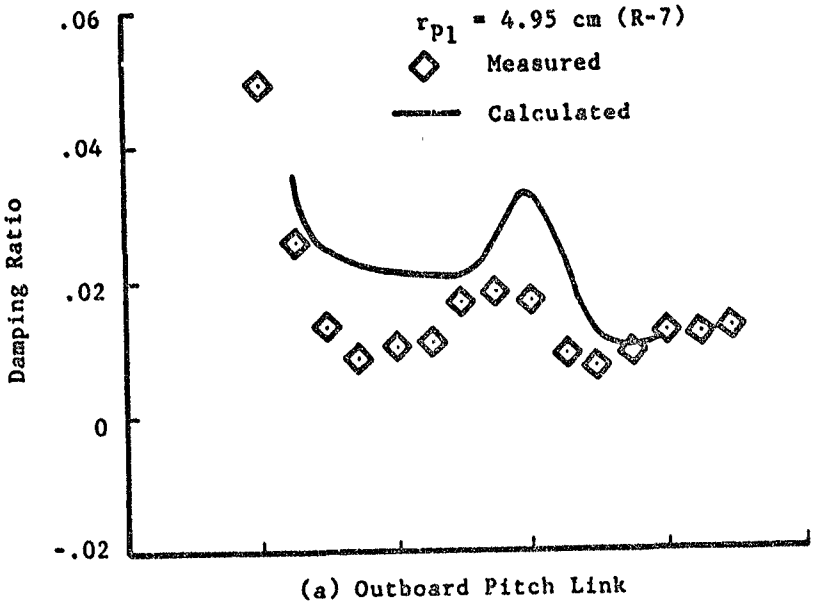

(a) Outboard Pitch Link

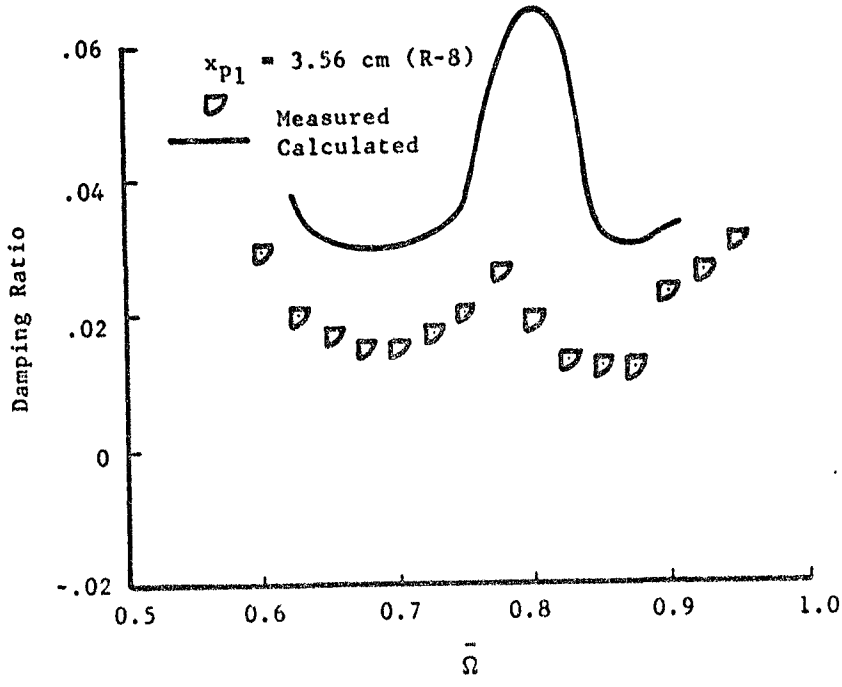

(b) Leading-Edge Pitch Link

Figure 24. Inplane Damping Variation With Pitch Link Location for Free-Hub (F-2) in Forward Flight (T-1g, V=27.7 kn).

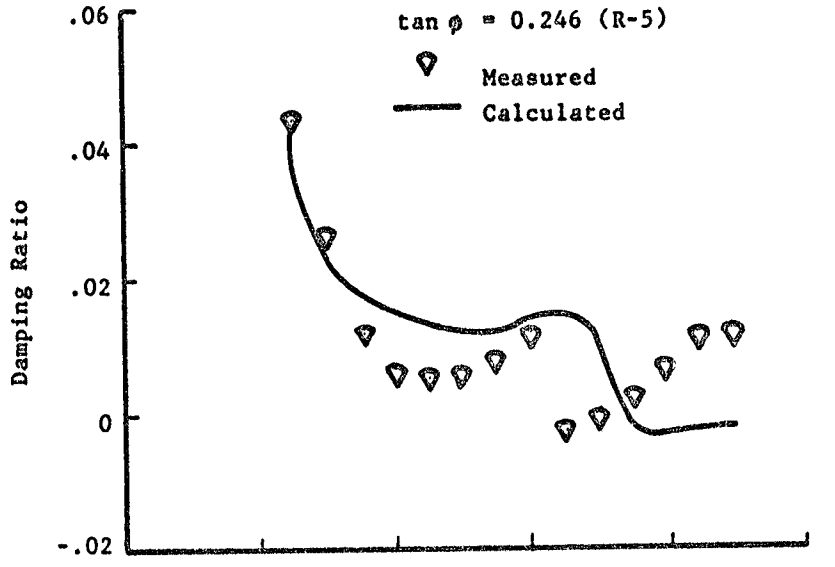

(a) Minimum Built-in Damping

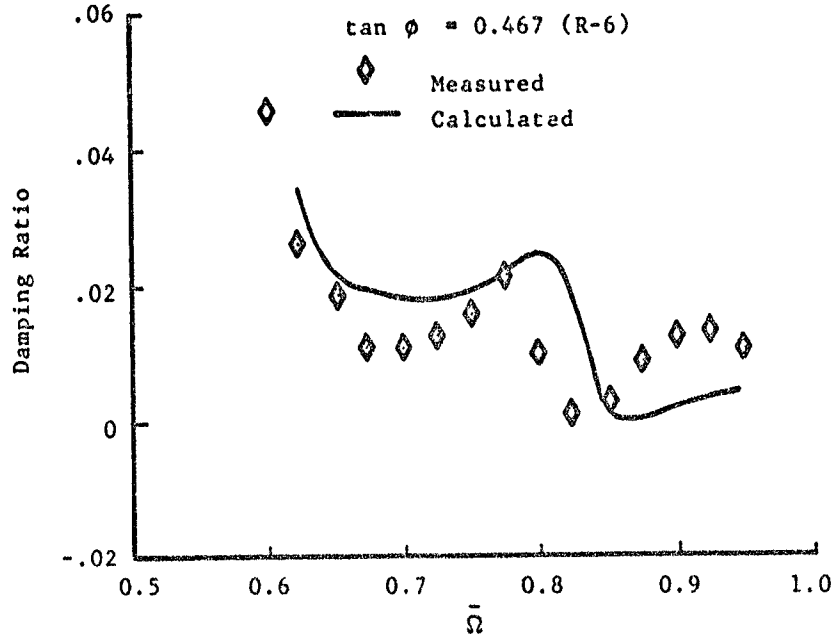

(b) Reduced Built-in Damping

Figure 25. Inplane Damping Variation With Blade Built-in Damping for Free-Hub (F-2) in Forward Flight (T-1g, V=27.7 kn).

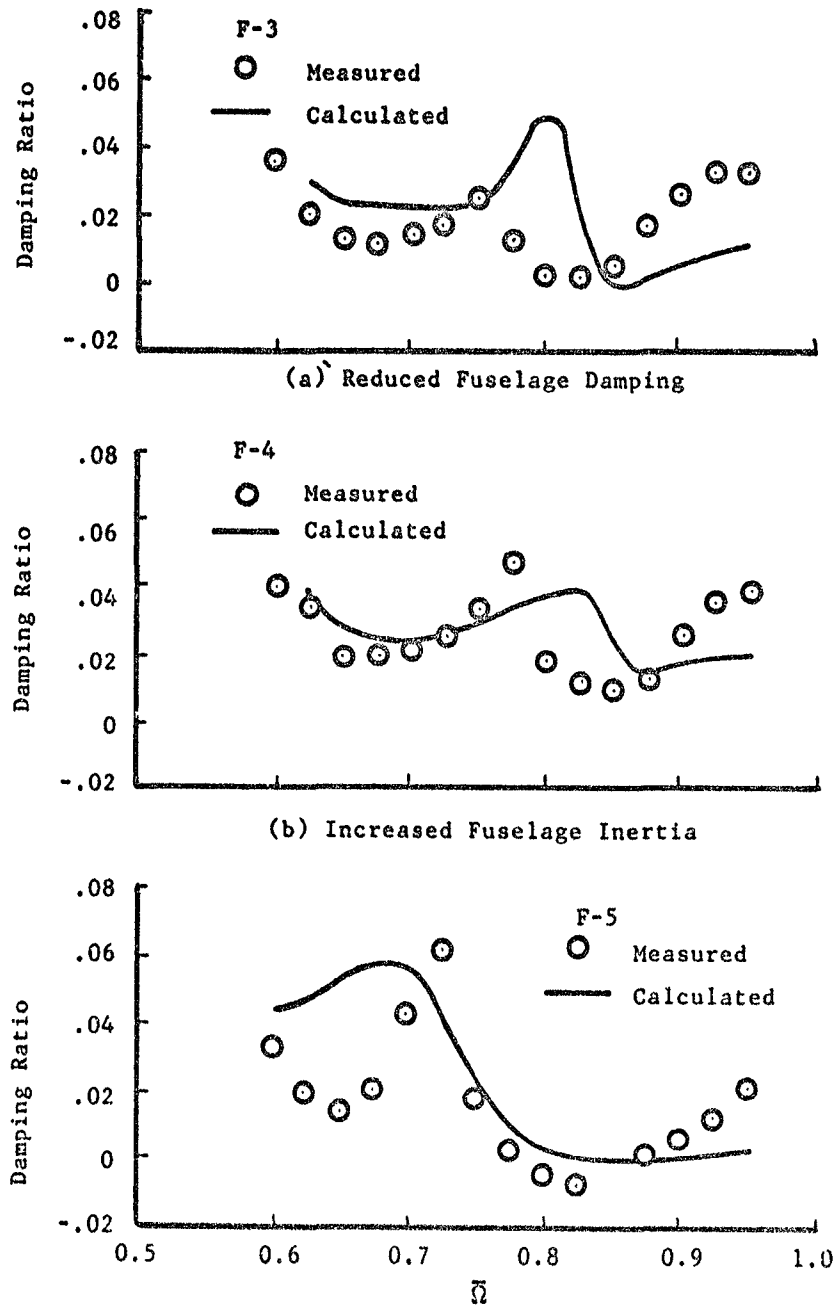

Figure 26. Inplane Damping Variation With Fuselage Structural Properties for Free-Hub (R-1) in Forward Flight (T-1g, V-27.7 kn).

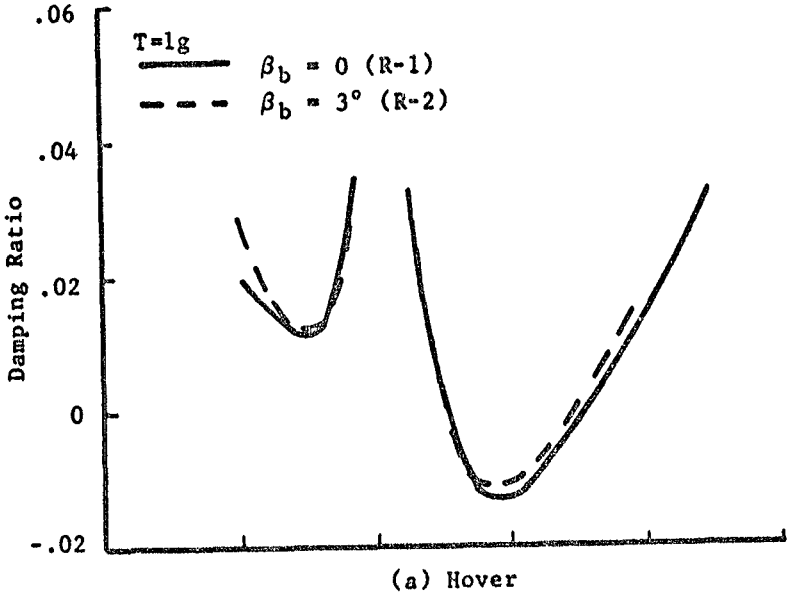

(a) Hover

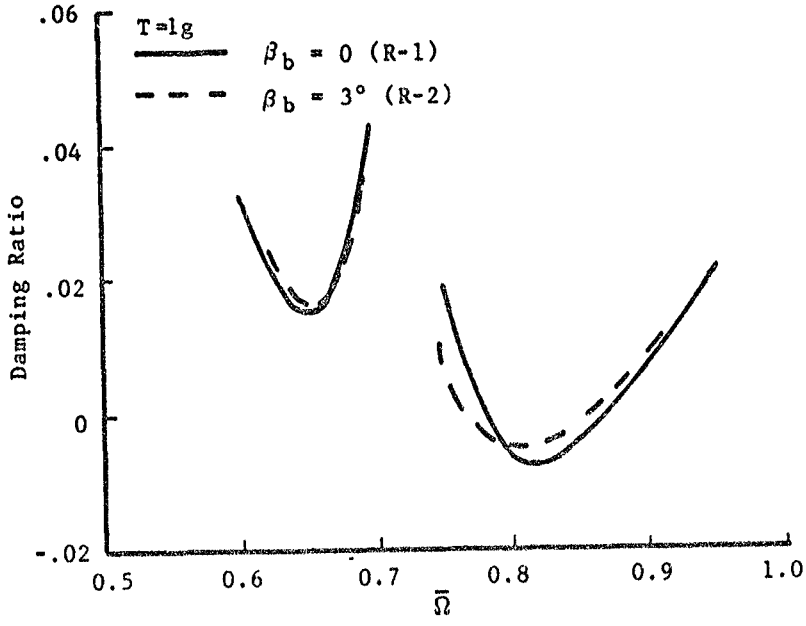

(b) Forward Flight (V=27.7 kn)

Figure 27. Measured Effect of Blade Cone Angle on Minimum Damping Ratios for Free-Hub (F-5).

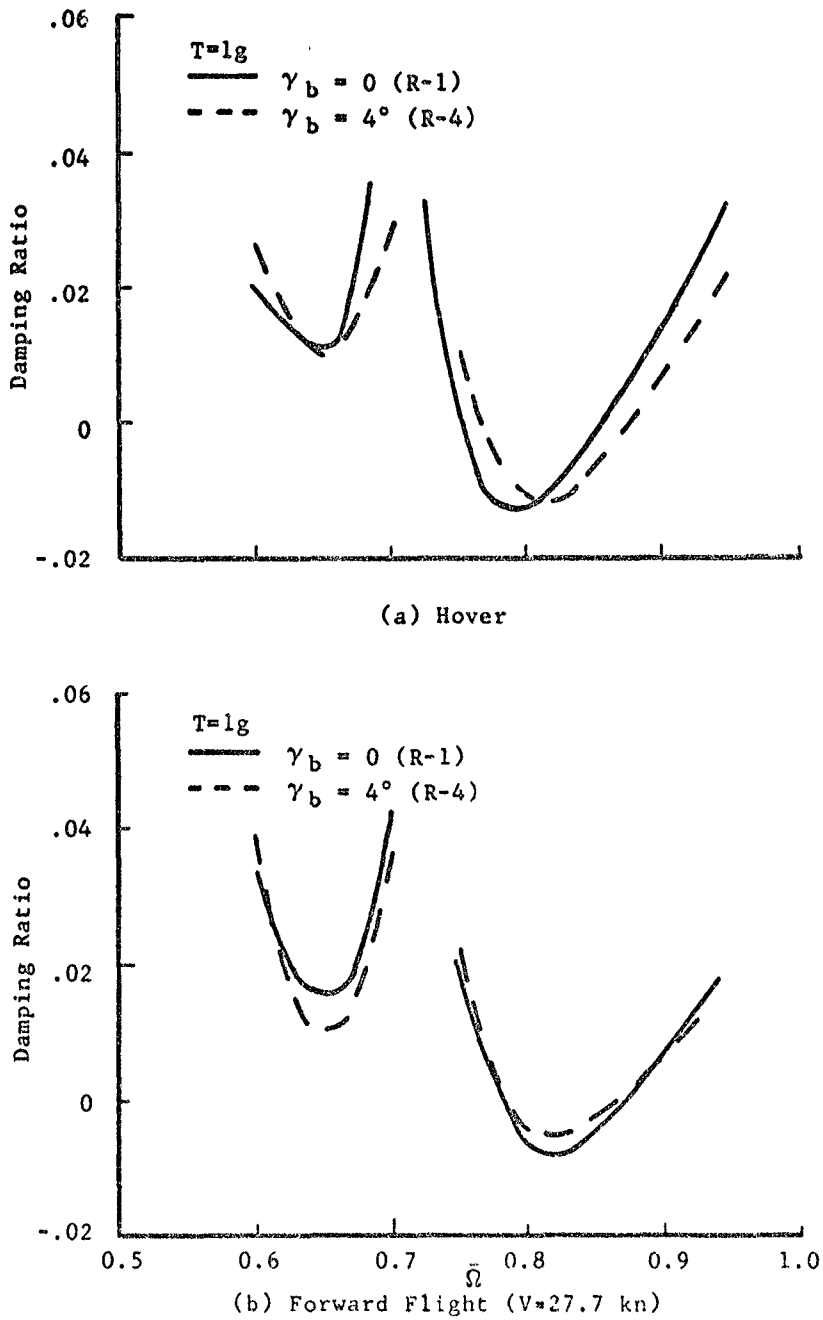

Figure 28. Measured Effect of Blade Sweep Angle on Minimum Damping Ratios for Free-Hub (F-5).

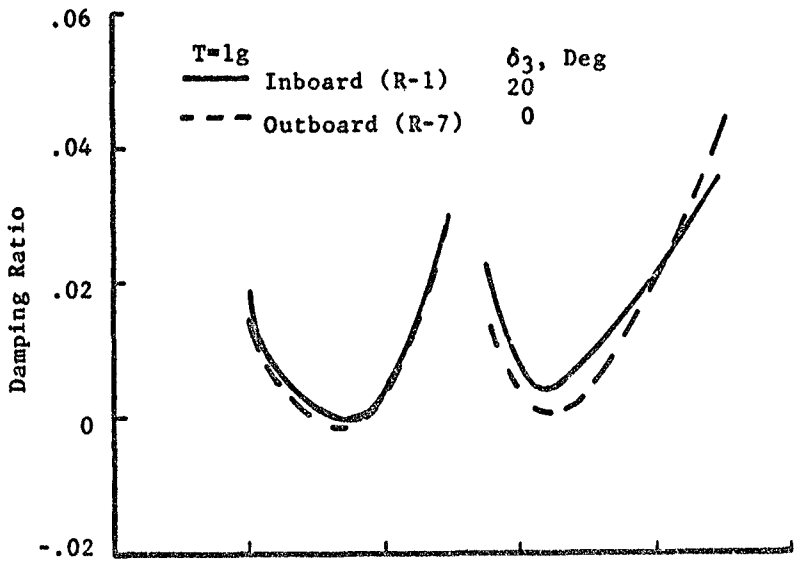

(a) Trailing-Edge Locations

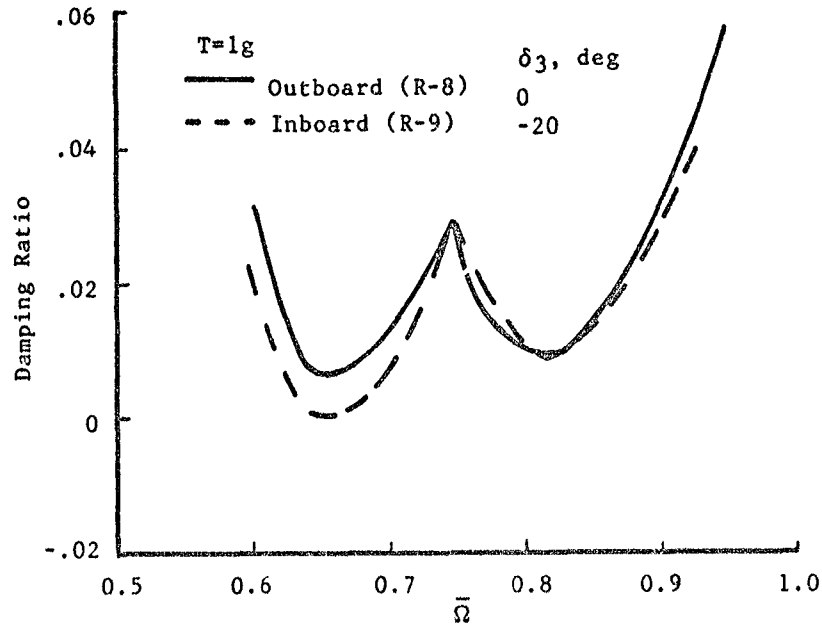

(b) Leading-Edge Locations

Figure 29. Measured Effect of Pitch link Location on Minimum Damping Ratios for Free-Hub (F-2) in Hover.

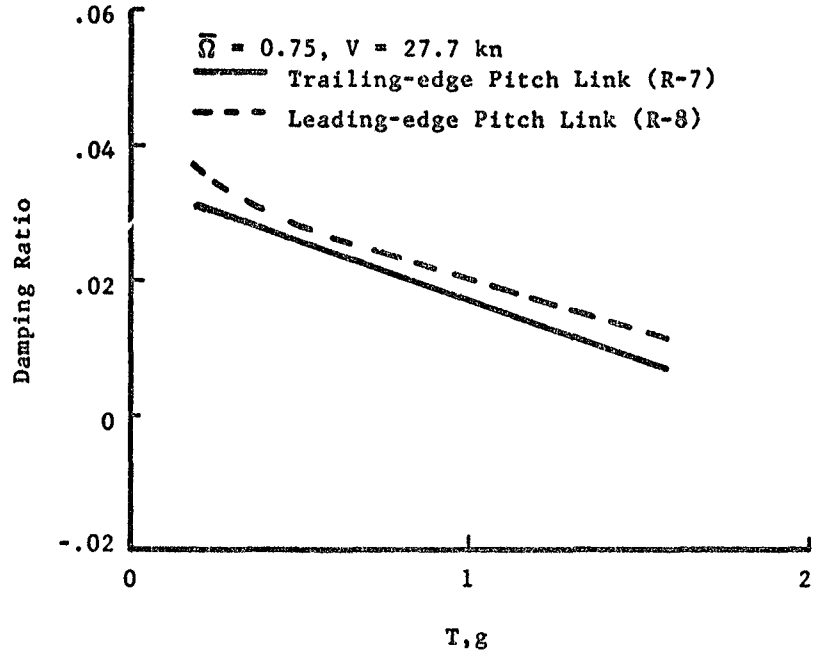

(a) Variation With Thrust

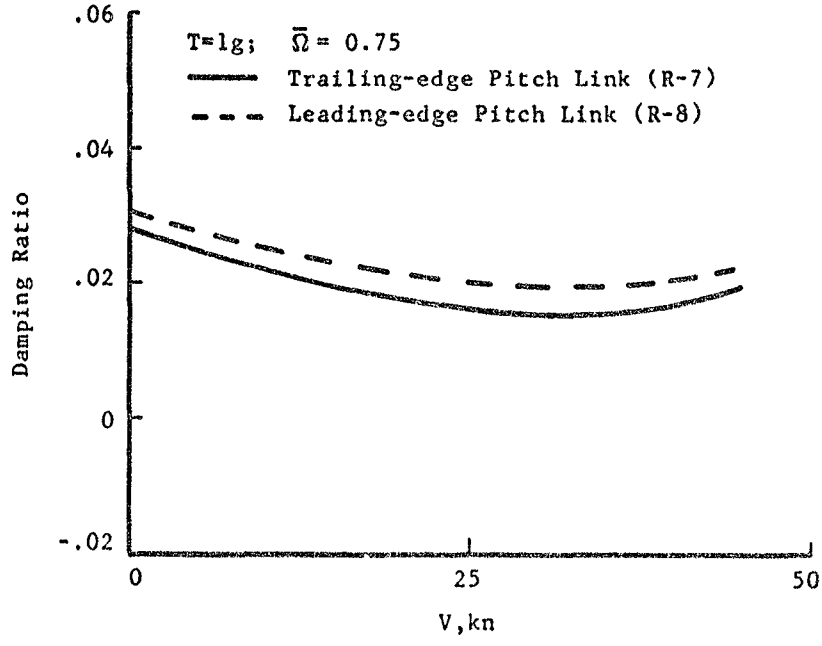

(b) Variation With Flight Speed

Figure 30. Measured Effect of Pitch Link Chordwise Location on Damping Ratios for Free-Hub (F-2) in Forward Flight

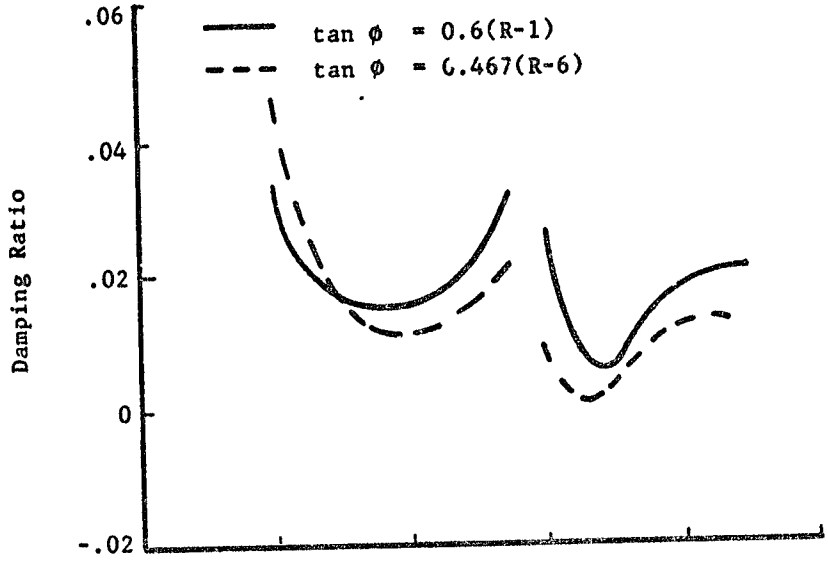

(a) Built-in Damping Effect

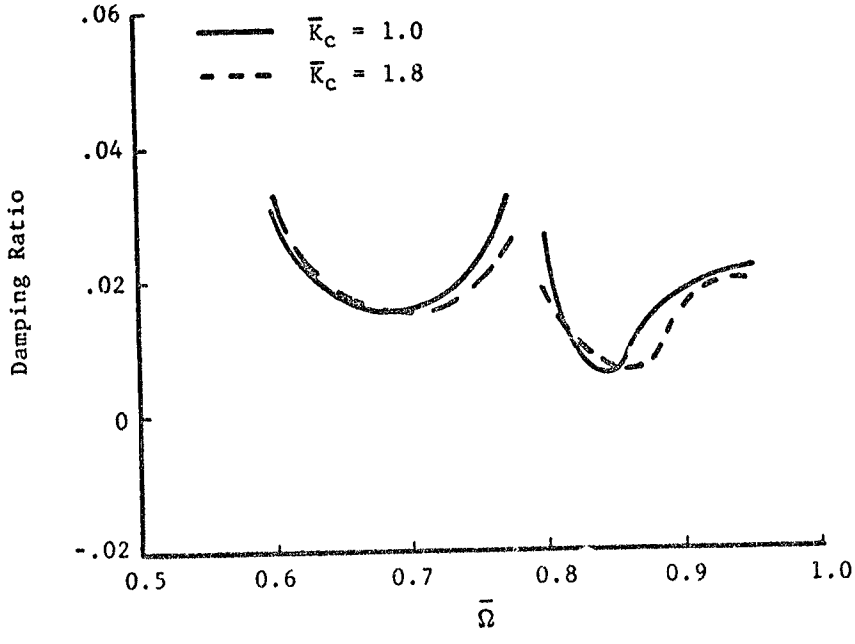

(b) Control System Stiffness Effect

Figure 31. Measured Effect of Blade Built-in Damping and Control System Stiffness for Free-Hub (F-2) in Forward Flight (T=1g, V=27.7 kn).

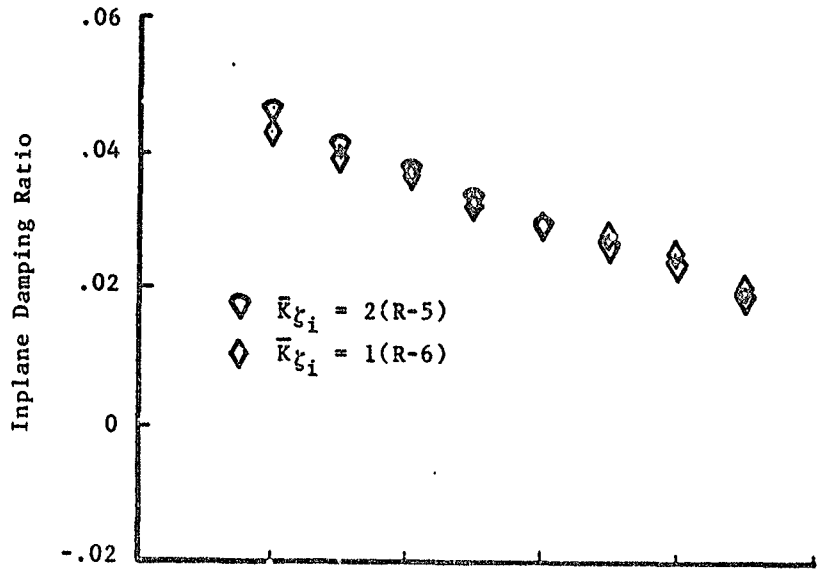

(a) Damping Comparison

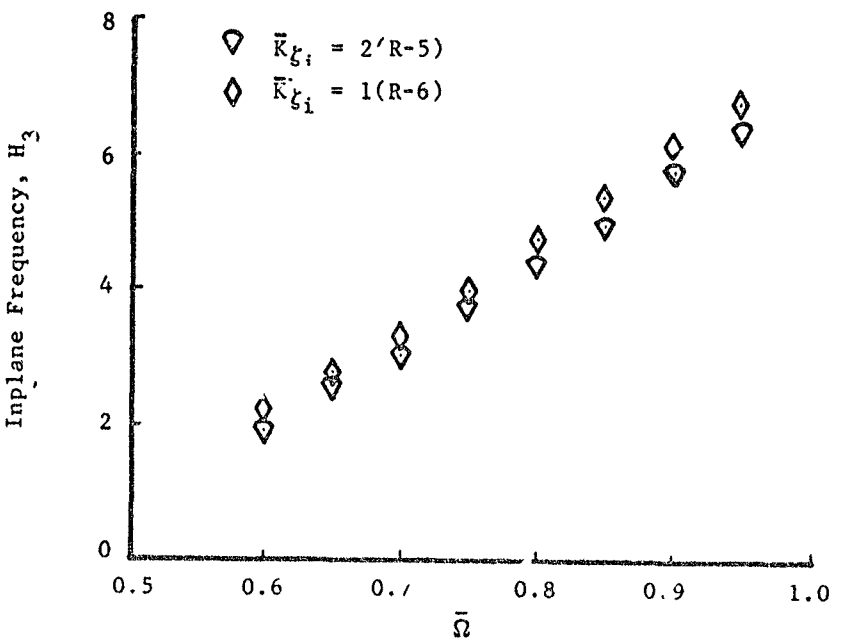

(b) Frequency Comparison

Figure 32. Comparison of Measured Isolated Rotor Inplane Characteristics for R-5 and R-6 in Hover (T-1g).

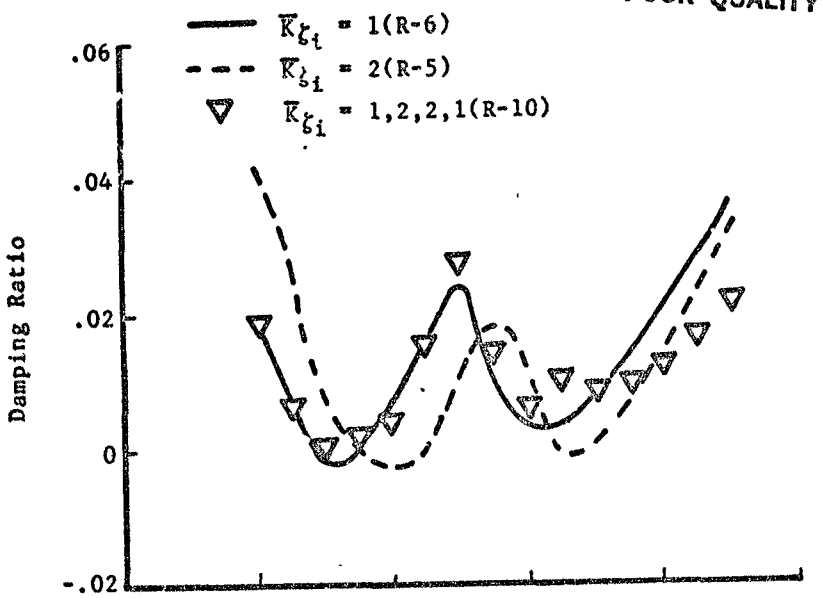

(a) Matched Adjacent Blades

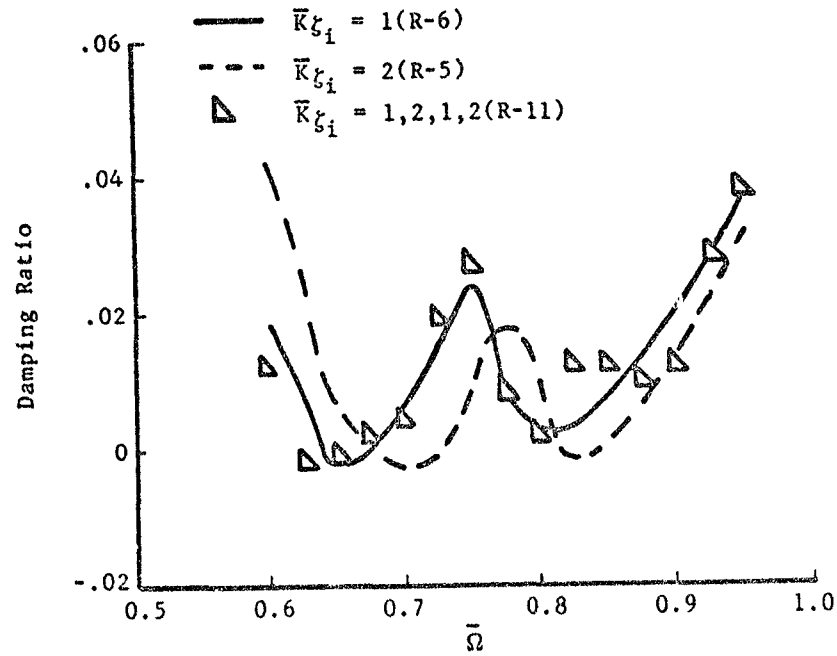

(b) Matched Opposite Blades

Figure 33. Measured Anisotropic Rotor Damping Characteristics for Free-Hub (F-2) in Hover (T-1g).

End of Document